535 Imaging, III
Thursday, May 07, 2015 12:00 PM–1:45 PM
Exhibit Hall Poster Session
Program #/Board # Range: 5900–5967/A0071–A0138
Organizing Section: Retina
Contributing Section(s): Anatomy/Pathology, Multidisciplinary Ophthalmic Imaging, Retinal Cell Biology

Program Number: 5900 **Poster Board Number:** A0071
Presentation Time: 12:00 PM–1:45 PM
In Vivo Multi-Level Vasculature Visualization in the Posterior Rodent Eye Using High Resolution Optical Coherence Tomography
Marco Augustin[1, 2], Stanislava Fialová[1, 2], Roberto Plasenzotti[3], Michael Pircher[1, 2], Christoph K. Hitzenberger[1, 2], Bernhard Baumann[1, 2]. [1]Center for Medical Physics and Biomedical Engineering, Medical University of Vienna, Vienna, Austria; [2]Medical Imaging Cluster, Medical University of Vienna, Vienna, Austria; [3]Division of Biomedical Research, Medical University of Vienna, Vienna, Austria.
Purpose: To show the ability of using optical coherence tomography (OCT) for in-vivo imaging of the vasculature in rodents' posterior eyes. This technique enables long-term follow up studies of ophthalmic pathologies where morphological changes of the vasculature can be observed, e.g. age-related macular degeneration (AMD) or diabetic retinopathy (DR).
Methods: A custom-made high resolution polarization sensitive (PS-) OCT system was used to image the posterior eye of mice and rats. Three-dimensional images of different rats (Long-Evans, Brown Norway, Sprague-Dawley) and Black-6 mice were acquired. The healthy rodents were anaesthetized and scanned with an angle of 11x11° and 21x21° around the papilla. Increasing the signal-to-noise ratio was achieved by averaging 5 repeated B-scans at each B-scan position. Motion artifacts due to breathing/heart beat were compensated between adjacent B-frames. To visualize different layers of retinal and choroidal vasculature a semi-automatic segmentation of the retinal layers is performed in a first step. In a second step, the segmented layers are used to restrict the volume in which the expected vasculature is visualized. To show the retinal blood vessels between nerve fiber layer and inner nuclear layer a maximum intensity (reflectivity) projection is used. The smaller capillaries in the outer plexiform layer (OPL) are also visualized by a maximum intensity projection. To visualize the vasculature in the choroid an average intensity projection is used and the resulting map is inverted.
Results: The resulting vascular maps of each level show the ability of visualizing different vasculature structures. The first (most inner) projection shows big retinal vessels and nerve fibers around the optic nerve head. Smaller capillaries can be observed in the OPL. Visualizing choroidal vasculature is a more challenging task as the vessels appear as hollow structures in the images. These vessels appear unsharp although vascular structures are clearly visible. Projection artefacts (shadows) from larger vessels remain visible in deeper layers.
Conclusions: The combination of high resolution PS-OCT and intensity projections between certain levels enables to visualize retinal and choroidal vasculature. The resolution of the custom-made system is high enough to visualize retinal capillaries of rodents in the OPL by using only the reflectivity information.

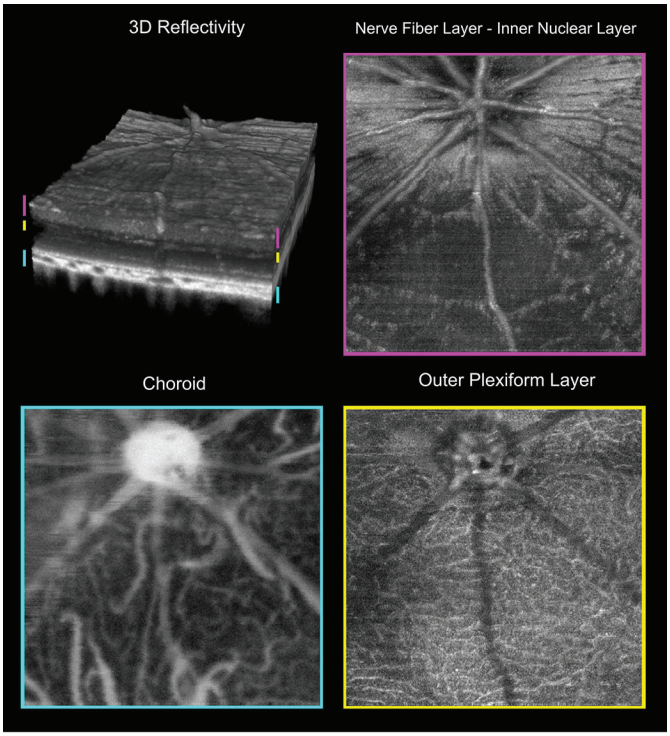

Figure 1. Exemplary three dimensional PS-OCT reflectivity image from Long-Evans rat and corresponding en-face projections between layers at different depths. The projection between the nerve fiber layer and the inner nuclear layer shows high reflectivity around the optic nerve head where the nerve fiber bundles show a strong reflection. Retinal capillaries are visible between the borders of the outer plexiform layer (OPL). An average projection through the choroid makes choroidal vasculature of different sizes visible. Projection artefacts (shadows) from big retinal vessels can be observed in the lower vascular maps of the OPL and the choroid.
(Field of view: 21 x 21°; corresponds to approximately 1.25 x 1.25 mm)

Commercial Relationships: Marco Augustin, None; **Stanislava Fialová**, None; **Roberto Plasenzotti**, None; **Michael Pircher**, None; **Christoph K. Hitzenberger**, None; **Bernhard Baumann**, None
Support: Austrian Science Fund (FWF) P25823-B24

Program Number: 5901 **Poster Board Number:** A0072
Presentation Time: 12:00 PM–1:45 PM
Thickness Mapping of Retinal Layers in Ins2(Akita) Diabetic and Wild Type Mice by Spectral Domain Optical Coherence Tomography
Andrew W. Francis, Justin Wanek, Mahnaz Shahidi. Ophthalmology and Visual Sciences, University of Illinois Eye and Ear Infirmary, Chicago, IL.
Purpose: The Ins2(Akita) mouse is a model of diabetes and heterozygous for a mutation in the insulin 2 gene resulting in beta-cell dysfunction, hypoinsulinemia, and hyperglycemia. The purpose of this study was to assess global and local inner and outer retinal thickness alterations in Ins2(Akita) diabetic mice by automated segmentation of spectral domain optical coherence tomography (SD-OCT) images.
Methods: SD-OCT imaging was performed in Ins2(Akita) diabetic mice (n = 5) and wild type mice (n = 5) at 12 weeks of age using a commercially available instrument (Spectralis; Heidelberg). In each mouse, 31 raster B-scans were acquired over a 30 x 25 degree retinal area nasal to the optic disk. Using an automated software algorithm developed in Matlab, 5 retinal cell layer interfaces were detected: 1) vitreous/internal limiting membrane; 2) inner nuclear/

outer plexiform; 3) outer nuclear/inner segment ellipsoid (ISe); 4) outer segment/retinal pigment epithelium (RPE); and 5) RPE/choroid. Based on automated segmentation, total retinal thickness (TRT), outer retinal thickness (ORT), inner retinal thickness (IRT), and photoreceptor outer segment length (OSL) were mapped. Mean and standard deviation (SD) of thickness measurements were compared using unpaired t-test. The percentage of retinal area with thickness above or below the normal confidence interval established in wild type mice was calculated for each retinal layer. Statistical significance was accepted at $p < 0.05$.
Results: Blood glucose levels in Ins2(Akita) diabetic mice (397 ± 109 mg/dL, n = 5) were significantly elevated compared to measurements in wild type mice (156 ± 23 mg/dL, n = 5) ($p = 0.001$), confirming the presence of diabetes. Automated segmentation of 4 retinal cell layers was successfully performed in both diabetic and wild type mice. There was no statistically significant difference in mean TRT ($p = 0.67$), IRT ($p = 0.15$), ORT ($p = 0.52$), OSL ($p = 0.09$) or the SDs of any retinal cell layer ($p > 0.09$). On average, less than 9% of the retinal area in diabetic mice had decreased TRT, IRT, ORT, or OSL and less than 8% had increased TRT, IRT, or ORT. However, on average, 17% of the retinal area in diabetic mice had increased OSL.
Conclusions: Alterations in inner and outer retinal thickness maps were not observed in Ins2(Akita) mice, indicating minimal global and local retinal structural changes at 12 weeks of age.
Commercial Relationships: Andrew W. Francis, None; **Justin Wanek**, None; **Mahnaz Shahidi**, None
Support: NIH EY017918, NIH EY001792, Research to Prevent Blindness, Illinois Society for the Prevention of Blindness

Program Number: 5902 **Poster Board Number:** A0073
Presentation Time: 12:00 PM–1:45 PM
Imaging Studies for the Management of Choroidal Neovascularization in Patients with Myopic Degeneration
Sarwar Zahid[1], KaPo Yeung[3], Kevin Chen[1], Richard T. Atallah[1], Daniel Simhaee[1], Joseph Tseng[3, 2], Kenneth Wald[3, 1]. [1]Ophthalmology, New York University, New York, NY; [2]Ophthalmology, SUNY Downstate, Brooklyn, NY; [3]Ophthalmology, Retina Associates of New York, New York, NY.
Purpose: To determine if optical coherence tomography (OCT) is a reliable method of detecting disease activity and therefore making management decisions in eyes with choroidal neovascularization (CNV) from Myopic Macular Degeneration (MMD). Fluorescein Angiography (FA) is considered the gold standard for detection of CNV from all causes. Long-term, ongoing management of patients with CNV most typically relies on OCT because it is rapid, inexpensive and noninvasive. Evidence of fluid on OCT imaging is considered a proxy for disease activity in eyes with Age-Related Macular Degeneration (ARMD), but its reliability is uncertain in MMD.
Methods: A retrospective study was conducted of 18 patients with CNV related to MMD. Clinical data collected include history, visual acuity, fundus examination, OCT and FA (on initial and some follow-up visits). MMD was defined as eyes that on examination exhibited posterior staphyloma, retinal pigment epithelial attenuation, obliquely inserted optic nerves, RPE atrophy, breaks in Bruch's membrane (lacquer cracks), and choroidal thinning on OCT. CNV was defined as progressive hyperfluorescence on FA.
Results: Average age at presentation was 60.7 years (range: 36 to 84). All patients had visual symptoms at presentation. In 12 of 18 patients, FA was able to detect CNV without OCT evidence of exudation. All eyes received anti-VEGF therapy (average 2.3 doses). Subsequent follow-up included 38 FA studies (in 15 patients) performed when symptoms recurred. Of those 38, 26 (68.4%) exhibited angiographic leakage, while only 12 (31.6%) had evidence of fluid on OCT.
Conclusions: Patients with myopic degeneration suspected of having active CNV (initially or on follow-up visits) should undergo FA if symptoms suggest recurrent disease. Management based on OCT evidence of disease activity may result in delay in diagnosis and/or treatment. OCT appears to have a lower sensitivity in detecting disease activity in eyes with MMD than in eyes with ARMD.
Commercial Relationships: Sarwar Zahid, None; **KaPo Yeung**, None; **Kevin Chen**, None; **Richard T. Atallah**, None; **Daniel Simhaee**, None; **Joseph Tseng**, None; **Kenneth Wald**, None

Program Number: 5903 **Poster Board Number:** A0074
Presentation Time: 12:00 PM–1:45 PM
The Choroid and Posterior Neural Retina in Posterior Microphthalmos: A Biometric and Optical Coherence Tomographic Analysis
Sawsan R. Nowilaty[1], Amani S. AlBakri[1], Ahmed Mousa[2], Nicola G. Ghazi[1]. [1]Vitreoretinal Division, King Khaled Eye Specialist Hospital, Riyadh, Saudi Arabia; [2]Department of Ophthalmology, College of Medicine, King Saud University, Riyadh 11411,, Saudi Arabia.
Purpose: To expand the phenotypic characterization of posterior microphthalmos (PM) by analyzing, using standard and enhanced depth imaging (EDI) spectral domain optical coherence tomography (SD-OCT), the retinal and choroidal thickness (RT, CT) and retinal and choroidal volume (RV, CV) as well as their spatial distribution across the macula in PM eyes, and how they correlate with biometric parameters of the globe.
Methods: Prospective comparative study of 15 PM eyes (8 patients) and 30 eyes of 15 age-matched controls. All eyes underwent refraction, axial length (AL) measurement, keratometry and macular SD-OCT in standard and EDI modes (radial and 19 horizontal raster scans). The 19 lines were manually segmented to measure the RT, CT, RV and CV in the 9 macular subfields of the ETDRS grid. The posterior pole curvature index (PPCI) was determined using the horizontal and vertical OCT scans. The RT, CT, RV and CV in PM eyes were compared to those of controls, the RT and CT distribution across the macula was evaluated in PM and controls, and the thickness and volume parameters were correlated with the refractive error, AL, keratometry and PPCI.
Results: The retina across the entire macula was significantly thicker in PM than in normal eyes ($p < 0.0001$). The mean RT in the central subfield was 429μm in PM eyes compared to 262μm in controls, and 350μm in the temporal outer field in PM eyes compared to 284μm in controls ($p < 0.0001$). The choroid throughout the macula was also substantially thicker in PM ($p < 0.0001$). The mean CT at the central subfield in PM was 481μm compared to 363μm in controls, and 504μm in the nasal inner subfield in PM compared to 343μm in controls ($p<0.0001$ for both). PM eyes had an abnormal distribution of the RT and CT across the macula with a characteristic shift of the maximum thickness of both layers to the nasal and inferior paracentral areas. Strong correlations exist between the central RV in PM and the AL, PMF height and corneal power ($r = 0.71$; $p=0.003$).
Conclusions: PM eyes have a significantly thicker retina and choroid throughout the macula, independent of the contribution of the PMF with a characteristic shift of the maximum thickness of these tissues to the nasal and inferior paracentral areas of the macula. In PM eyes, the retinal volume at the center of the macula correlates strongly with each of the inverse AL, PMF height and corneal curvature.
Commercial Relationships: Sawsan R. Nowilaty, None; **Amani S. AlBakri**, None; **Ahmed Mousa**, None; **Nicola G. Ghazi**, None

Program Number: 5904 **Poster Board Number:** A0075
Presentation Time: 12:00 PM–1:45 PM
Comparison Of Spectralis Fundus Autofluorescence Blue (486 nm) And Green Mode (518 nm) In A Consecutive Series Of Patients With Retinal Disorders
Simone Kellner[1, 2], Silke Weinitz[1, 2], Ghazaleh Farmand[1], Ulrich Kellner[1, 2]. [1]AugenZentrum Siegburg, MVZ ADTC Siegburg GmbH, Siegburg, Germany; [2]RetinaScience, Bonn, Germany.
Purpose: Lipofuscin-related fundus autofluorescence (FAF) can be elicited by different wavelengths. The most detailed experience is available using 488 nm laser light with the Spectralis HRA imaging system (Heidelberg Engineering, Germany). FAF elicited by longer wavelengths (> 500 nm) should be less affected by macular pigment blocking in the foveal area. The present study was performed to evaluate the difference in FAF elicited by either 486 or 518 nm provided by the novel Spectralis MultiColor system in patients with retinal disorders.
Methods: Between February 2013 and November 2014 a consecutive series of 657 patients with various retinal disorders were examined clinically and with 2 wavelength fundus autofluorescence (B-FAF, 486 nm; G-FAF, 518 nm; Spectralis MultiColor HRA & OCT, Heidelberg Engineering, Germany)). Imaging was performed in 30 or 50 degree mode. Further retinal imaging techniques (e.g. MultiColor reflectance imaging, near-infrared autofluorescence (NIA), spectral domain OCT (SD-OCT), fluorescein angiography (FAG) were performed with the same system when indicated.
Results: The series of patients included a variety of retinal disorders (e.g. age-related macular degeneration, inherited retinal dystrophies, toxic or autoimmune retinopathies). Regarding the peripheral and perifoveal FAF in 30 and 50 degree mode, no difference between B-FAF and G-FAF was noted. All lesions with either increased or decreased FAF intensity detected by B-FAF were also observed with G-FAF. In contrast, within the foveal area G-FAF was less affected by blockage from macular pigment with higher FAF intensity in normal eyes and in addition G-FAF revealed foveal lesions that were not detectable by B-FAF.
Conclusions: In comparison to B-FAF, G-FAF provides the opportunity to observe more details in the foveal area without missing other FAF imaging details. G-FAF therefore appears to be the more preferable wavelength for FAF imaging.
Commercial Relationships: Simone Kellner, None; **Silke Weinitz**, None; **Ghazaleh Farmand**, None; **Ulrich Kellner**, None

Program Number: 5905 **Poster Board Number:** A0076
Presentation Time: 12:00 PM–1:45 PM
Spectral-domain optical coherence tomography findings in Combined Hamartoma of the Retina and Retinal Pigment Epithelium in 5 consecutive patients
Julia Nemiroff[1], Tara A. McCannel[1], Colin A. McCannel[1], Irene Voo[2]. [1]Ophthalmology, UCLA Jules Stein Eye Institute, Los angeles, CA; [2]Ophthalmology, Retina Consultants of Nevada, Los Vegas, NV.
Purpose: To identify characteristics on Spectral-domain optical coherence tomography (SD-OCT) that contribute to the diagnosis of Combined Hamartoma of the Retina and retinal pigment epithelium (CHR-RPE).
Methods: Retrospective, observational cases series highlighting clinical and spectral domain OCT features of CHR-RPE. Patient demographics, visual acuity, clinical examination findings, ultrasonography and OCT features were reviewed.
Results: There were 5 consecutive patients who had a CHR-RPE which had been imaged with OCT. The mean age of presentation was 50.4 (Range 7-70). In all cases, the tumor was unilateral and unifocal. The presenting symptom was decreased vision in 2 cases and asymptomatic in 3 cases, with only 1 patient experiencing vision less than 20/30. The location of the tumor was in the optic nerve head in 2 cases, the superotemporal vascular arcade in 2 cases, and the macula in 1 case. SD-OCT revealed a posterior vitreous detachment present in 3/5 cases, an epiretinal membrane in 3/5 cases, and vitreoretinal traction in 4/5 cases. Retinal disorganization was seen in all cases, as well as marked loss of photoreceptor outer segments. 4/5 cases were associated with subretinal or intraretinal fluid. The basal diameter was measured at a mean of 4027.6 micrometers (Range 2461-6216). The height of the lesion was measured as a mean of 806.52 micrometers (Range 511-1127).
Conclusions: This report highlights the OCT characteristics of 5 cases of CHR-RPE. Our mean age of presentation was 50.4, older than previously reported, likely due to our practice's focus on adult ocular tumors. A prominent epiretinal membrane was associated with all cases that were associated with decreased vision. Our study revealed that retinal disorganization and loss of photoreceptor outer segments are prominent features on SD-OCT. Our findings demonstrate that SD-OCT is a helpful modality in the diagnosis of these tumors, particularly in atypical smaller tumors in a non-peripapillary location.

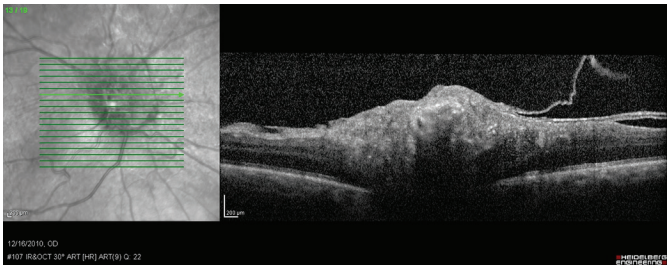

SD-OCT of Patient 1, a 57 year old male, demonstrating a prominant peripapiallary lesion with retinal disorganization and loss of photoreceptor outer segments, as well as an epiretinal membrane.

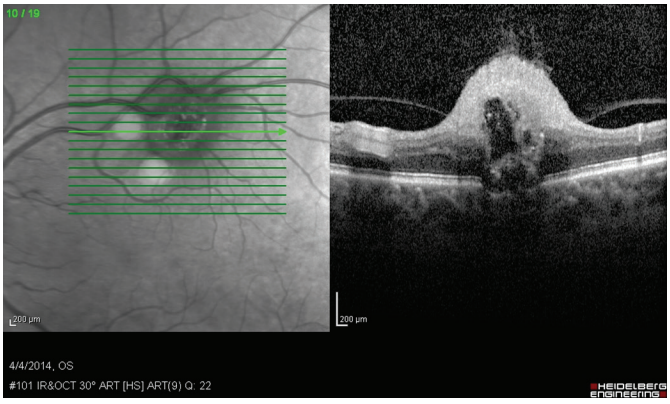

SD-OCT of Patient 5, a 56 year old female, demonstrating a promiant lesion in the superotemperal arcade with retinal disorganization and loss of photoreceptor outer segments.
Commercial Relationships: Julia Nemiroff, None; **Tara A. McCannel**, None; **Colin A. McCannel**, None; **Irene Voo**, None

Program Number: 5906 **Poster Board Number:** A0077
Presentation Time: 12:00 PM–1:45 PM
Restoration of foveal thickness and architecture after macula-off retinal detachment repair.
Roberto Dell'Omo[1], Mariaelena Filippelli[1, 2], Dario Giorgio[1], Roberto Di Iorio[1], Ermanno dell'Omo[1], Ciro Costagliola[1]. [1]Medicine and Health Sciences, University of Molise, Campobasso, Italy; [2]Second University of Naples, Napoli, Italy.

Purpose: To investigate the foveal changes after repair of macula-off rhegmatogenous retinal detachment (RRD).
Methods: Prospective comparative case series. Twenty-four eyes of 24 patients with macula-off/ fovea-on detachment (n= 9) and fovea-off detachment (n=15) were studied. Serial optical coherence tomography (OCT) images taken at the same location were recorded at month 1,3,6 and 12 after operation. Fellow eyes were used as controls.
Results: No significant changes of the central foveal thickness (CFT) were recorded in the fovea-on group over the follow-up. From month 1 to month 12, CFT increased significantly in the fovea-off group (P< 0.001). In this group, a significant increase of the Henle fiber and outer nuclear layer thickness(P=0.004), and of the ellipsoid zone (EZ)-retinal pigment epithelium (RPE) thickness (P < 0.001) was recorded. Significant restoration of the integrity of the external limiting membrane in the fovea-off group (P <0.001) and significant restoration of the EZ and cone interdigitation zone in the fovea-on group and the fovea-off group were observed (P <0.02 and P<0.001, and P<0.00 and P<0.001, respectively). Twelve months after operation the foveal bulge restored in 8 out of 15 eyes of the fovea-off group.
Conclusions: OCT scans taken serially at the same location show a progressive increase of foveal thickness and restoration of the integrity of outer retinal bands after repair of fovea-off RRD. The ELM-RPE thickness correlates with BCVA.
Commercial Relationships: Roberto Dell'Omo, None; **Mariaelena Filippelli**, None; **Dario Giorgio**, None; **Roberto Di Iorio**, None; **Ermanno dell'Omo**, None; **Ciro Costagliola**, None

Program Number: 5907 **Poster Board Number:** A0078
Presentation Time: 12:00 PM–1:45 PM
Clinical utility of retinal and choroidal OCT in the assessment of chronic kidney disease
James R. Cameron, Shyamanga Borooah, Craig Balmforth, Titia Ruijs, Tom MacGillivray, Baljean Dhillon, David Webb, Neeraj Dhaun. University of Edinburgh, Edinburgh, United Kingdom.
Purpose: Patients with chronic kidney disease (CKD) have a 10-30 fold increased risk of mortality due to cardiovascular disease (CVD). There is an established association between the vasculopathy affecting the kidney and the retina, suggesting common pathological mechanisms. Consequently, the examination of ocular vasculature and structure may be a valuable clinical aid in studying CVD risk and systemic microvascular damage, particularly in patients with CKD. The aim of this prospective, cross-sectional study was to examine the retina and choroid in patients with CKD, using Spectral-Domain Optical Coherence Tomography (SD-OCT), and correlate measurements with established biomarkers of CKD.
Methods: 24 patients with CKD, 24 patients with hypertension, and 25 age and sex matched healthy controls were recruited. Exclusion criteria included severe CKD requiring dialysis. All participants were imaged with SD-OCT (Heidelberg Spectralis). Measurements included retinal thickness, retinal nerve fibre layer (RNFL) thickness, macular volume and choroidal thickness. Blood and urinary measurements were also taken, including glomerular filtration rate (GFR), urinary protein and plasma Interleukin-6 (IL-6).
Results: Retinal thickness was reduced across the macula in CKD patients compared to both those with hypertension (p<0.01), and controls (p<0.05). RNFL thickness did not differ between groups. Macular volume was lower in CKD patients compared to both patients with hypertension (p<0.0001) and controls (p<0.001). Similarly, CKD was associated with a reduced choroidal thickness (across all three separate locations measured on the macula) compared to both patients with hypertension (p<0.001) and controls (p<0.01).
Interestingly, in those with CKD, a thinner choroid was associated with a lower GFR (p<0.01) and more severe proteinuria (p<0.01), both important independent CVD risk factors. A thinner choroid also correlated with higher plasma levels of IL-6 (r=-0.61, p<0.01), an inflammatory cytokine thought to be a marker of vascular inflammation.
Conclusions: The decreases in retinal and choroidal thickness seen in CKD may represent significant systemic microvascular injury. It remains unclear how these may change with therapy. Thus, OCT may offer potential utility in assessing microvascular damage in patients at high CVD risk as well as a potential biomarker of efficacy for therapies used to reduce this risk.
Commercial Relationships: James R. Cameron, None; **Shyamanga Borooah**, None; **Craig Balmforth**, None; **Titia Ruijs**, None; **Tom MacGillivray**, None; **Baljean Dhillon**, None; **David Webb**, None; **Neeraj Dhaun**, None

Program Number: 5908 **Poster Board Number:** A0079
Presentation Time: 12:00 PM–1:45 PM
Functional Optical Coherence Tomography of Transient Intrinsic Optical Signal Changes in Retinal Rod and Cone Photoreceptors
Xincheng Yao[1, 2], Qiuxiang Zhang[3], Benquan Wang[1]. [1]Department of Bioengineering, University of Illinois at Chicago, Chicago, IL; [2]Department of Ophthalmology and Vision Sciences, University of Illinois at Chicago, Chicago, IL; [3]National Institute on Deafness and Other Communication Disorders, Bethesda, MD.
Purpose: This study is to characterize intrinsic optical signals (IOSs) in retinal photoreceptors, and to test the potential of optical coherence tomography (OCT) mapping of rod and cone functions.
Methods: A custom-designed OCT was employed to achieve high spatiotemporal resolution imaging. An adaptive data processing algorithm was developed to achieve a high signal-to-noise ratio (SNR) in single-pass IOS recordings. Grass frog (*Rana pipiens*), which has rod and cone photoreceptors stratified into different axial depths, was selected for quantitative evaluation of rod and cone responses. Both short (10 ms) and prolonged (500 ms) visible light flashes were employed to evoke fast IOSs in the retina. Variable background light controls were conducted to test IOS difference in rod and cone photoreceptors.
Results: High spatiotemporal resolution OCT revealed robust IOSs, without an averaging requirement for multiple trials. Transient IOSs, which might reflect an early stage of light phototransduction, were consistently observed almost immediately (<4 ms) after retinal stimulation. Combined OCT-IOS (structural-functional) images allowed precise identification of anatomic sources of the IOSs. With visible short (10 ms) flash stimulation, fast IOSs were predominantly observed in the outer retina, particularly in the photoreceptor outer segments (OSs). However, prolonged (500 ms) stimulation evoked additional IOSs in the inner retina, with a delayed time course (1.5–2 s). In the dark condition, transient IOSs were observed in both cone and rod OSs. In contrast, under the light condition, the IOS distribution was significantly shifted to the cone OS area.
Conclusions: In coordination with adaptive data processing, functional OCT enabled robust IOS detection in single-pass measurements. The OS was identified as the primary IOS source in retinal photoreceptors. Comparative study of dark- and light-adapted retinas demonstrated the potential of functional OCT-IOS mapping of rod and cone photoreceptors, which promises a new method for improved detection and treatment evaluation of age-related macular degeneration (AMD) and other eye diseases that can cause photoreceptor damage.

Commercial Relationships: Xincheng Yao, None; **Qiuxiang Zhang**, None; **Benquan Wang**, None
Support: NIH R01 EY023522, NIH R01 EY024628, NIH P30 EY001792 and NSF CBET-1055889.

Program Number: 5909 **Poster Board Number:** A0080
Presentation Time: 12:00 PM–1:45 PM
Clinical experience with the first commercially available intraoperative optical coherence tomography system (iOCT)
Matthias D. Becker[1, 2], Maximilian Pfau[1], Stephan Michels[1].
[1]Ophthalmology, Triemli Hospital, Zürich, Switzerland; [2]Ophthalmology, University of Heidelberg, Heidelberg, Germany.
Purpose: A retrospective, single-center, case-series was initiated to evaluate the first clinical experience with the first commercially available intraoperative optical coherence tomography system (iOCT) for the enhancement of ophthalmic surgery.
Methods: The Rescan 700 system (Zeiss, Oberkochen, Germany), a spectral-domain OCT system integrated into a Lumera 700 surgical-microscope (Zeiss, Oberkochen, Germany), was used in 40 consecutive cases. A standardized review was used to assess whether the iOCT-imaging resulted in additional information or/and altered decision-making. Additionally, the preoperative diagnosis, surgical procedures and total iOCT-imaging time were documented to analyze potentially increased surgery time.
Results: For anterior and posterior segment surgical procedures, iOCT-imaging was found to be beneficial.
The surgeons in this study reported that iOCT-imaging provided additional information in 74.1% of the posterior and combined surgical cases (n=31), which resulted in 41.9% of the cases in altered decision-making. The iOCT imaging time amounted on average to 167 seconds (SD =77 seconds). In addition, it showed to be usable in conjunction with common chromovitrectomy-dyes and different tamponades. Furthermore, iOCT-imaging allowed evaluation of iatrogenic effects during surgery and subsequent minimization.
In anterior procedures (n=9), the surgeons reported gain of additional information in 22.2% of all cases and no case of altered decision-making. In these procedures, the iOCT imaging time amounted on average to 117 seconds. Among others, the following aspects were evaluated: corneal incisions with regard to size, positioning and extension; anterior capsular rhexis; hydrodisection with imaging of the posterior capsule; phacoemulsification and incision closure by hydration.
Novel intraoperative-alterations of the macula, peripheral retina and sclera, which can only be seen on iOCT, were discovered, described and evaluated.
Conclusions: The Rescan 700 system fits into the surgical process and allows intraoperative life-scanning to evaluate different ocular structures for surgical decision making. The here shown results suggest that iOCT has the potential to improve the quality of posterior and anterior segment surgery.
Commercial Relationships: Matthias D. Becker, Alcon (F), Allergan (F), Bayer (F), Novartis (F), Santen (F); **Maximilian Pfau**, None; **Stephan Michels**, Alimera (C), Allergan (C), Bayer (C), Clanotech (C), Esbatech (C), Novartis (C), Roche (C), Sucampo (C)
Clinical Trial: pending

Program Number: 5910 **Poster Board Number:** A0081
Presentation Time: 12:00 PM–1:45 PM
Evidence of Macular Pigment in the Central Macula in Albinism
Yulia Wolfson[1], Emily Fletcher[3], Rupert W. Strauss[1, 2], Hendrik P. Scholl[1]. [1]Ophthalmology, Johns Hopkins University, Baltimore, MD; [2]Ophthalmology, Medical University Graz, Graz, Austria; [3]Ophthalmology, Gloucestershire NHS Trust, Gloucester, United Kingdom.
Purpose: Albinism represents a spectrum of disorders with diminished to absent amounts of melanin pigmentation including the posterior segment of the eye. The role of melanin in visual development is not completely understood, but a correlation was found between the amount of fundus pigmentation and visual function in albinos.
Macular pigment (MP) consists of two main carotenoids, lutein and zeaxanthin, concentrated in the macula. MP serves as blue light absorbent, antioxidant, and is believed to reduce chromatic aberration and glare.
It remains unclear if albinos have detectable MP. An increase of MP deposition in the macula may allow improving visual performance by reducing light scatter and glare. Our purpose was to investigate the distribution of MP in albino patients with psychophysical and imaging techniques.
Methods: 4 albino patients were enrolled in the study and multimodal ophthalmic imaging was performed. Macular pigment was measured either by heterochromatic flicker perimetry (QuantifEye; MPS 9000 series: Tinsley Precision Instruments Ltd., Croydon, Essex, UK) or by scanning laser ophthalmoscopy (MPOD module, MultiColor Spectralis®, Heidelberg Engineering). The study followed the tenets of the Declaration of Helsinki and was approved by the local Ethics Review Board. Informed written consent was obtained from each patient.
Results: 3 patients had genetically confirmed oculo-cutaneous albinism. Visual acuity ranged from 20/32 to 20/125, significant nystagmus was present in 2 patients, and all 4 patients showed typical foveal hypoplasia on fundus exam and optical coherence tomography. Fundus autofluorescence (FAF) demonstrated various degrees of central FAF signal attenuation (Fig. 1). Measurable amounts of MP were detected in all 4 patients and ranged from 0.05 to 0.24.
Conclusions: MP can be demonstrated and measured in albinos. Further studies are needed to investigate MP accumulation following supplementation and its consequences for visual performance in albino patients. This is currently being investigated in The Effects of Lutein and Zeaxanthin Supplementation on Vision in Patients with Albinism (LUVIA) Study (ClinicalTrials.gov Identifier: NCT02200263).

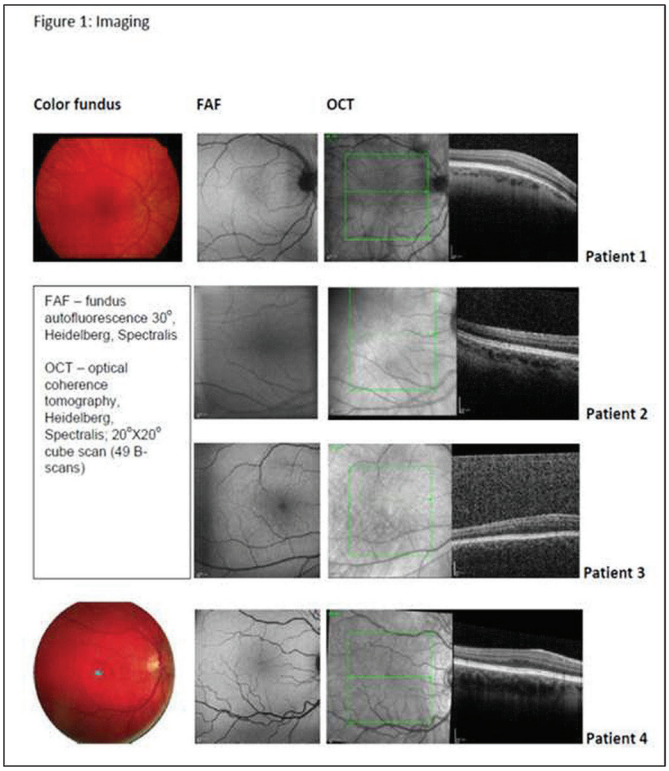

Commercial Relationships: Yulia Wolfson, None; **Emily Fletcher**, Bayer (C); **Rupert W. Strauss**, None; **Hendrik P. Scholl**, QLT Inc. (C), QLT Inc. (F), Sanofi-Fovea Pharmaceuticals (C), Vision Medicines, Inc (C)

Support: Dr. Hendrik Scholl is supported by the Foundation Fighting Blindness Clinical Research Institute (FFB CRI) and a grant to FFB CRI by the U.S. Department of Defense USAMRMC TATRC, Fort Meade, Maryland (grant numbers W81-XWH-07-1-0720 and W81XWH-09-2-0189); The Shulsky Foundation, New York, NY; Ocular Albinism Research Fund (Clark Enterprises Inc.); Unrestricted grant to the Wilmer Eye Institute from Research to Prevent Blindness; Baylor-Johns Hopkins Center for Mendelian Genetics (National Human Genome Research Institute, NHGRI/NIH; Identification number: 1U54HG006542-01). H.P.N.S. is the Dr. Frieda Derdeyn Bambas Professor of Ophthalmology

Program Number: 5911 **Poster Board Number:** A0082
Presentation Time: 12:00 PM–1:45 PM

Polarization uniformity imaging of macular disease using jones-matrix optical coherence tomography

Aaron C. Chan[1, 3], Shuichi Makita[1, 3], Young-Joo Hong[1, 3], Masahiro Miura[2, 3], Yoshiaki Yasuno[1, 3]. [1]Computational Optics Group, University of Tsukuba, Tsukuba, Japan; [2]Department of Ophthalmology, Ibaraki Medical Center, Tokyo Medical University, Ami, Japan; [3]Computational Optics and Ophthalmology Group, University of Tsukuba, Tsukuba, Japan.

Purpose: Imaging retinal pigment epithelium (RPE) abnormalities can help in macular degeneration diagnosis. The use of Jones-matrix optical coherence tomography (JM-OCT) to create 3D maps of pigmented tissue can highlight RPE abnormalities and complement the existing methods of fluorescein angiography (FA) and fundus auto-fluorescence (FAF). Here clinical case studies are used to compare JM-OCT observations of macular disease with FA and FAF images.

Methods: Eight eyes of eight patients with macular disease were examined, with conditions ranging from choroidal neovascularization (CNV, 3 cases), angioid streaks (1 case), polypoidal choroidal vasculopathy (PCV, 2 cases), geographic atrophy (GA, 1 case) and wet age-related macular degeneration (AMD, 1 case). Pathologic regions were scanned with 512 A-lines × 256 B-scans × 4 frames using a 1μm wavelength JM-OCT at 100,000 A-scans/s. A newly developed pigmented tissue imaging method called modified degree of polarization uniformity (M-DOPU) was applied to the JM-OCT images. M-DOPU has high noise immunity, thereby providing robust and quantitative imaging. As its imaging contrast originates from the randomization of the polarization state of backscattered light, it mainly contrasts the melanin of the posterior part of the eye. Three-dimensional mapping of pigmented tissues and en-face images of the distribution of melanin were visualized. En-face M-DOPU images were compared with FA and FAF images, and details were investigated in the cross-sectional M-DOPU images.

Results: Figure 1 shows an example of PCV in the left eye of a 58 year old man. The (b) FA shows a region of hyper- fluorescence. The corresponding location in (a) FAF shows hypo-autofluorescence. The (c) en-face M-DOPU image indicates a region with high M-DOPU (arrows), suggesting RPE damage (or pigmentation reduction). By examining the B-scan at the corresponding location in Fig. 2(b), the region of the RPE shows a high M-DOPU value (circle). Similar features of high M-DOPU at FA hyper-fluorescence were seen in four other subjects (2 PCV, 1 CNV and 1 GA).

Conclusions: As M-DOPU provides selective contrast related to the depigmentation of the posterior part of the eye, it may be a useful complement to AF and FAF in identifying abnormalities in the RPE.

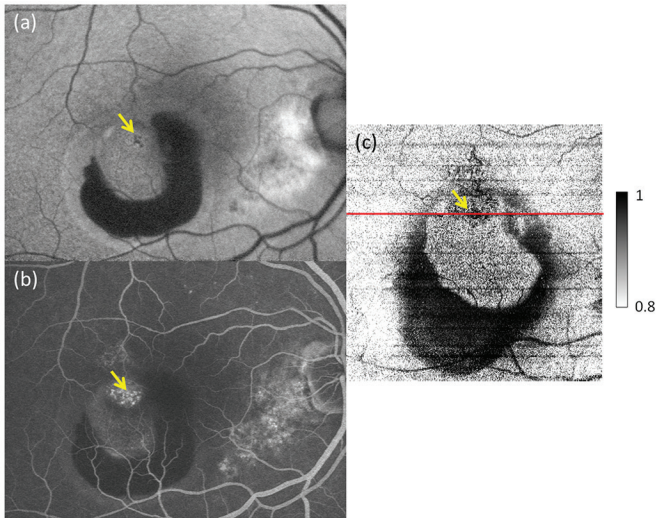

Fig. 1: Eye with PCV (a) FAF (b) FA (c) DOPU-OCT en-face.

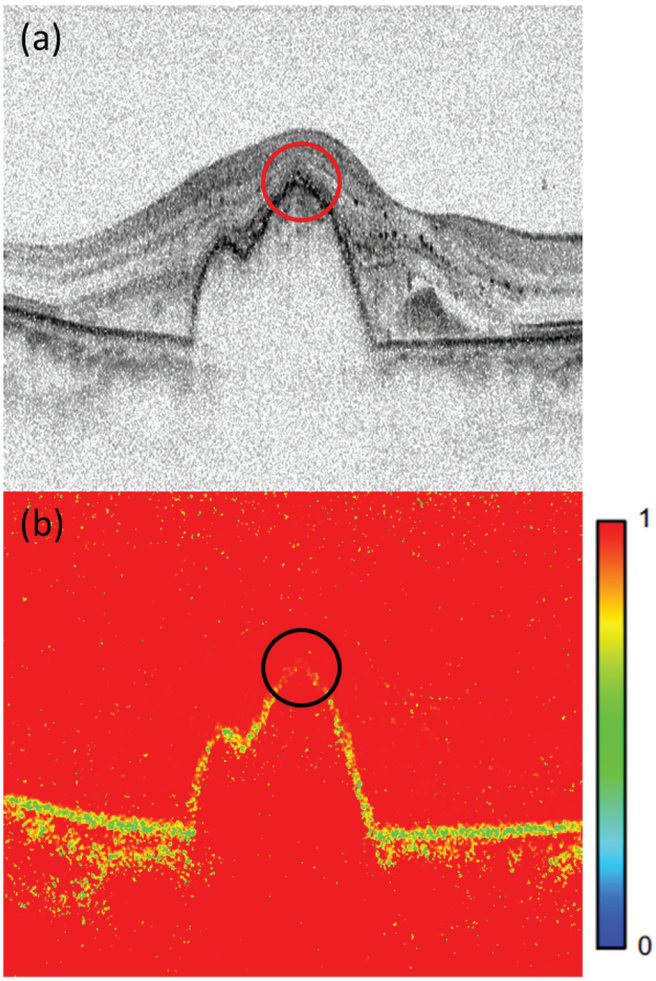

Fig. 2: B-scans (a) OCT (b) M-DOPU.

Commercial Relationships: Aaron C. Chan, Tomey (F), Topcon (F); **Shuichi Makita**, Tomey (F), Tomey (P), Topcon (F); **Young-Joo Hong**, Tomey (F), Topcon (F); **Masahiro Miura**, Novartis (R); **Yoshiaki Yasuno**, Tomey (F), Tomey (P), Topcon (F)

Program Number: 5912 **Poster Board Number:** A0083
Presentation Time: 12:00 PM–1:45 PM

Comparing the effectiveness of single posterior pole retinal images against binocular indirect ophthalmoscopic exam in detecting retinal hemorrhages in pediatric cerebral malaria

Sheila C. Nemeth[1], Ian J. MacCormack[2, 3], Simon P. Harding[2], Susan Lewallen[4], Terrie E. Taylor[5, 6], Peter Soliz[1], Vinayak S. Joshi[1].
[1]VisionQuest Biomedical LLC, Albuquerque, NM; [2]Eye and Vision Science, institute of Ageing and Chronic Disease, University of Liverpool, Liverpool, United Kingdom; [3]Malawi-Liverpool-Wellcome Trust Clinical Research Programme, Blantyre, Malawi; [4]Kilimanjaro Centre for Community Ophthalmology, University Cape Town Groot Schuur Hospital, Cape Town, South Africa; [5]Osteopathic Medical Specialties, Michigan State University, East Lansing, MI; [6]Blantyre Malaria Project, Blantyre, MI.

Purpose: Detecting malarial retinopathy (MR) is important for accurate case classification and clinical diagnosis of cerebral malaria (CM). The use of portable retinal cameras has potential for MR detection in low-resource clinical environments. However, they may have limitations in their field of view (FOV). We investigated the ability of single FOV retinal images to detect one of the characteristic lesions of MR, retinal hemorrhages.

Methods: We analyzed images the posterior pole from 42 consecutive pediatric admissions with suspected CM (Research Ward, Blantyre, Malawi, 2014). Images were acquired with a Topcon 50-EX fundus camera, and were graded for the presence/absence of retinal hemorrhages in the macula, defined as a circle centered on the center of the fovea with a radius of 3.8mm, or, 2.5 ETDRS disc diameters. The clinical binocular indirect ophthalmoscopy examination (BIO) of the entire retina was then compared to these findings. Specificity and sensitivity of the detection of hemorrhages were calculated in relation to the BIO findings.

Results: The manual grading of a posterior pole image for presence/absence of hemorrhages against BIO as the reference standard achieved the following performance metrics: sensitivity = 0.68 (95% CI, 0.48-0.83); specificity = 1.0 (95% CI, 0.73-1); Positive predictive value = 1.0 (95% CI, 0.79-1); Negative predictive value = 0.61 (95% CI, 0.39-0.80).

Conclusions: Single field posterior pole photography has only moderate sensitivity at 68% for the detection of hemorrhages associated with MR. As expected, single field posterior pole imaging is highly specific in determining the absence of hemorrhages characteristic of CM. Our preliminary findings suggest that peripheral detection of the retina using portable cameras for MR detection will need to be included to add the ability to detect hemorrhages outside the posterior pole. Including other signs of CM (such as retinal whitening) may also increase the sensitivity.

Commercial Relationships: Sheila C. Nemeth, VisionQuest Biomedical LLC (E); **Ian J. MacCormack**, VisionQuest Biomedical LLC (C); **Simon P. Harding**, VisionQuest Biomedical LLC (C); **Susan Lewallen**, VisionQuest Biomedical LLC (C); **Terrie E. Taylor**, None; **Peter Soliz**, VisionQuest Biomedical LLC (I); **Vinayak S. Joshi**, VisionQuest Biomedical LLC (E)
Support: NIH Grant 1R43AI112164-01

Program Number: 5913 **Poster Board Number:** A0084
Presentation Time: 12:00 PM–1:45 PM

Gaze-Induced Axial Length Changes in Emmetropic Eyes as Gauged by Magnetic Resonance Imaging

Alexander Vu[1, 2], Amanda Chi[1, 2], Jennifer Nguyen[3], Quan V. Hoang[1].
[1]Ophthalmology, Harkness Eye Institute, Columbia Univ, New York, NY; [2]Institute of Human Nutrition, Columbia University, New York, KS; [3]St. Thomas Aquinas, Overland Park, KS.

Purpose: Our group previously reported that in highly myopic eyes with staphyloma, a reversible, instantaneous axial length elongation occurs in downgaze. Here we determine if axial length changes occur in emmetropic eyes undergoing the stress and strain of normal eye movement.

Methods: A prospective imaging study was performed on 12 eyes of 6 emmetropic patients (with uncorrected visual acuity of 20/20 or better). 3-D MRI scans were acquired while subjects gazed in 5 directions (primary, nasal, temporal, superior and inferior). Volume renderings were manually reoriented so that the plane of the limbus (the cornea-sclera interface) was normal to the plane of the screen. Four axial length measurements were taken at 90 degree rotations around the central axis and averaged for each eye in every gaze. Eye axial lengths at each eccentric gaze were compared to the axial length in primary gaze using a fixed effects regression allowing for person-specific and eye-specific effects.

Results: The mean change in axial length was near-zero and not statistically significant when comparing the primary gaze to the nasal gaze ($p = 0.619$), temporal gaze ($p = 0.406$) or up gaze ($p = 0.340$).

Axial lengths lengthened when changing from primary gaze to downgaze by +0.117 mm (p = 0.001, 95% CI 0.051 to 0.183).
Conclusions: A reversible, instantaneous axial length elongation appears to occur in downgaze, not only in highly myopic patients with staphyloma, but also in emmetropic patients without staphyloma. This is of interest given past clinical studies suggesting an association between excessive near work and myopia development and progression.
Commercial Relationships: Alexander Vu, None; **Amanda Chi**, None; **Jennifer Nguyen**, None; **Quan V. Hoang**, None
Support: This work was supported in part by Career Development Awards from Research to Prevent Blindness (QVH), K08 Grant (QVH, 1 K08 EY023595, National Eye Institute, NIH) the Louis V. Gerstner Jr. Scholars Program (QVH), AR Peacock Trust (QVH) and JR Peacock Trust (QVH).

Program Number: 5914 **Poster Board Number:** A0085
Presentation Time: 12:00 PM–1:45 PM
Ultra-wide Field Angiography for Diabetic Retinopathy
Jordan Burnham, Ching J. Chen. University of Mississippi Medical Center, Jackson, MS.
Purpose: To investigate the effectiveness of ultra-wide field angiography in evaluating diabetic retinopathy versus traditional 7 field angiography
Methods: CPT codes were used to generate a report of all Diabetic patients who had received a fluoroscein angiogram with the Optos (Optos plc) ultra-wide field imaging system since January 2014. Images from the Optos image database were then collected and those that were of poor quality were excluded. The remainder of the images were evaluated for single frames that provided the highest diagnostic yield and these single frames were printed on standard photo paper. A stencil cut-out was then made to "crop" the ultra-wide field image and show only the areas that are included in the standard 7 field (ETDRS) collage. A diagnosis was made by a single Vitreoretinal surgeon using this 7 field collage stencil and then again with the stencil removed. Thus 7 field collage was directly compared to ultra-wide imaging for the same fluoroscein angiogram image. Images were then classified into four categories: Level 0 images had no difference in information, diagnosis, or treatment basis between ultra-wide and 7 field. Level 1 images revealed additional information with the ultra-wide image, but no change in diagnosis or treatment. Level 2 images revealed additional information that altered the diagnosis but did not change the treatment plan. Level 3 images revealed information that changed both the diagnosis and the treatment plan.
Results: This study evaluated 366 photos, 21 (5.7%) level 0, 294 (80.3%) level 1, 36 (9.8%) level 2, and 25 (6.8%) level 3. Thus, there were only 5.7% of the images in which the Optos did not provide any additional information compared to the 7 field collage while 94.3% at least revealed additional information and in some cases even affected the diagnosis and treatment decisions.
Conclusions: Ultra-wide field angiography has a clear benefit when monitoring diabetic retinopathy and should be the standard of care. Ultra-wide field angiography provides valuable information of the retinal periphery that is not seen in standard 7 field imaging and can change the diagnosis and treatment plans of patients.
Commercial Relationships: Jordan Burnham, None; **Ching J. Chen**, None

Program Number: 5915 **Poster Board Number:** A0086
Presentation Time: 12:00 PM–1:45 PM
Predictive power of retinal layer responses to intravitreal ranibizumab treatment for diabetic macular edema
Andreas Ebneter, Abhishek Jain, Sebastian Wolf, Martin S. Zinkernagel. Department of Ophthalmology, University of Bern, Bern, Switzerland.
Purpose: Indicators forecasting benefit from intravitreal anti vascular endothelial growth factor treatment for diabetic macular edema are lacking. We described the thickness change of individual retinal layers in eyes treated with ranibizumab as per RESOLVE protocol, and investigated the predictive value of individual layer responses on the 1-year (1y) visual acuity outcome.
Methods: Retrospective interventional case series including 33 eyes of 33 patients. Retinal layers were segmented on high-resolution optical coherence tomography scans (Heidelberg Spectralis®) at baseline and 1y using automated software (Heidelberg Eye Explorer) with manual correction if needed. Layer thickness changes and other parameters were analyzed using correlation matrices. A model predicting final visual acuity was built using multiple linear regression.
Results: The only significant layer thickness change was observed in the inner ring for the inner plexiform layer (Image 1). The correlation matrices showed a similar pattern for inner and outer ring of the standard ETDRS grid (Image 2). Thickness changes in the outer plexiform, the outer and the inner nuclear layers were significant factors in the multiple linear regression model predicting 1y visual acuity.
Conclusions: A differential response of individual retinal layers was observed in diabetic macular edema treated with ranibizumab. Analysis of individual layer responses to initial treatment might be useful to predict treatment benefit. Further prospective studies are needed to determine suitable time points for imaging.

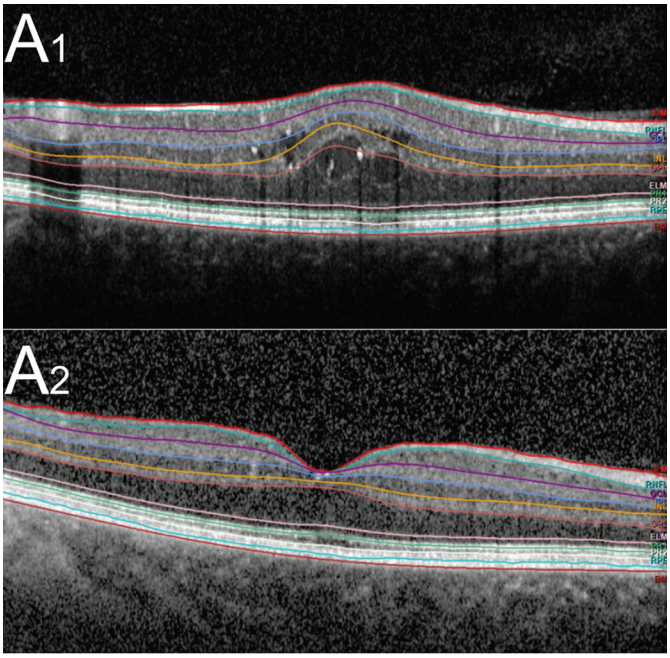

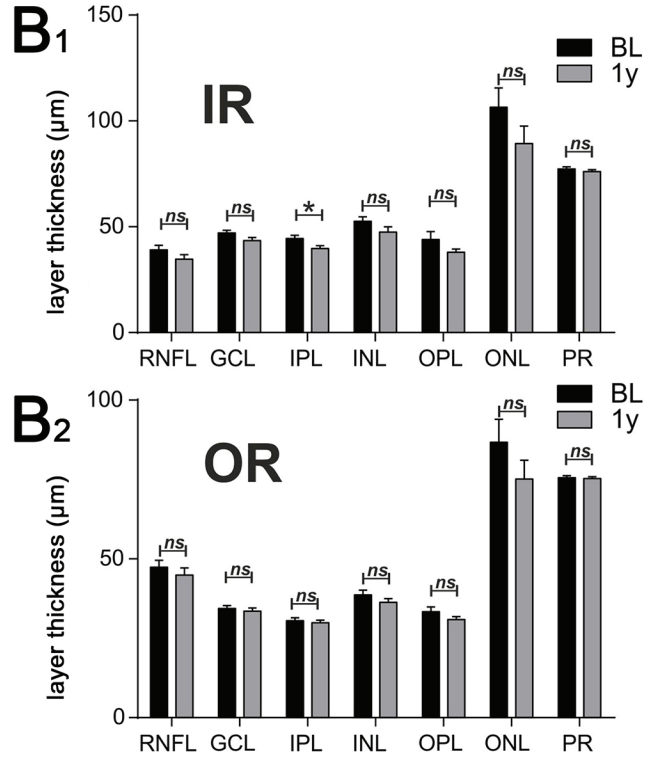

Representative image at **A_1)** baseline (BL) and **A_2)** 1 year after treatment initiation (1y). Individual layer thickness for the **B_1)** inner ring (IR) and **B_2)** outer ring (OR) of the standard ETDRS grid. [*< 0.05; *t*-test]

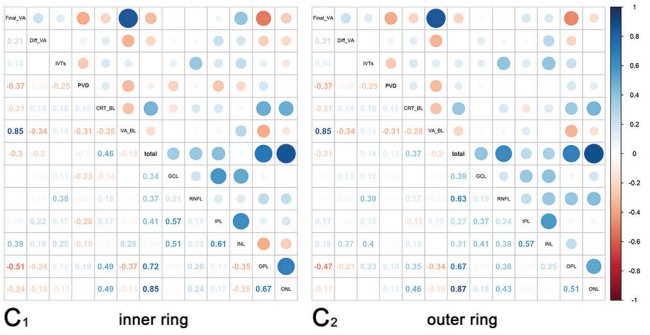

Correlation matrix for **C_1)** inner ring and **C_2)** outer ring of standard ETDRS grid: Best-corrected visual acuity at 1y (Final_VA), BL (VA_BL) and difference from BL (Diff_VA), number of IVT injections (IVTs), presence of posterior vitreous detachment (PVD), central retina thickness at BL (CRT_BL), decrease of thickness from BL for whole retina (total), ganglion cell layer (GCL), retinal nerve fiber layer (RNFL), inner plexiform layer (IPL), inner nuclear layer (INL), outer plexiform layer (OPL), outer nuclear layer (ONL).

Commercial Relationships: Andreas Ebneter, Bayer (R); **Abhishek Jain**, None; **Sebastian Wolf**, Bayer (C), Heidelberg Engineering (C), Heidelberg Engineering (F), Novartis (C), Optos Plc (C), Optos Plc (F), Zeiss (C); **Martin S. Zinkernagel**, Bayer (C), Heidelberg Engineering (F), Novartis (C)
Support: Project Grant, OPOS Foundation, 9014 St. Gallen, Switzerland

Program Number: 5916 **Poster Board Number:** A0087
Presentation Time: 12:00 PM–1:45 PM

Reproducibility and reliability of intraretinal layer thickness measurements in mice using optical coherence tomography

Andrés Cruz-Herranz[1], Philipp Albrecht[2], Hao Yiu[1], Lisanne Balk[3], Ari Green[1]. [1]Neurology, University of California San Francisco, San Francisco, CA; [2]Heinrich-Heine University, Düsseldorf, Germany; [3]VU University Medical Center, Amsterdam, Netherlands.

Purpose: Spectral domain optical coherence tomography (OCT) allows *in vivo* measurements retinal layers. However, the utilization of OCT for tracking retinal degeneration in mice has been challenged because of the absence of data regarding test-retest reliability for the parameters measured. As opposed to histology, OCT offers the opportunity to perform longitudinal measures. We aimed to identify the most suitable scan protocols for the quantitative analysis of the retinal layers in cross-sectional and longitudinal studies in mice.
Methods: Retinal images from 10 C57BL/6 mice were obtained using spectral domain (SD)–OCT (Heidelberg Spectralis). We performed raster based volume, peripapillary ring, and horizontal and vertical line scans with semi-automated segmentation of retinal layers to analyze the retest reliability of consecutive measurements. Independent investigators performed semi-automated segmentation to assess inter-rater reliability.
Results: We obtained the best reproducibility with retinal layer thickness measurements from consecutive volume scans (interclass correlation coefficient (ICC), 95% confidence interval (CI), total retinal thickness: 0.96, 0.83-0.99; retinal nerve fiber layer: 0.81, 0.04-0.96; ganglion cell layer plus inner plexiform layer: 0.94, 0.75-0.99; inner nuclear layer: 0.81, 0.16-0.96; outer plexiform layer: 0.61, -0.33-0.91; outer nuclear layer: 0.96, 0.83-0.99; photoreceptor layer: 0.93, 0.64-0.99). Peripapillary ring scans showed the poorest reliability and reproducibility. The inner retinal layers showed more inter-rater reliability (0.995, 0.989-0.998) and reproducibility (0.94, 0.73-0.99) than the outer retinal layers.

Conclusions: Our data suggest that among the different scan protocols, volume scans are most suitable to assess the thickness of the different retinal layers. The measurement of inner retinal layers thickness showed better reliability and reproducibility than the deeper retinal layers. These data indicate that OCT reliability is dependent on the scan protocols selected and that particular scan protocols in mice show promise for monitoring longitudinally.

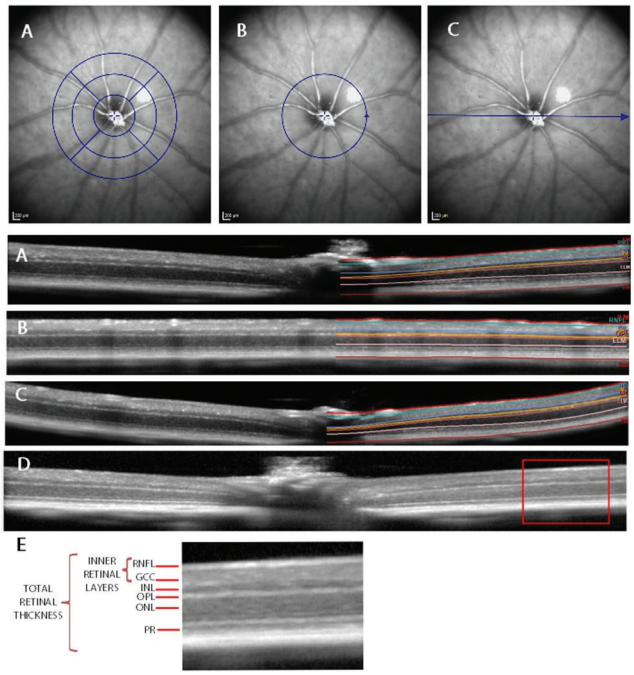

Figure 1: Segmentation of OCT Scans
Examples of volume (A) and peripapillary ring scans (B) as well as horizontal and vertical line scans (C). On the right side of the scans the results of the semi-automated segmentation of the layers is depicted, E shows a close-up of D, the different layers are labelled on the side.

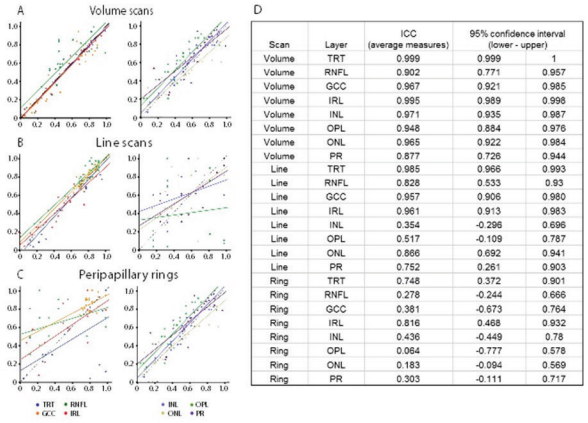

D

Scan	Layer	ICC (average measures)	95% confidence interval (lower - upper)	
Volume	TRT	0.999	0.999	1
Volume	RNFL	0.902	0.771	0.957
Volume	GCC	0.967	0.921	0.985
Volume	IRL	0.995	0.989	0.998
Volume	INL	0.971	0.935	0.987
Volume	OPL	0.948	0.884	0.976
Volume	ONL	0.965	0.922	0.984
Volume	PR	0.877	0.726	0.944
Line	TRT	0.985	0.966	0.993
Line	RNFL	0.828	0.533	0.93
Line	GCC	0.957	0.906	0.980
Line	IRL	0.961	0.913	0.983
Line	INL	0.354	-0.296	0.696
Line	OPL	0.517	-0.109	0.787
Line	ONL	0.866	0.692	0.941
Line	PR	0.752	0.261	0.903
Ring	TRT	0.748	0.372	0.901
Ring	RNFL	0.278	-0.244	0.666
Ring	GCC	0.381	-0.673	0.764
Ring	IRL	0.816	0.468	0.932
Ring	INL	0.436	-0.449	0.78
Ring	OPL	0.064	-0.777	0.578
Ring	ONL	0.183	-0.094	0.569
Ring	PR	0.303	-0.111	0.717

Figure 2: Interreater reliability
The different OCT scans were consecutively segmented by two independent raters and the results plotted along with a linear regression line. Each point represents a single eye of a mouse the dotted line the reference for 100% agreement between both raters.

Commercial Relationships: Andrés Cruz-Herranz, None; **Philipp Albrecht**, None; **Hao Yiu**, None; **Lisanne Balk**, None; **Ari Green**, None

Program Number: 5917 **Poster Board Number:** A0088
Presentation Time: 12:00 PM–1:45 PM
Disease Modelling & Prediction: Automated Fovea Detection as a Key Registration Landmark for Construction of a Population Reference Frame

Jing Wu[1], Sebastian M. Waldstein[1], Bianca S. Gerendas[1], Roland Leitner[1], Sinziana Birta[1], Georg Langs[2], Christian Simader[1], Ursula Schmidt-Erfurth[1]. [1]Christian Doppler Laboratory for Ophthalmic Image Analysis, Vienna Reading Center, Department of Ophthalmology, Medical University of Vienna, Vienna, Austria; [2]Christian Doppler Laboratory for Ophthalmic Image Analysis, Computational Imaging Research Lab, Department of Biomedical Imaging and Image-guided Therapy, Medical University of Vienna, Vienna, Austria.

Purpose: To automatically compute the foveal position in multi-vendor retinal spectral domain optical coherence tomography (SD-OCT) scans of patients with exudative macular disease (neovascular age-related macular degeneration (nAMD), diabetic macular edema and retinal vein occlusion (RVO)), used as key landmarks in the construction of a population reference frame for cross-patient spatio-temporal and group-wise disease modelling and prediction.
Methods: Initially, preprocessing is performed on each OCT scan: *Z* dimension motion correction, denoising by block matching

collaborative filtering, and graph cut segmentation to delineate the internal limiting membrane (ILM) and cysts.
First, the fovea type is distinguished. Combining the segmented contiguous ILM segments generates a 3D model of the probable fovea region (Fig 1.), from which 3 distinct fovea types are examined: 1) normal foveal depression (NFD), seen as a prominent depression spanning several contiguous B-scans (Fig 1.a); 2) minor foveal depression (MFD) which features a smaller depression elevated by asymmetric retinal edema and the presence of cysts (Fig 1.b); 3) absent foveal depression type (AFD) where no depression is seen due to retinal edema by cysts (Fig 1.c).
Fovea position computation for NFD (Fig 2.a) identifies the centroid of all zero thickness positions between the ILM and RNFL surfaces in the masked region. For MFD & AFD (Fig 2.b,c), pairwise distance comparison between the ILM and cyst boundary point sets is performed. From the resulting closest spatial co-ordinate pair, the position x_{fovea} in the B-scan plane is taken as x_{ILM}, y_{fovea} is the current B-scan and z_{fovea} is the corresponding position on the ILM surface z_{ILM}.
Results: Results from three disease groups each with 100 SD-OCT scans present mean (±SD) absolute distances between automated fovea detection results and manual annotated fovea for nAMD, branch RVO and central RVO to be 176.5±156.8 μm, 159.5±127.0 μm, and 165.0±143.8 μm respectively.
Conclusions: The presented method automatically and accurately computes the fovea position, the key landmark for creating a population reference frame, in diseased scans from "big data". Thus this allows patient scans from different time points, vendors and modalities to be analysed in a common reference frame facilitating further advanced clinical analysis, disease modelling and prediction.

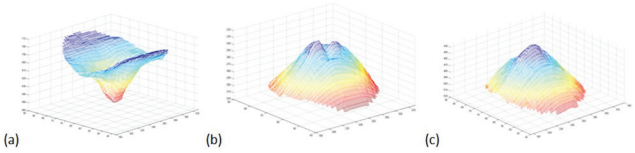

Figure 1. Fovea type examples (a) NFD, (b) MFD, and (c) AFD.

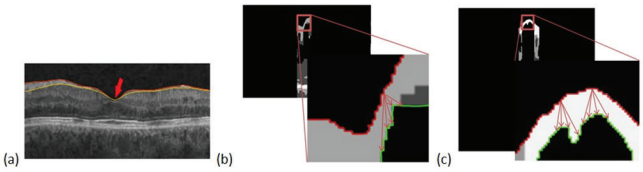

Figure 2. Exemplar fovea point computation for (a) NFD where ILM and retinal nerve fibre layer (RNFL) surfaces are the red and yellow lines respectively. In (b) MFD and (c) AFD, the red and green boundaries depict the masked region ILM and cyst boundaries respectively with the red arrows depicting the pairwise distance computation.

Commercial Relationships: Jing Wu, None; **Sebastian M. Waldstein**, None; **Bianca S. Gerendas**, None; **Roland Leitner**, None; **Sinziana Birta**, None; **Georg Langs**, None; **Christian Simader**, None; **Ursula Schmidt-Erfurth**, Alcon (C), Bayer (C), Boehringer Ingelheim (C), Novartis (C)
Support: Austrian Federal Ministry of Science, Research and Economy; National Foundation for Research, Technology and Development

Program Number: 5918 **Poster Board Number:** A0089
Presentation Time: 12:00 PM–1:45 PM
Depth-resolved imaging of the parafoveal capillary network in diabetic retinopathy using swept source OCT-microangiography
Laura Kuehlewein[1, 2], Tudor Tepelus[1, 2], Lin An[3], Mary K. Durbin[3], Srinivas R. Sadda[1, 2]. [1]Doheny Image Reading Center, Doheny Eye Institute, Los Angeles, CA; [2]Department of Ophthalmology, David Geffen School of Medicine, University of California - Los Angeles, Los Angeles, CA; [3]Carl Zeiss Meditec, Inc., Dublin, CA.
Purpose: To characterize the foveal avascular zone (FAZ) and the parafoveal capillary network at different retinal layers using swept source OCT-microangiography (OMAG) in normal subjects and patients with diabetic retinopathy.
Methods: OMAG images were acquired in 15 eyes of 11 patients with diabetic retinopathy, and 19 eyes of 13 healthy individuals using a prototype swept source OCT (Carl Zeiss Meditec), with a central wavelength of 1050nm. Scans were taken in clusters of 4 repeated B-scans from 3x3x3mm cubes centered on the fovea. *En-face* images of the retinal vasculature were generated from the superficial and deeper inner retinal layer (SRL/DRL) using a proprietary intensity differentiation algorithm. The area of the FAZ was computed at each *en-face* level following manual segmentation of the FAZ border. In addition, the parafoveal vessel density in a ring with a distance of 500 microns from the border of the foveal avascular zone was computed following automatic extraction using the publically available GNU Image Manipulation Program GIMP 2.8.14 (http://gimp.org). Vessel density was expressed as percent retinal area occupied by vessels.
Results: The values for mean ± SD area of the FAZ are shown in Table 1. The mean size of the FAZ was statistically significantly larger in patients with diabetic retinopathy for both the SRL and DRL ($p<0.001$ and $p=0.002$). The mean ± SD vessel density in the parafoveal ring is shown in Table 1. The mean parafoveal vessel density at the SRL was statistically significantly smaller in patients with diabetic retinopathy ($p<0.001$). At the DRL, however, there was no statistically significant difference in the vessel density when comparing patients with diabetic retinopathy and healthy individuals ($p=0.552$).
Conclusions: The foveal avascular zone was significantly larger in patients with diabetic retinopathy. The parafoveal vessel density was significantly smaller in patients with diabetic retinopathy at the superficial inner retinal layer. At the deeper inner retinal layer, however, the vessel density in patients with diabetic retinopathy was comparable to those in healthy subjects.

	Diabetic retinopathy		Healthy individuals	
	SRL	DRL	SRL	DRL
Area of the FAZ mean ± SD (mm^2)	0.450 ± 0.130	0.658 ± 0.204	0.282 ± 0.116	0.455 ± 0.148
Parafoveal vessel density mean ± SD (%)	55.8 ± 8.6	51.9 ± 7.2	70.5 ± 5.4	53.3 ± 6.3

Table 1. Mean and standard deviation (SD) of the area of the foveal avascular zone (FAZ) and parafoveal vessel density in patients with diabetic retinopathy and healthy individuals at the superficial and deeper inner retinal layer (SRL/DRL).

Commercial Relationships: Laura Kuehlewein, None; **Tudor Tepelus**, None; **Lin An**, Carl Zeiss Meditec, Inc., Dublin, CA (E); **Mary K. Durbin**, Carl Zeiss Meditec, Inc., Dublin, CA (E); **Srinivas R. Sadda**, Carl Zeiss Meditec (C), Carl Zeiss Meditec (F), Carl Zeiss Meditec (R), Optos (C), Optos (F), Optos (R)

Program Number: 5919 **Poster Board Number:** A0090
Presentation Time: 12:00 PM–1:45 PM
Interactive, Stereoscopic, Three Dimensional, Virtual Reality Visualization of Optical Coherence Data Sets of Vitreo-Macular Tractions Before and After Enzymatic Vitreolysis
Enikoe Bukaty, Carl G. Glittenberg, Susanne Binder. Ophthalmology, Rudolf Foundation Hospital, Vienna, Austria.
Purpose: To design a visualization system, which displays solid–mesh segmentation reconstructions with reflection intensity based texturing of optical coherence tomography (OCT) data sets in an interactive head mounted virtual reality display.
Methods: OCT data sets of 4 patients with vitreo-macular traction was collected before, one week after, 4 weeks after, 3 months after, 6 months after, and one year after intravitreal injections of Ocriplasmin. The OCT data sets were imported into MAXON Cinema 4D™ where they were segmented into a triangle mesh based on the OCT threshold intensities using custom built algorithms. The resulting meshes were given UV texture coordinates and a vertex map relating to the nearest reflection intensity was applied. These textured meshes were then exported to UNITY 3D™ and visualized using an Oculus Rift™ virtual reality head set.
Results: 6 data sets were collected from 4 patients resulting in 24 collected and converted data sets. Visualizations of each data set achieved a crisp and clear display of the pathology changing over time. The end-user was able to freely move around in the data set using a joystick. Any movement of the end-user's head was immediately translated into corresponding changes of the virtual cameras direction, angle, and pitch, allowing the end-user to freely explore and look around inside the pathology. With the click of a button the end-user was able to scroll through the data sets temporally, making it possible to visualize not only the three dimensional structures of the pathology, but also its changes over time in reaction to the surgical intervention.
Conclusions: The achieved interactivity and visualization quality of the virtual reality head set was very high. The primary drawback of this generation of displays is the pixel resolution, which is still slightly too low, making single pixels still discernable and causing slight ghosting. This problem will be addressed in the next iteration. This technology promises to aid clinical understanding of vitreo-retinal pathologies both in educational and research settings.

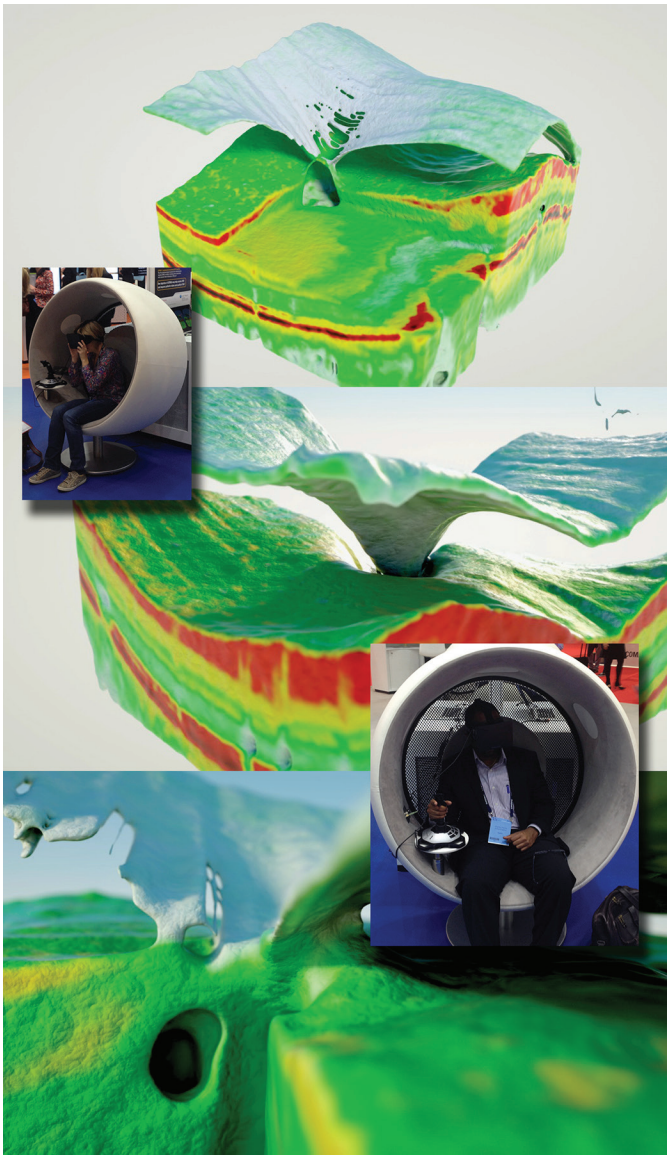

Commercial Relationships: Enikoe Bukaty, None; **Carl G. Glittenberg**, Alcon (C), Lutronic (C), Novartis (C), Thea (C), Topcon (C), Zeiss (C); **Susanne Binder**, None

Program Number: 5920 **Poster Board Number:** A0091
Presentation Time: 12:00 PM–1:45 PM
Automatic segmentation and classification of intraretinal cystoid fluid and subretinal fluid in 3D-OCT using convolutional neural networks
Thomas Schlegl[1], Ana-Maria Glodan[2], Dominika Podkowinski[2], Sebastian M. Waldstein[2], Bianca S. Gerendas[2], Ursula Schmidt-Erfurth[2], Georg Langs[1]. [1]Christian Doppler Laboratory for Ophthalmic Image Analysis, Computational Imaging Research Lab, Department of Biomedical Imaging and Image-guided Therapy, Medical University of Vienna, Vienna, Austria; [2]Christian Doppler Laboratory for Ophthalmic Image Analysis, Vienna Reading Center, Department of Ophthalmology, Medical University of Vienna, Vienna, Austria.
Purpose: The key driver for vision loss in macular diseases such as neovascular age-related macular degeneration is the accumulation

of macular edema. Out of the two components of macular edema, intraretinal cystoid fluid (IRC) leads to severe vision loss. Conversely, recent evidence suggests that subretinal fluid (SRF) may be associated with better visual acuity outcomes. The precise classification and quantification of IRC and SRF are therefore of paramount importance for disease management. We propose a fully automated segmentation and classification method for IRC and SRF in spectral-domain optical coherence tomography (SD-OCT) images.
Methods: We use convolutional neural networks (CNN) to capture characteristic visual appearance patterns and classify normal retinal tissue, IRC and SRF. The CNN is trained in a supervised manner using approximately 300,000 2D image patches extracted from 157 OCT image volumes available at the Vienna Reading Center. All image patches are sampled at random positions. 73% of the patches show healthy tissue, 8% show IRC and 18% show SRF. Besides the visual appearance of the image patches we provide the CNN with the Euclidean distances of the patch centers to the fovea and the 3D coordinates of the patch centers. We evaluate the automatic segmentation performing four-fold cross-validation. Based on the image patches of the training set the CNN learns representative and discriminative features appropriate for pixel-wise image classification. The pixel-wise classification results in a segmentation of the whole OCT volume into normal retinal tissue, IRC and SRF.
Results: The amount of spatial overlap between predicted class labels and the corresponding ground truth annotations is computed as performance measure. The classifier achieves an overall accuracy over all three classes of 96%. The pixel-based class-wise accuracies of normal retinal tissue, IRC and SRF are 98%, 90% and 92%, respectively.
Conclusions: Our CNN classifier automatically and highly accurately segments and discriminates between normal retinal tissue, IRC and SRF in retinal SD-OCT. This may enable precise structure-function correlations, and the prediction of visual function based on SD-OCT on the large scale.

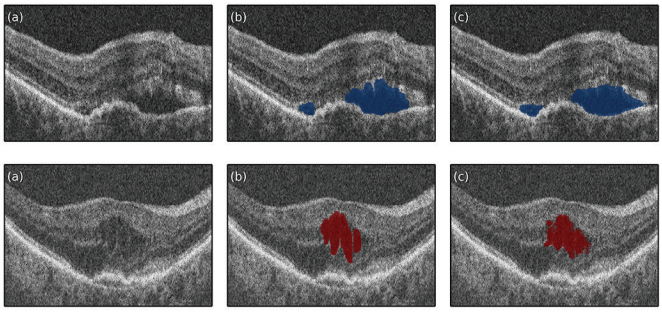

Figure 1: Intensity image (a), ground truth (b) and segmentation result (c) of a case showing SRF (top) and IRC (bottom).
Commercial Relationships: Thomas Schlegl, None; **Ana-Maria Glodan**, None; **Dominika Podkowinski**, None; **Sebastian M. Waldstein**, None; **Bianca S. Gerendas**, None; **Ursula Schmidt-Erfurth**, Alcon (C), Bayer (C), Boehringer Ingelheim (C), Novartis (C); **Georg Langs**, None
Support: Austrian Federal Ministry of Science, Research and Economy; National Foundation for Research, Technology and Development

Program Number: 5921 **Poster Board Number:** A0092
Presentation Time: 12:00 PM–1:45 PM
Analysis of changes in retinal and choroidal thickness in population-based normal elderly people and its correlation with major AMD associated single nucleotide polymorphisms (SNPs) in the complement factor H (CFH) and age-related maculopathly susceptibility 2 (ARMS2) genes
Na-Kyung Ryoo, Se Joon Woo, Kyu Hyung Park. Ophthalmology, Seoul National University Bundang Hospital, Seongnam-Si, Korea (the Republic of).
Purpose: We aimed to analyze the changes in retinal and choroidal thickness in healthy elderly people over 65 years of age. The relationships between retinal and choroidal thickness on EDI-OCT and major AMD-associated SNPs were also evaluated.
Methods: A population-based, prospective cohort study in Korean elders aged 65 year and older was conducted. Among the participants, spectral domain optical coherence tomography (SD-OCT) and blood samples were obtained from 352 individuals. Thickness of the retina and choroid were measured according to the ETDRS subfields. The subfields were grouped into mean minimal foveolar thickness (MMFT), central foveolar thickness (CFT), mean central thickness (MCT), mean peripheral thickness (MPT) and mean total region thickness (MTT). Subfoveal choroidal thickness (SFCT) was also measured on EDI-OCT. Statistical analysis was done to evaluate the correlation of thickness with age and gender. Each individual was also genotyped for the major AMD-associated SNPs – rs800292 and rs1061170 from CFH gene, and rs10490924 from ARMS2. Correlation with the genotype and retinal or subfoveal choroidal thickness was further explored.
Results: Data from 255 individuals with an average age of 76.7 years were available for analysis. The mean retinal thicknesses were - MMFT 217.3 (± 21.4), CFT 264.7 (± 24.1), MCT 326.6 (± 20.3), MPT 288.8 (± 59.3), MTT 303.0 (± 29.9), retinal nerve fiber layer (RNFL) thickness 95.2 (± 11.9) and SFCT 181.5 (± 69.1). The overall decrease in thickness was observed in the RNFL, MCT, and SFCT. With aging, the thickness declined at the rate of 6.17 / 10yrs ($p<0.001$) in RNFL, 6.02 / 10yrs ($p=0.003$) in MCT, and 2.78 /yrs ($p<0.001$) in SFCT. CFT and MCT were thicker by 8.45 ± 2.99 um ($p=0.005$) and 5.82 ± 2.50 um, respectively, in males than females. The genetic analysis showed an association between SFCT and CFH rs10611700 (Y402H).
Conclusions: Age and gender-related differences of retinal and choroidal thickness exist in the normal healthy geriatric population. Acquisition of such normative data and genetic analysis in healthy eyes may provide insight on the pathophysiology of retinal and choroidal diseases.
Commercial Relationships: Na-Kyung Ryoo, None; **Se Joon Woo**, None; **Kyu Hyung Park**, None

Program Number: 5922 **Poster Board Number:** A0093
Presentation Time: 12:00 PM–1:45 PM
Correlation between the elongation of photoreceptor inner/outer segment and visual acuity after surgery for rhegmatogenous retinal detachment
Misato Kobayasi, Takeshi Iwase, Kentaro Yamamoto, Hiroko Terasaki. Ophthalmology, Nagiya University Graduate School of Medicine, Nagoya, Japan.
Purpose: To evaluate changes of the length of photoreceptor of inner (IS) and outer segment (OS) and a correlation between the changes and visual acuity after surgery for rhegmatogenous retinal detachment (RRD).
Methods: Patients who had undergone successful RRD repair with vitrectomy or scleral buckling and could be observed the IS /OS

line at the central fovea in the spectral-domain optical coherence tomographic (OCT) images were retrospectively studied. Twenty-eight eyes of 28 patients were evaluated, and the eyes were classified preoperatively into those with macula-on RRD (n = 15, age 48.0 ± 16.9 years) and those with macula-off RRD (n = 13, age 54.8 ± 15.0 years). The central foveal thickness (CFT), the outer nuclear layer (ONL) thickness, and the length of IS and OS on the OCT images, and visual acuity were measured at 2 weeks, 1, 3, 6, and 12 months after surgery, respectively. We compared the length and the visual acuity.

Results: In the macula-off RRD group, the mean CFT and ONL thickness were 212 ± 51μm and 127 ± 54 μm, respectively, at 2 weeks after surgery and did not change with time significantly. However, the mean IS length was 25 ± 5 μm at 2 weeks after surgery and increased to 34 ± 3 μm at 12 months after surgery, and after postoperative 3 months elongated significantly compared to that at 2 weeks after surgery ($p<0.001$, ANOVA). Also, the mean OS length was 17 ± 10 μm 2 weeks after surgery and increased to 39 ± 9 μm at 12 months after surgery, and after postoperative 1 month elongated significantly compared to that at 2 weeks after surgery ($p<0.01$, ANOVA). In the macula-on RRD group, the mean CFT, ONL thickness, IS and OS length were 238 ± 15 μm, 126 ± 14 μm, 34 ± 3 μm and 44 ± 4 μm at 2 weeks after surgery and did not change with time. There was a significant difference in the OS length between the macular-off group and the macular-on group ($p=0.042$, t-test) at 12 months after surgery. The mean postoperative IS and OS length were significant correlated with the visual acuity in the macular-off group ($r=-0.41$, $p<0.001$; $r=-0.63$, $p<0.001$, Pearson).

Conclusions: The length of IS and OS was elongated with time significantly and was correlated with the visual acuity significantly in the macular-off RRD group. It was indicated that the restoration of IS and OS was correlated with the improvement of visual acuity after surgery for macular-off RRD.

Commercial Relationships: Misato Kobayasi, None; **Takeshi Iwase**, None; **Kentaro Yamamoto**, None; **Hiroko Terasaki**, None

Program Number: 5923 **Poster Board Number:** A0094
Presentation Time: 12:00 PM–1:45 PM
Retinal layer thickness measurement using automated retinal segmentation with SD-OCT

Gisele Soubrane[1], Isabelle Aknin[2]. [1]Ophthalmology, Hotel Dieu, Univ Paris Descartes, Paris, France; [2]Ophthalmology, Clinique Oxford, Antibes, France.

Purpose:
To obtain normative database of the different retinal layer thickness, using recently developed automatic retinal segmentation, and to evaluate the relationship between retinal layers and aging.

Methods: A prospective study of healthy controls, with no clinical evidence of retinal or glaucomatous disease was performed. The automated layer segmentation protocol of the HRA Spectralis and OCT (Heidelberg Engineering, Heidelberg, Germany) was used. The different retinal layers identified were inner limiting membrane (ILM), retinal nerve fiber layer (RNFL), ganglion cell layer (GCL), inner plexiform layer (IPL), inner nuclear layer (INL), outer plexiform layer (OPL), external limiting membrane (ELM), interface of the inner and outer segments of the photoreceptor layer (PR1), outer segment-RPE interdigitation (PR2), RPE and Bruch's membrane complex.The respective measured thickness of each layer was reported beneath the fovea, at 500 μm and 1500 μm intervals, nasally and temporally to the center of the fovea respectively
Inclusion criteria: in the L
Patients presenting at our practice for visual control have been clinically thoroughly examined. They were included in the study if visual acuity on the ETDRS scale was superior to 80 letters and no anomaly was detected until each decade of age group contained 10 subjects. The protocol was then carried out with the Spectralis SD-OCT.

Results: 60 eyes of 30 healthy subjects were included. The groups were distributed between 30 years to 80 years in 10 years gap. Each group comprises a minimum of 10 eyes.
Primary endpoint: obtain the scale of the thickness of the retinal layers, and the different layers shape.
The details of the measures showed that the thickness of the RNFL nasally (at 500 and 1500μm) was thicker as expected than temporally.
Secondary endpoint: point out retinal layers thickness modification through aging.
The PR1 layer is the one that showed a consistant thickness decrease with age. The other layers had a more variable course needing probably a larger asample size.

Conclusions: This attempt to obtain normative data base of the measure retinal layers with automatic retinal segmentation provides interesting results. This work needs a confirmation in a larger study group before predating pathological studies.

Commercial Relationships: Gisele Soubrane, None; **Isabelle Aknin**, None

Program Number: 5924 **Poster Board Number:** A0095
Presentation Time: 12:00 PM–1:45 PM
Quantitative Characteristics of Spectral-Domain Optical Coherence Tomography (SDOCT) in Corresponding Areas of Decreased Autofluorescence in Patients with Stargardt Disease

Alexander Ho[1], Laura Kuehlewein[1, 2], Amirhossein Hariri[1, 2], Yulia Wolfson[3], Rupert W. Strauss[3], Hendrik P. Scholl[3], Srinivas R. Sadda[1, 2]. [1]Doheny Image Reading Center, Doheny Eye Institute, Los Angeles, CA; [2]Doheny Eye Center, UCLA David Geffen School of Medicine, Los Angeles, CA; [3]Wilmer Eye Institute, Johns Hopkins University, Baltimore, MD.

Purpose: Fundus autofluorescence (FAF) has been proposed as a method to monitor Stargardt disease (STGD), but various patterns of abnormal FAF may be observed, potentially confounding longitudinal assessments. Outer retinal substructure alterations on optical coherence tomography (OCT) have also been demonstrated in STGD patients to correlate with visual outcomes. In this analysis, we explored the relationship between these OCT alterations and areas of definitely and questionably decreased autofluorescence (DDAF, QDAF).

Methods: 34 eyes from 19 STGD patients with exclusively DDAF or QDAF in the central subfield on confocal scanning laser ophthalmoscope FAF images were identified from the ongoing Natural History of the Progression of Atrophy Secondary to Stargardt Disease (ProgStar) studies. DDAF was defined as regions of decreased FAF greater than 125 μm in diameter with a blackness level comparable to the optic disc. QDAF was defined as regions of decreased FAF greater than 125 μm in diameter and relatively less dark than the optic disc, but still substantially more hypo-autofluorescent than the background (Figure 1). Corresponding SDOCT B-scans (49-section 20°x20° high resolution volume scans) were independently segmented using proprietary software (OCTOR) for the following layers: inner retina (inner limiting membrane [ILM] to dendritic outer plexiform layer [OPL]), outer nuclear layer (ONL; dendritic OPL to external limiting membrane [ELM]), and combined layers between ELM and Bruch's membrane (BM). Central subfield layer metrics from DDAF and QDAF were compared using the Mann-Whitney-Wilcoxon test.

Results: The averages and standard deviations of mean thicknesses and preserved areas in the central subfield are shown for DDAF

and QDAF in Table 1. The ONL and ELM-BM layer were both significantly thinner in areas of DDAF compared to QDAF ($p<0.05$).
Conclusions: Thickness and preservation of the ONL and ELM-BM layer appear to be linked to the visible differences in DDAF and QDAF lesions. This finding is consistent with the proposed models for STGD progression, if QDAF is considered a transition state between healthy retina and later stages of STGD.

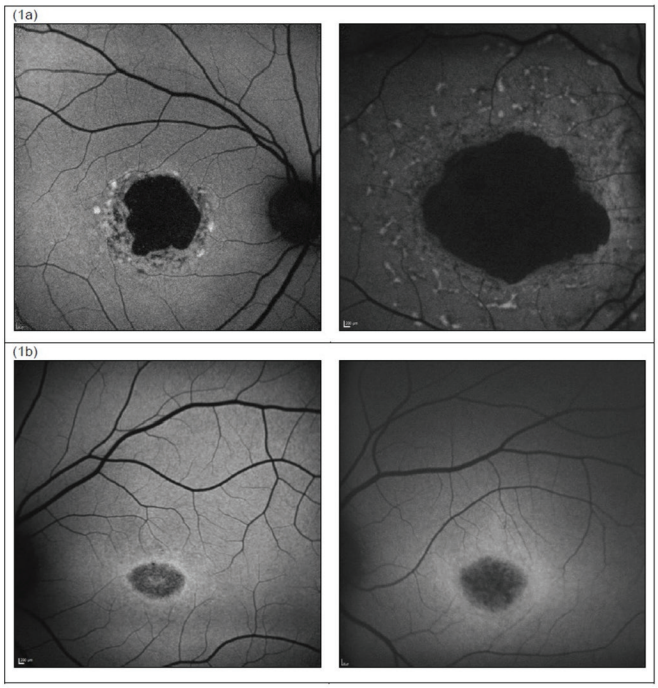

Figure 1. Examples of lesions categorized as (1a) DDAF and (1b) QDAF.

Layer	Mean Thick. DDAF (n=23) (avg ± std. dev, µm)	Mean Thick. QDAF (n=11) (avg ± std. dev, µm)	p-value
Inner retina	68 ± 17	68 ± 19	0.418
ONL	18 ± 20	34 ± 19	0.015
ELM to BM	12 ± 11	26 ± 21	0.043
Layer	**Area - DDAF (n=23)** (avg ± std. dev, mm^2)	**Area - QDAF (n=11)** (avg ± std. dev, mm^2)	**p-value**
Inner retina	0.76 ± 0.06	0.78 ± 0.01	0.084
ONL	0.38 ± 0.28	0.65 ± 0.19	0.004
ELM to BM	0.37 ± 0.32	0.58 ± 0.29	0.033

Table 1. Averages and standard deviations of mean thicknesses and areas of layers in the central subfield per SDOCT.
Commercial Relationships: Alexander Ho, None; **Laura Kuehlewein**, None; **Amirhossein Hariri**, None; **Yulia Wolfson**, None; **Rupert W. Strauss**, None; **Hendrik P. Scholl**, QLT Inc. (C), QLT Inc. (F), Sanofi-Fovea Pharmaceuticals (C), Vision Medicines, Inc. (C); **Srinivas R. Sadda**, Carl Zeiss Meditec (C), Carl Zeiss Meditec (F), Carl Zeiss Meditec (R), Optos (C), Optos (F), Optos (R)
Support: Foundation Fighting Blindness Clinical Research Institute; Research to Prevent Blindness.
Clinical Trial: NCT01977846

Program Number: 5925 **Poster Board Number:** A0096
Presentation Time: 12:00 PM–1:45 PM
Improvement of hyper reflective dots visualization on OCT by gold nanoparticles
Patricia Fernandez-Robredo[1], Michael Powner[1], Senthil Selvam[1], Dawn A. Sim[2, 1], Pearse A. Keane[2, 1], Marcus Fruttiger[1]. [1]Cell Biology, UCL Institute of Ophthalmology, London, United Kingdom; [2]NIHR Biomedical Research Centre for Ophthalmology, Moorfields Eye Hospital NHS Foundation Trust, London, United Kingdom.

Purpose: In previous work, we showed in a mouse model of choroidal neovascularisation (CNV) that circulating monocytes invading the retina can be labelled by indocyanine green (ICG) and imaged *in vivo*. Here we aimed to investigate the feasibility of using gold nanoparticles as contrast agents to label invading inflammatory cells on the OCT in the retina.
Methods: Gold nanoshells, nanorods, nanobypiramids and silver plates were pre-screened in a tissue phantom (agar sheets) to establish the best suitable contrast agent in OCT. Gold nanoshells (GNS) were selected for *in vivo* analyse in the mouse CNV model. Mice (n=5) were i.p. injected with GNS 3 days before the animals were lasered with a 532 nm diode laser (Micron III, Phoenix Research) and compared with control animals (n=5). Three to four laser spots were made close to the optic nerve in each eye. OCT images were taken on SD-OCT (Envisu R2200, Bioptigen), immediately after and 7 days post CNV induction. Fluorescein angiography was performed 7 days after laser. Animals were sacrificed, eyes flatmounted and subjected to lectin (IB4) staining and analysed using fluorescence microscopy.
Results: Hyper reflective dots (HRDs) were visible in OCT images one week after the CNV induction, surrounding CNV lesion area. Those dots were brighter in animals injected with nanoshells compared to controls. The HRD observed in the OCT correlated with lectin positive cells observed in the flatmount samples with macrophage-like morphology.
Conclusions: This study shows that gold nanoparticles can improve the visualisation of inflammatory cells on OCT. HRDs in OCT are observed clinically, but it has been difficult to prove what cells the HRDs exactly represent. Further studies are needed to characterise these cells.
Commercial Relationships: Patricia Fernandez-Robredo, None; **Michael Powner**, None; **Senthil Selvam**, None; **Dawn A. Sim**, None; **Pearse A. Keane**, None; **Marcus Fruttiger**, None
Support: Marie Sklodowska Curie Actions: PIEF-GA-2012-331855; Starting Grant for Clinical Lecturers, Academy of Medical Sciences

Program Number: 5926 **Poster Board Number:** A0097
Presentation Time: 12:00 PM–1:45 PM
Spectrum of Retinal Vascular Diseases Associated with Paracentral Middle Maculopathy
Xuejing Chen[5], Ehsan Rahimy[4], Netan Choudhry[1], Amani A. Fawzi[6], Allen C. Ho[4], Jean-Pierre Hubschman[5], Marion R. Munk[2], Robert Sergott[4], Eduardo C. Souza[7], David Sarraf[5, 3]. [1]Herzig Eye Institute, Toronto, ON, Canada; [2]Ophthalmology, Northwestern University Feinberg School of Medicine, Evanston, IL; [3]Great Los Angeles Veterans Affairs Healthcare Center, Los Angeles, CA; [4]Wills Eye Hospital, Philadelphia, PA; [5]Stein Eye Institute, Department of Ophthalmology, University of California, Los Angeles, Los Angeles, CA; [6]Department of Ophthalmology, Northwestern University Feinberg School of Medicine, Evanston, IL; [7]Department of Ophthalmology, Universidade Federal of Sao Paulo, Sao Paulo, Brazil.

Purpose: Paracentral middle maculopathy (PAMM) is a newly described hyper-reflective, parafoveal band at the level of the inner nuclear layer (INL) on spectral domain optical coherence tomography (SD-OCT) that co-localizes with the intermediate (ICP) and deep capillary plexuses (DCP). This is an observational, retrospective, multi-centered case series to evaluate the spectrum of retinal diseases that demonstrate PAMM.
Methods: Nine patients (10 eyes) from 4 centers with PAMM lesions and associated retinal vascular diseases are included. Clinical presentations and multimodal imaging, including color photographs, near infrared reflectance, fluorescein angiography, SD-OCT, and

color doppler imaging are described. Baseline and follow-up findings are correlated with demographics and systemic associations.
Results: PAMM lesions are verified by SD-OCT at baseline presentation in 5 men and 4 women (age 27 to 66 years). Follow-up SD-OCT analysis of these PAMM lesions demonstrated subsequent thinning of the INL. Novel systemic associations between retinal vasculopathy and PAMM include eye compression injury causing global ocular ischemia, sickle cell crisis, Purtscher's retinopathy, occlusive retinal vasculitis, post-H1N1 vaccine, hypertensive retinopathy, migraine disorder, and post-upper respiratory infection.
Conclusions: PAMM lesions may develop in a wide spectrum of retinal vascular diseases. They are best identified with SD-OCT and may represent ischemia of the ICP and DCP. These lesions typically result in permanent thinning of the INL and are critical to identify in order to determine the cause of unexplained vision loss.

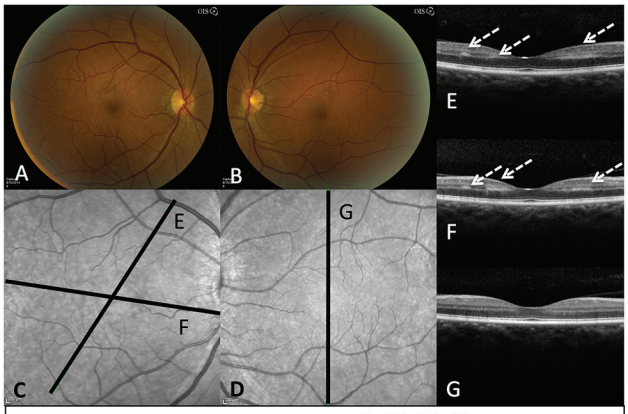

	Systolic Velocities			
	CRA (cm/s)	NPCA (cm/s)	TPCA (cm/s)	OA (cm/s)
At presentation				
OD	0	0	0	40.6
OS	6.3	0	5.0	15.5
2 days later				
OD	3.0	0	8.9	36.7
OS	14.9	6.6	10.1	22.2

Case 1: Prolonged globe compression leading to severe compromise in CRA and PCA blood flow as measured by color doppler imaging leading to PAMM. At baseline presentation, the flow for the CRA, NPCA, TPCA are severely reduced. Upon follow up, there was improved flow for each, except the NPCA OD, corresponding to slow reperfusion after relief of extended orbital pressure. OD: right; OS: left; CRA: central retinal artery; PCA: posterior cilary artery; NPCA: nasal PCA; TPCA: temporal PCA; OA: ophthalmic artery

Case No.	Age/ Sex	Presentation	Systemic Disease	Eye Disease	Eye	Baseline VA	Follow-up VA
2	28/F	Acute onset of bilateral paracentral scotomas in the absence of other signs of occlusive crisis.	Sickle cell disease	Sickle cell retinopathy with chronic temporal BRAOs OU and nasal PAMM OU	OD OS	20/50 20/200	20/20 20/20
3	36/F	Acute onset of central scotoma OD and floaters OS for 1 week, associated with right-sided retro-orbital pain.	Pregnancy-induced DVT, recent flu-like illness with GI symptoms	Papillitis/occlusive vasculitis/multifocal retinal infiltrates OU, inferotemporal retinal ischemia with temporal PAMM OD	OD	20/150	20/25
4	29/M	Vision loss OS in the setting of recent blunt trauma	Recent MVA with loss of consciousness and trauma OS	Purtscher's retinopathy OS	OS	CF	-
5	27/F	2-3 months of vision loss OS and "changing vision" OD. In clinic BP was 180/80.	Migraines, OCP, Adderall use, HTN	Hypertensive retinopathy	OD OS	20/20 CF	20/20 CF
6	50/M	Acute onset blurry vision OD. Recent BP ranged from 112/71 to 195/88 depending on medication compliance.	HTN, CHF, pulmonary HTN, alcohol abuse	Hypertensive retinopathy, pseudophakia	OD	20/30	20/40
7	28/M	Acute onset paracentral scotoma OD	Migraine with visual aura	-	OD	20/20	20/20
8	53/F	Acute onset of paracentral scotomas OD 2-3 days after H1N1 vaccine	Hypo-thyroidism, HTN, anxiety	Pseudophakia	OD	20/50	20/50
9	37/F	Acute onset of scotoma OD 2 weeks after a URI	Recent URI	-	OD	20/25	20/20

Cases 2-9. F:female; M:male; OD:right; OS:left; OU:bilateral, CF:count fingers; BRAO:branch retinal artery occlusion; DVT:deep vein thrombosis, GI:gastrointestinal; OCP:oral contraceptive pills; HTN:hypertension; CHF:congestive heart failure; DM:diabetes mellitus; URI:upper respiratory infection
Commercial Relationships: Xuejing Chen, None; **Ehsan Rahimy**, None; **Netan Choudhry**, None; **Amani A. Fawzi**, None; **Allen C. Ho**, None; **Jean-Pierre Hubschman**, None; **Marion R. Munk**, None; **Robert Sergott**, None; **Eduardo C. Souza**, None; **David Sarraf**, None

Program Number: 5927 **Poster Board Number:** A0098
Presentation Time: 12:00 PM–1:45 PM
The foveal shape is not predictive of visual acuity and treatment response in macular edema due to retinal vein occlusion
Dominika Podkowinski, Jing Wu, Ana-Maria Glodan, Bianca S. Gerendas, Alessio Montuoro, Roland Leitner, Christian Simader, Sebastian M. Waldstein, Ursula Schmidt-Erfurth. Christian Doppler Laboratory for Ophthalmic Image Analysis, Vienna Reading Center, Department of Ophthalmology, Medical University of Vienna, Vienna, Austria.
Purpose: The fovea as the functional center of the retina is a key structure when investigating visual function in retinal disease. It is common clinical belief that an abnormal shape of the fovea (such as eversion by macular edema) is a sign of poorer visual acuity and treatment outcomes; however, systematic investigations are lacking. The aim of this study was to characterize the foveal shape and to investigate corresponding functional and anatomical response patterns in patients with branch retinal vein occlusion (BRVO) and central retinal vein occlusion (CRVO).
Methods: Patients with CRVO or BRVO enrolled in phase III randomized multicenter trials with data available at the Vienna Reading Center were included. All patients were treated with ranibizumab injections. Baseline spectral-domain optical coherence tomography (OCT) scans of the study eye were processed using an automated image analysis pipeline consisting of denoising, motion correction, layer segmentation and foveal shape classification. Each scan was automatically assigned one of three foveal shape categories: 1) normal foveal depression, 2) minor foveal depression and 3) absent foveal depression. Best-corrected visual acuity (BCVA) at baseline, change in BCVA from baseline to month six, number of treatments, retinal thickness at baseline, and the change in thickness from baseline to six months were compared between these groups.

Results: 72 eyes with CRVO and 56 eyes with BRVO were analyzed. In BRVO, 22 eyes (39%) presented a normal foveal depression, 7 (13%) a minor foveal depression, and 27 (48%) an absent foveal depression. In CRVO, 17 eyes (24%) showed a normal foveal depression, 16 (22%) a minor foveal depression and 39 (54%) an absent foveal depression. The comparison of anatomical and functional characteristics and treatment outcomes are presented in Table 1. There was a statistically significant difference in mean retinal thickness at baseline and change in retinal thickness, with thinner retinas in the normal foveal depression group and larger changes in the other groups. All other variables showed no statistically significant differences between the different foveal shapes.
Conclusions: Contrary to common clinical belief, baseline BCVA, change in BVCA and number of treatments seem independent of the foveal shape in macular edema due to retinal vein occlusion.

Central retinal vein occlusion (CRVO)

	Normal foveal depression	Minor foveal depression	Absent foveal depression
Mean BCVA at baseline (letters) (95% confidence interval)	50 (41 – 60)	55 (47 – 64)	54 (51 – 58)
Mean change in BCVA from baseline to month 6 (letters) (95% confidence interval)	14 (6 – 22)	18 (14 – 23)	14 (11 – 17)
Mean number of ranibizumab treatments (95% confidence interval)	4.2 (3.6 – 4.9)	4.5 (3.9 – 5.0)	4.9 (4.6 – 5.3)
Mean central retinal thickness at baseline (µm) (95% confidence interval)	490 (382 – 598)	636 (556 – 715)	684 (634 – 734)
Mean reduction in central retinal thickness from baseline to month 6 (µm) (95% confidence interval)	185 (95 – 274)	357 (265 – 450)	359 (293 – 425)

Branch retinal vein occlusion (BRVO)

	Normal foveal depression	Minor foveal depression	Absent foveal depression
Mean BCVA at baseline (letters) (95% confidence interval)	59 (53 – 64)	55 (44 – 66)	59 (55 – 64)
Mean change in BCVA from baseline to month 6 (letters) (95% confidence interval)	18 (14 – 22)	9 (5 – 13)	15 (11 – 19)
Mean number of ranibizumab treatments (95% confidence interval)	4.2 (3.7 – 4.7)	5.3 (4.3 – 6.3)	4.7 (4.3 – 5.2)
Mean central retinal thickness at baseline (µm) (95% confidence interval)	420 (378 – 462)	486 (417 – 554)	599 (536 – 648)
Mean reduction in central retinal thickness from baseline to month 6 (µm) (95% confidence interval)	123 (81 – 164)	111 (10 – 233)	295 (229 – 361)

Table 1

Commercial Relationships: Dominika Podkowinski, None; **Jing Wu**, None; **Ana-Maria Glodan**, None; **Bianca S. Gerendas**, None; **Alessio Montuoro**, None; **Roland Leitner**, None; **Christian Simader**, None; **Sebastian M. Waldstein**, None; **Ursula Schmidt-Erfurth**, Alcon (C), Bayer (C), Boehringer Ingelheim (C), Novartis (C)
Support: Austrian Federal Ministry of Science, Research and Economy; National Foundation for Research, Technology and Development

Program Number: 5928 **Poster Board Number:** A0099
Presentation Time: 12:00 PM–1:45 PM
Segmental analysis of the retinal single-layers in de novo drug-naïve Parkinson's disease
Hyeong Min Kim[1], Jee yun Ahn[1, 2], Tae Wan Kim[1, 2], Martha Kim[3], Jee-Young Lee[4, 5]. [1]Department of Ophthalmology, Seoul National University College of Medicine, Seoul, Korea (the Republic of); [2]Department of Ophthalmology, Seoul Metropolitan Government Seoul National University Boramae Medical Center, Seoul, Korea (the Republic of); [3]Department of Ophthalmology, Dongguk University Ilsan Hospital, Goyang, Korea (the Republic of); [4]Department of Neurology, Seoul Metropolitan Government Seoul National University Boramae Medical Center, Seoul, Korea (the Republic of); [5]Department of Neurology, Seoul National University College of Medicine, Seoul, Korea (the Republic of).
Purpose: To perform segmental analysis of the retinal single-layers in de novo drug-naïve Parkinson's disease (PD) in order to assess the presence and degree of structural retinal change in the early stage of PD.
Methods: Fifty-four de novo PD (99 eyes) and 23 age-matched controls (39 eyes) were recruited. General ophthalmologic examination and optical coherence tomography (OCT) scans were done. Using automated segmentation software, the parafoveal retina was separated into 10 layers and the mean thickness of each retinal layer was calculated in the 9 sectors of the Early Treatment of Diabetic Retinopathy Study (ETDRS) macular map. The whole retinal layer (WRT), retinal nerve fiber layer (RNFL), ganglion cell layer (GCL), inner plexiform layer (IPL), inner nuclear layer (INL), outer plexiform layer (OPL), outer nuclear layer (ONL) and photoreceptor layer (PR) thicknesses were compared between de novo PD and control.
Results: There were no significant differences in baseline demographic factors such as age, sex, logMAR visual acuity, spherical equivalent and axial length. De novo PD patients showed OPL thinning in the inferior and nasal sectors of the inner ETDRS circle (35.67±8.75 vs 39.79±12.00 mm, p=0.056 and 33.69±8.06 vs 39.79±11.04 mm, p=0.003). Conversely, the GCL inferior and nasal sectors of the outer circle, the center fovea of the GCL and IPL, and ONL nasal sector of the inner circle showed increased thickness compared to control. (33.43±4.06 vs 30.87±3.65 mm, p=0.001, 38.73±4.01 vs 37.03±4.11 mm, p=0.027, 13.58±5.58 vs 11.82±2.53 mm, p=0.012, 19.37±3.73 vs 18.03±1.94 mm, p=0.006, and 70.47±12.21 vs 65.15±14.43 mm, p=0.030).
Conclusions: Segmental analysis of the retinal single-layers showed evident structural changes in de novo drug-naïve PD. Future studies are warranted to further characterize the topographic pattern and the degree of retinal single-layer change in early stage PD.
Commercial Relationships: Hyeong Min Kim, None; **Jee yun Ahn**, None; **Tae Wan Kim**, None; **Martha Kim**, None; **Jee-Young Lee**, None

Program Number: 5929 **Poster Board Number:** A0100
Presentation Time: 12:00 PM–1:45 PM
Retinal Fluorescence Lifetime Characteristics in Mouse Models of Pharmacologically Induced Retinal Degeneration
Chantal Dysli[1, 2], Muriel Dysli[1, 2], Martin S. Zinkernagel[1, 2], Volker Enzmann[1, 2]. [1]Ophthalmology, University Hospital Bern, Bern, Switzerland; [2]Department of Clinical Research, University Hospital Bern, Bern, Switzerland.
Purpose: Fluorescence Lifetime Imaging Ophthalmoscopy (FLIO) is used for non-invasive in vivo measurement of fluorescence lifetimes of natural fluorophores of the retina.

By directed induction of degeneration of the photoreceptors (PR) and the retinal pigment epithelium (RPE), the contribution of these individual layers to the measured fluorescence lifetime signal are investigated.
Methods: Wildtype C57BL/6 mice (6-8 weeks) were used for this experiment. Degeneration of the RPE was induced by intravenous injection of sodium iodate (NaIO3, 35 mg/kg). N-methyl-N-nitrosourea (MNU, 45 mg/kg) injected intraperitoneally was used for degeneration of the photoreceptor cell layer. NaIO3 mice, MNU mice, and control mice (NaCl) were measured at day 3, 7, 14, and 28 after injection. Fluorescence lifetime imaging was performed using a fluorescence lifetime imaging ophthalmoscope (FLIO, Heidelberg Engineering, Germany). The fluorescence excitation wavelength was 473 nm and decay times were measured in a short and in a long spectral channel (SSC: 498–560 nm, LSC: 560–720 nm). Corresponding optical coherence tomography images were acquired and histology (H&E) was performed from all retinas at the latest time point.
Results: At day 28, fluorescence lifetimes were prolonged by 8% in the short and 61% in the long spectral channel in NaIO3 mice compared to control animals (p=0.21 and p=0.004, respectively). In MNU mice, retinal lifetimes were shortened by 27% in the short and 51% in the long spectral channel (both p=0.0028). OCT images and histology verified the cell type-specific degeneration process over time.
Conclusions: Specific degeneration of the RPE by NaIO3 lead to longer mean fluorescence lifetimes of the retina compared to control mice, whereas in degeneration of the photoreceptor layer induced by MNU shorter lifetimes are measured. Therefore, short retinal fluorescence lifetimes may origin from the RPE and may be modified by the overlaying retinal layers.
Commercial Relationships: Chantal Dysli, Heidelberg Engineering, Germany (F); **Muriel Dysli**, None; **Martin S. Zinkernagel**, Heidelberg Engineering, Germany (F); **Volker Enzmann**, None
Support: Swiss National Science Foundation (SNSF) #320030_156019

Program Number: 5930 **Poster Board Number:** A0101
Presentation Time: 12:00 PM–1:45 PM
Usual Multimodal Imaging Versus Spectralis "En-Face" OCT 2 Angiography: a new semiologic approach in healthy and AMD patients.
Gabriel J. Coscas[1, 2], Florence Coscas[1, 2], Marco Lupidi[2, 3], Valérie Krivosic[1], Catherine Favard[2], Catherine Francais[2], Eric H. Souied[1].
[1]Department of Ophthalmology, Creteil Eye Clinic Univ Hospital, Creteil, France; [2]75006, Centre Ophtalmologique de l'Odeon, Paris, France; [3]Eye Clinic, S. Maria Della Misericordia Hospital, Perugia, Italy.
Purpose: To compare the results obtained with standard multimodal imaging versus En-Face OCT 2 ANGIOGRAPHY (OCT2-A) in Patients with exudative AMD and identify similarities or differences in 4 types of choroidal neovascularization.
Methods: Case series of 10 healthy and 80 eyes of 50 consecutive AMD patients (39 females, mean age 79.4 ± 5.3) diagnosed with different types of CNV (53 type I,12 predominantly classic, 6 Retinal Angiomatous Proliferation, 9 Polypoidal choroidal vasculopathy). Initial diagnosis was based on Fluorescein Angiography (FA), Indocyanine green angiography (ICGA), B-Scan OCT with two different examiners to the ones achieved with En-Face OCT2-A (Spectralis, Heidelberg Engineering) to help for the diagnosis and the decision of treatment. In conventional multimodal imaging, lesions were classified into subepithelial or preepithelial and mixed. The lesion's activity was evaluated according to leakage in FA and fluid accumulation in OCT. The new imaging with OCT2-A associated with En Face allowed to recognize the pattern of active CNV as hyperdense multiramified network due to active blood flow corresponding to hyperreflective network and fluid accumulation on "En Face". The system used by Spectralis is an Amplitude Decorrelation OCT device able to show in a B-scan OCT2-A the relationship between CNV and RPE layer.
Results: OCT2-A allows recognition of localization of CNV as sub or pre epithelial. The two methods achieved the same diagnosis about presence of subfoveal CNV (52/80).The diagnosis of active CNV based on FA leakage (25/52) was more easy than based on qualitative changes of morphology of CNV on OCT2-A (14/52) . The classification into 4 groups as usual, was applicable for both type I and II with OCT2-A using the unique possibility to have a B-scan section in OCT2-A. The diagnosis of active CNV was achieved with non invasive method (OCT2-A and En Face OCT) in all 52 cases.
Conclusions: Our study highlights the capability of the method of OCT2-A to determine the presence of subfoveal CNV, the diagnosis of activity, the classification into the well known four groups and particularly to distinguish sub and pre epithelial CNV. Nevertheless, even if FA remains the gold standard for the presence of leakage, the En-Face OCT could easily show fluid accumulation and its variations.

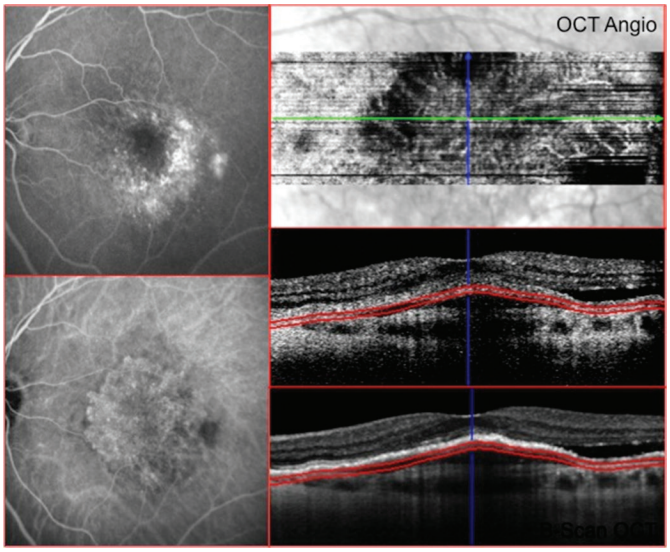

Commercial Relationships: Gabriel J. Coscas, Allergan (C), Bayer (C), Novartis (C); **Florence Coscas**, Allergan (C), Bayer (C), Novartis (C); **Marco Lupidi**, None; **Valérie Krivosic**, allergan (C), bayer (C), novartis (C); **Catherine Favard**, None; **Catherine Francais**, Bayer (C), Novartis (C), roche (C); **Eric H. Souied**, Allergan (C), Bayer (C), Novartis (C)

Program Number: 5931 **Poster Board Number:** A0102
Presentation Time: 12:00 PM–1:45 PM
Quantitative fundus autofluorescence in age-related macular degeneration and other retinal diseases associated with drusen
Martin Gliem, Philipp Mueller, Frank G. Holz, Peter Charbel Issa.
Department of Ophthalmology, University of Bonn, Germany, Bonn, Germany.
Purpose: Lipofuscin accumulation in the retinal pigment epithelium (RPE) has been suggested to play a pathophysiological role in various monogenetic and complex retinal diseases including age-related macular degeneration (AMD) with direct evidence for this assumption in Stargardt disease. The aim of this study was to quantitatively measure lipofuscin-related fundus autofluorescence

(AF) in early or intermediate AMD and other retinal diseases associated with drusen.
Methods: Fundus AF images were acquired with a modified scanning laser ophthalmoscope equipped with an internal fluorescent reference (modified Spectralis HRA-OCT, Heidelberg Engineering, Heidelberg, Germany). All patients were younger than 65 years of age. The disease spectrum included early or intermediate AMD, reticular pseudodrusen with or without geographic atrophy (GA), basal laminar drusen (BLD), colloidal drusen and membranoproliferative glomerulonephritis (MPGN) type 2. For every subject, the mean gray value of a defined circular region at an eccentricity of approximately 7° to 9° centered on the fovea was determined. The quantitative AF (qAF) value was calculated after adjustment to the reference, the optical magnification, the density of the ocular media, the laser offset and a device-specific correction factor. Data was compared to normative qAF values derived from 90 healthy subjects.
Results: Thirty-nine patients were investigated. Mean±SD age was 52±6 years (range: 35-61 years). All patients with early and intermediate AMD (n=7) revealed qAF levels within the 95% confidence interval (CI) of age-matched controls. In patients with BLD (n=11), colloidal drusen (n=3) and RPD without GA (n=12), qAF levels were within the 95% CI in 91%, 67% and 75%, respectively. The remaining patients of these groups as well as all patients with GA (n=4) and the patient with MPGN type 2 (n=1) had qAF values below the age-matched 95% CI. No patient showed a qAF value above the age-matched 95% CI.
Conclusions: QAF measurements showed no increased lipofuscin-related fundus-AF in early or intermediate AMD or other diseases associated with drusen which may serve as model diseases for AMD. Lower qAF-levels in certain subgroups may point to subnormal lipofuscin concentration in the RPE or disease-specific limitations to detect true RPE lipofuscin content.
Commercial Relationships: Martin Gliem, Carl Zeiss Meditec, Germany (F), Heidelberg Engineering, Germany (F), Optos, UK (F); **Philipp Mueller**, Carl Zeiss Meditec, Germany (F), Heildelberg Engineering, Germany (F), Optos, UK (F); **Frank G. Holz**, Acucela (C), Acucela (C), Acucela (F), Allergan (C), Allergan (F), Bayer (C), Bayer (F), Boehringer Ingelheim (C), Genentech (C), Genetech (F), Heidelberg Engineering (C), Heidelberg Engineering (F), Merz (C), Novartis (F), Novertis (C), Optos (F), Roche (C), Zeiss (F); **Peter Charbel Issa**, Heildelberg Engineering, Germany (F)
Support: BONFOR research grant O-137.0018, ProRetina

Program Number: 5932 **Poster Board Number:** A0103
Presentation Time: 12:00 PM–1:45 PM
Three dimensional vascular imaging of diabetic retinopathy by Doppler optical coherence tomography
Daisuke Muramatsu[1], Young-Joo Hong[2], Yoshiaki Yasuno[2], Takuya Iwasaki[1], Hiroshi Goto[3], Masahiro Miura[1]. [1]Ophthalmology, Tokyo Medical University Ibaraki medical center, Inashiki gun, Japan; [2]Computational Optics Group, University of Tsukuba, Tsukuba, Japan; [3]Opthalmology, Tokyo Medical University, Tokyo, Japan.
Purpose: To evaluate 3-D vascular architecture in diabetic retinopathy with Doppler optical coherence tomography (OCT).
Methods: 33 eyes of 26 patients with diabetic retinopathy (simple type: 16 eyes, pre-proliferative:10 eyes, proliferative: 7 eyes) were evaluated. 3-D vascular flow imaging (OCT angiography) was obtained using 1 μm swept source Doppler OCT (100,000 Ascan/s, axial resolution 6.4 μm). In a single scan, the system simultaneously provided both an intensity-based standard OCT image and a Doppler OCT image. High sensitive vascular image was obtained by calculating power of Doppler phase signals between two A-lines of two successive B-scans.
Results: 3-D vascular imaging of vascular lesions could be clearly detected with Doppler OCT. Doppler OCT images clearly depicted three dimensional vascular architecture of microaneurysm (22 eyes), neovascularization elsewhere (NVE: 4 eyes), and intraretinal microvascular anomaly (IRMA: 2 eyes). Microaneurysms were located in inner plexiform layers in 22 eyes and outer plexiform layers in 2 eyes. In one eye, NVE was located in the inner retina and standard OCT shows a focal hyperreflective mass at inner retinal NVE. After breaking through internal limiting membrane, new vessels in NVE formed loop formations, and were pulled towards the vitreous body. IRMAs were located in inner plexiform layers. In contrast to inner retinal NVE, the hyperreflective lesion was not confirmed in the area of IRMA in the standard OCT image.
Conclusions: Doppler OCT is useful for detection and evaluation of the 3-D vascular structure of diabetic retinopathy. Doppler OCT allows visualization of the core vascular lesions in diabetic retinopathy without flurorescein dye.
Commercial Relationships: Daisuke Muramatsu, None; **Young-Joo Hong**, Nidek (F), Tomey (F), Topcon (F); **Yoshiaki Yasuno**, Nidek (F), Tomey (F), Topcon (F); **Takuya Iwasaki**, None; **Hiroshi Goto**, None; **Masahiro Miura**, Novartis (R)

Program Number: 5933 **Poster Board Number:** A0104
Presentation Time: 12:00 PM–1:45 PM
Cone loss in Type 2 Macular Telangiectasia Demonstrated by Adaptive Optics Scanning Laser Ophthalmoscopy in a Phase 1 Clinical Trial of Ciliary Neurotrophic Factor
Hongxin Song[1], Austin Roorda[2], Jacque L. Duncan[3], Mina M. Chung[4,1]. [1]Center for Visual Science, University of Rochester, Rochester, NY; [2]School of Optometry and Vision Science Graduate Group, University of California, Berkeley, Berkeley, CA; [3]Department of Ophthalmology, University of California, San Francisco, San Francisco, CA; [4]Flaum Eye Institute, University of Rochester, Rochester, NY.
Purpose: Macular telangiectasia (MacTel) has been considered primarily a vascular disease, but recent evidence suggests that neuronal changes may occur early in disease development. The NT-501 ciliary neurotrophic factor (CNTF) implant (Neurotech USA, Inc.) uses encapsulated cell technology to deliver CNTF to the retina and has been shown to reduce photoreceptor cell loss in retinal degeneration. To study the rate of cone photoreceptor loss in MacTel treated with CNTF, we used AOSLO to examine patients enrolled in a Phase 1 clinical trial.
Methods: Three patients with MacTel were imaged using AOSLO at two centers. In each patient, the more severely affected eye had received the CNTF implant and the fellow eye served as a control. AOSLO imaging was conducted at baseline and 18 months after implantation in all 3 subjects. 1 subject was additionally imaged at 24 and 36 months. At least 10 regions of interest (ROIs) were selected and tracked across imaging sessions. Individual cones within each ROI were labeled. At each time point, at each ROI, the percent change in cone spacing from baseline was measured. The mean percent change was compared from baseline to each time point using one-way ANOVA, and the treated eyes were compared to controls using an independent t-test.
Results: Combining the treated and control eyes from all 3 patients, AOSLO showed a statistically significant increase in cone spacing after 18 months ($p<0.05$). In 1 patient studied at 24 and 36 months, the increase was significant in the control ($p<0.01$) but not the treated eye ($p=0.06$) at 24 months, and significant in each eye at 36 months ($p<0.01$). The difference between treated and control eyes was not statistically significant at 18 months in the 3 patients studied ($p =0.4$).

In 1 patient, the increase in cone spacing was significantly lower in the treated eye at 24 months (p =0.02) and 36 months (p=0.01).
Conclusions: Although MacTel has been classically defined by its clinically detectable changes in the retinal vasculature, AOSLO demonstrates that cone photoreceptor spacing increases with time in MacTel. AOSLO can provide a highly sensitive method to measure microscopic changes in MacTel in the clinical trial setting. Further study, including greater numbers of patients, is needed to determine whether the CNTF implant is effective in treating MacTel.
Commercial Relationships: Hongxin Song, None; **Austin Roorda**, University of Houston (P), University of Rochester (P); **Jacque L. Duncan**, None; **Mina M. Chung**, None
Support: R01 EY021786Edward N. & Della L. Thome Memorial FoundationP30 EY001319, Lowy Medical FoundationResearch to Prevent Blindness, NIH Grants EY002162, R01FD004100, Foundation Fighting Blindness, The Bernard A. Newcomb Macular Degeneration Fund, That Man May See, Inc., Hope for Vision, Claire Giannini Fund

Program Number: 5934 **Poster Board Number:** A0105
Presentation Time: 12:00 PM–1:45 PM
In-vivo Detection of Choroidal Abnormalities Related to Neurofibromatosis Type 1: Feasibility and Comparison with Standard NIH Diagnostic Criteria in Pediatric Patients.
Raffaele Parrozzani[1], Luisa Frizziero[2], giacomo miglionico[2], Pierdavide Perrini[2], Olympia Kotsafti[1], Enrica Convento[2], Edoardo Midena[2, 1]. [1]Ocular Oncology and Toxicology Research Unit, G.B. Bietti Foundation, IRCCS, Roma, Italy; [2]Department of Ophthalmology, University of Padova, Padova, Italy.
Purpose: To evaluate the feasibility of near infrared (NIR) imaging acquisition in a large sample of consecutive pediatric patients with neurofibromatosis type 1 (NF1), to evaluate the diagnostic performance of NF1 related choroidal abnormalities as a diagnostic criterion of the disease and to compare this criterion with those established by original Institutes of Health Consensus Development Conference.
Methods: One-hundred and forty consecutive pediatric patients (0-16 years old) affected by NF1 (at least two diagnostic criteria), fifty-nine suspected (a single diagnostic criterion) and forty-two healthy subjects (no diagnostic criterion) were consecutively included. Each patient underwent genetic, dermatologic and ophthalmologic examination to evaluate the presence/absence of each NIH diagnostic criterion. The presence of NF1 related choroidal abnormalities was investigated using NIR confocal ophthalmoscopy (Spectralis®, Heidelberg Engineering, Heidelberg, Germany).
Results: NF1-related choroidal abnormalities where detected in seventy-two affected (60.5%), one suspected (2.4%) and in no-one healthy subject, reaching a feasibility rate of 85%. Sensitivity, specificity, positive and negative predictive values were 0.60, 0.97, 0.98 and 0.46, respectively. Compared whit standard NIH criteria, the presence of NF1-related choroidal abnormalities is the third parameter (after café-au-lait macules and freckling) for sensitivity, positive and negative predictive value, and the fourth for specificity. The introduction of this sign has anticipated the diagnosis in a single case (0.5%). The subject who moved from suspected to affected group by using this sign was a 2-year-old boy that eventually developed other NIH diagnostic criteria.
Conclusions: Although the sign NF1-related choroidal abnormalities, compared with standard NIH criteria, is third in order of sensitivity, positive and negative predictive value, and fourth for specificity. It should be therefore considered a new clinical marker of the disease, but does not appear to add diagnostic performance to standard NIH diagnostic criteria.

Diagnosis of NF1: comparison between epidemiological indicators.

	Sensitivity (C.I. 95%)	Specificity (C.I. 95%)	PPV	NPV
Café au lait spots	0.98 (0.96-1.00)	0.30 (0.18-0.43)	0.79	0.88
Axillary or inguinal freckling	0.92 (0.88-0.97)	1.00 (1.00-1.00)	1.00	0.83
Lish nodules	0.57 (0.49-0.45)	0.94 (0.88-1.00)	0.96	0.46
Familiarity	0.26 (0.18-0.33)	0.84 (0.74-0.94)	0.81	0.29
Neurofibromas	0.32 (0.25-0.40)	0.98 (0.94-1.00)	0.97	0.35
Optic Pathway Glioma	0.20 (0.13-0.26)	0.80 (0.95-1.00)	0.96	0.34
Distinctive osseous lesions	0.02 (0.00-0.04)	1.00 (1.00-1.00)	1.00	0.27
NF1 related choroidal abnormalities	0.60 (0.51-0.69)	0.97 (0.92-1.00)	0.98	0.46

PPV=positive predictive value; NPV=negative predictive value; C.I.=Confidence Interval.

Commercial Relationships: Raffaele Parrozzani, None; **Luisa Frizziero**, None; **giacomo miglionico**, None; **Pierdavide Perrini**, None; **Olympia Kotsafti**, None; **Enrica Convento**, None; **Edoardo Midena**, None
Support: The research for this paper was supported by Ministry of Health and Fondazione Roma.

Program Number: 5935 **Poster Board Number:** A0106
Presentation Time: 12:00 PM–1:45 PM
Enface OCT Angiography (OCTA) Techniques for Enhanced Visualization of Choroidal Neovascularization
Utkarsh Sharma[1], Douglas Matsunaga[3], Lin An[1], Mary K. Durbin[1], Carmen A. Puliafito[2], Amir H. Kashani[3]. [1]R&D, Carl Zeiss Meditec, Inc., Dublin, CA; [2]Office of the Dean, Keck School of Medicine, Los Angeles, CA; [3]Ophthalmology, University of Southern California, Los Angeles, CA.
Purpose: OCTA is a promising non-invasive imaging technique that may be used for detecting and monitoring vascular abnormalities such as choroidal neovascularization (CNV). The goal of this study is to demonstrate that CNV can be detected using OCTA on a spectral-domain OCT system. Furthermore, new OCTA visualization tools are used that provide 3D impressions in 2D enface projections to better assess the extent of neovascularization growth.
Methods: Cirrus 5000 HD-OCT based prototype system (Carl Zeiss Meditec Inc., Dublin, CA) was used to obtain OCTA scans at 67.5 kHz. OCT microangiography (OMAG) technique with 2D cross-correlation based motion correction was used to obtain OCTA results. Line scanning ophthalmoscope (LSO) based tracking was used to minimize motion artifacts. Three subjects diagnosed with CNV were included in the study. Color fundus (CF) images and fluorescein angiograms (FA) were also obtained and used for correlating the results of OCTA images. Depth-encoded OCTA color maps were generated to better appreciate the depth information as well as to delineate the CNV growth. For depth-encoded color maps, vasculature in the inner-retina, mid-retina and outer-retina were encoded in the red, green and blue color, respectively.
Results: CNV was well visualized by OMAG technique and the results correlated well with the CF and FA images. Figure 1 shows the foveal region of 3mm x 3mm from the CF and FA image and the corresponding OMAG images of the left eye for a 70 year old female subject with CNV. While, the inner-retina vasculature (superficial retinal capillary plexus) looks relatively normal (1C), CNV region is well delineated and emphasized with the blue color in the depth-encoded color map (1D). CNV region in OCTA images corresponds well with the pathology shown in FA and CF images.
Conclusions: Cirrus based SD-OCT prototype system demonstrated fine spatial resolution of the CNV complex. In addition, OCT angiography maps can provide detailed depth encoded information of retinal vasculature that is not possible with traditional FA.

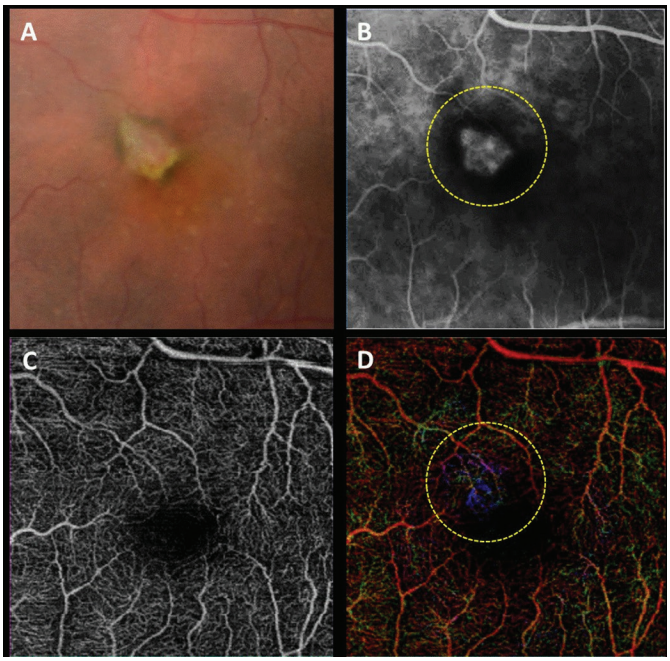

Fig. 1 Imaging CNV. A) CF image. B) FA image. C) OCTAimage of inner-retina vasculature. D). Depth-encoded color OCTA color map where the growth of CNV membrane is emphasized in the blue color and corresponds well with FA image (dashed yellow circles).

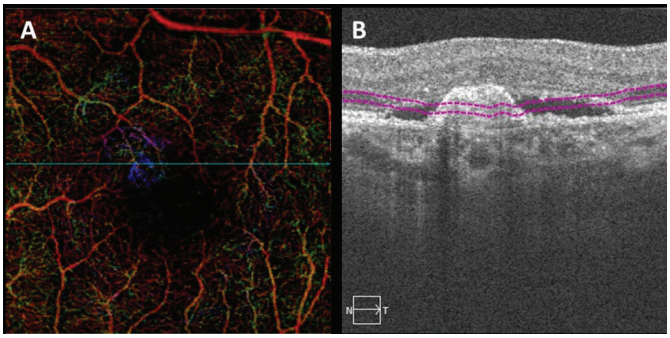

Fig. 2 B-scan (right) corresponding to the line across the CNV growth as shown in OCTA enface image (left).
Commercial Relationships: Utkarsh Sharma, Carl Zeiss Meditec, Inc. (E); **Douglas Matsunaga**, Carl Zeiss Meditec Inc. (F); **Lin An**, Carl Zeiss Meditec, Inc. (E); **Mary K. Durbin**, Carl Zeiss Meditec, Inc. (E); **Carmen A. Puliafito**, Carl Zeiss Meditec Inc. (F); **Amir H. Kashani**, Carl Zeiss Meditec Inc. (F)

Program Number: 5936 **Poster Board Number:** A0107
Presentation Time: 12:00 PM–1:45 PM
Peripapillary choroidal thickness in eyes with neovascular age-related macular degeneration: Is choroid outside the macula affected after intravitreal ranibizumab injections?
Jaeryung Oh[1], Cheolmin Yun[1], Kwang-Eon Choi[1], So-Eun Ahn[1], Jong-Hyun Oh[2], Kuhl Huh[1]. [1]Ophthalmology, Korea University College of Medicine, Seoul, Korea (the Republic of); [2]Ophthalmology, Dongguk University Ilsan Hospital, Goyang, Korea (the Republic of).
Purpose: To investigate whether the choroidal thickness (CT) outside the macula is affected after intravitreal ranibizumab injections (IVR) in eyes with neovascular age-related macular degeneration (AMD).
Methods: Peripapillary and subfoveal CT were measured on the images obtained by spectral domain optical coherence tomography from 39 eyes of neovascular AMD patients and 39 age-matched controls. The patients were treated with 0.5 mg IVRs monthly for 3 months, and retreated as needed. Peripapillary CT was measured at four locations (superior, nasal, inferior and temporal area) at baseline, 3 months and 6 months.
Results: The mean peripapillary and subfoveal baseline CTs (153.3 ± 45.3 μm and 228.6 ± 78.6 μm) were not different from those of controls (149.0 ± 42.3 μm and 221.4 ± 54.1 μm; P = 0.665 and P = 0.639, respectively). Among peripapillary CTs, only the temporal peripapillary CT decreased from baseline (167.1 ± 54.5 μm) to at 3 months (159.4 ± 50.8 μm, P = 0.010), and it was sustained at 6 months (160.6 ± 49.6, P = 0.026). However, superior, nasal and inferior peripapillary CT did not show significant changes after IVRs. Subfoveal CT decreased at 3 (213.8 ± 75.8 μm, P < 0.001) and 6 months (215.1 ± 72.8 μm, P = 0.002).
Conclusions: Change in peripapillary CT after IVR was limited to the macular area. This result may suggest that IVR does not affect CT outside of the macula of eyes in patients with neovascular AMD.
Commercial Relationships: Jaeryung Oh, None; **Cheolmin Yun**, None; **Kwang-Eon Choi**, None; **So-Eun Ahn**, None; **Jong-Hyun Oh**, None; **Kuhl Huh**, None
Support: Supported by a grant from Korean Ministry of Environment (2012001350010)

Program Number: 5937 **Poster Board Number:** A0108
Presentation Time: 12:00 PM–1:45 PM
Standardized assessment of RPE and retina thickness from SDOCT volume scans in a large multicenter trial
Ronald P. Danis, Amitha Domalpally, Yijun Huang. Ophthalmology & Visual Sciences, Univ of Wisconsin-Madison, Madison, WI.
Purpose: To evaluate the methodology and reproducibility for assessment of retinal pigment epithelium thickness (RPE) and central retina thickness in a large clinical trial setting using a custom spectral domain optical coherence tomography (SD-OCT) software application after conversion of files to a standard format.
Methods: In a clinical trial of geriatric patients under study for non-ocular disease, a preliminary analysis of the baseline OCT volume scan images from 946 eyes (473 participants) enrolled from 82 reading-center certified clinical sites were centrally collected for analysis. Exclusions included intermediate AMD or worse or other confounding ocular abnormalities and age range was >54 to <86 years . After conversion to DICOM OPT format, macular volume scan files collected from 4 different SDOCT machines were displayed in the same software and segmented for ILM, RPE and Bruch's membrane layers in a unified display and analysis platform using an algorithm developed at the University of Wisconsin's Fundus Photograph Reading Center (Huang, et al, PLoS One. 2013 Dec 26;8(12):e82922) . Reading center graders reviewed each volume scan and edited boundary line placement if required. Reproducibility was tested through masked regrading to assess intergrader variabilty.
Results: Of 947 eyes, the proportion of ungradable scans was 5% for center retinal thickness and 2% for center RPE thickness. The standardized assessment of mean center RPE thickness was 33.3 microns (SD 4.6) and mean center retinal thickness was 244.1 microns (SD 27.4). From masked regrading, the Weighted Variance of intergrader difference in center subfield RPE thickness was 0.682 microns and for center subfield retina thickness 38.57 microns. Intraclass correlation coefficients were 0.97 for central subfield RPE thickness and 0.90 for center subfield retina thickness.
Conclusions: Standardized analysis of retinal and RPE thickness from multiple types of SDOCT machines is feasible in large clinical trials via conversion to standard file format, storage in a single database, and standardized assessment using the same segmentation

algorithm. With reading center certification of the clinical sites, the ungradable image rate was low in this elderly population. Reproducibility for reading center determination of center subfield RPE and retina thickness was excellent .

Commercial Relationships: Ronald P. Danis, Merck (F); **Amitha Domalpally**, None; **Yijun Huang**, None
Support: Grant to the University of Wisconsin from Merck for for ophthalmic reading center services
Clinical Trial: NCT01739348

Program Number: 5938 **Poster Board Number:** A0109
Presentation Time: 12:00 PM–1:45 PM

Imaging vascular pathologies in the chorioretinal complex by phase-variance SSOCT system with real-time retinal motion correction with an SLO

Justin Migacz, Iwona Gorczynska, Narendran Sudheendran, Robert J. Zawadzki, Ala Moshiri, Susanna S. Park, Lawrence S. Morse, John S. Werner. Ophthalmology and Vision Science, UC Davis, Davis, CA.

Purpose: A phase-variance contrast optical coherence tomography (pvOCT) system was combined with a video-rate scanning laser ophthalmoscope (SLO) to correct eye motion of subjects. The system was used to collect motion-corrected OCT volume mosaics of subjects with age-related macular degeneration (AMD) and the data were analyzed for phase-variance contrast to reveal the vasculature. A comparison of vascular maps with and without motion correction are presented. The maps were also compared with fluorescein angiography (FA) images.

Methods: Six subjects were imaged with the joint OCT and tracking SLO system, including three subjects with age-related macular degeneration (AMD) and three with no known pathology. The OCT light source was a swept-source laser operating at 1060 nm with a sweep repetition rate of 100 kHz. The optical power of the OCT light beam on the cornea was 1.4 mW. The system provided axial resolution of 5.4 μm in tissue. Phase variance data were calculated from sets of 5 B-scans acquired at each location in the volume. These data highlight the flow of blood cells. Scanning areas were 1x1 mm^2 and multiple locations were imaged during each imaging session. The SLO system tracked the motion in a 1.5x1.5 mm^2 region of the retina with a 0.4mW beam. Motion of the SLO images was tracked in real-time to adjust the OCT scanner position, thus allowing the system to follow eye movements.

Results: The vascular images of subjects had a noticeable reduction in motion artifacts when motion tracking was activated. Figure 1 shows a comparison of the OCT imaging with and without tracking. The top panel shows a representative OCT intensity B-scan from a subject with no pathology. The subsequent images show the pvOCT processed en-face projections of the inner retinal capillaries and choriocapillaris. Retinal capillaries appear to have fewer discontinuities when tracking is activated, although it cannot correct for large saccades. Fluorescein angiography images of the same retinal locations show vascular patterns that agree well with those captured with pvOCT, validating the accuracy of the system (Figure 2).

Conclusions: The combination of OCT with a tracking SLO is a complex system and requires careful alignment and calibration. The improvement in image quality, however, is significant when compared to standard OCT systems and standard clinical tools such as FA.

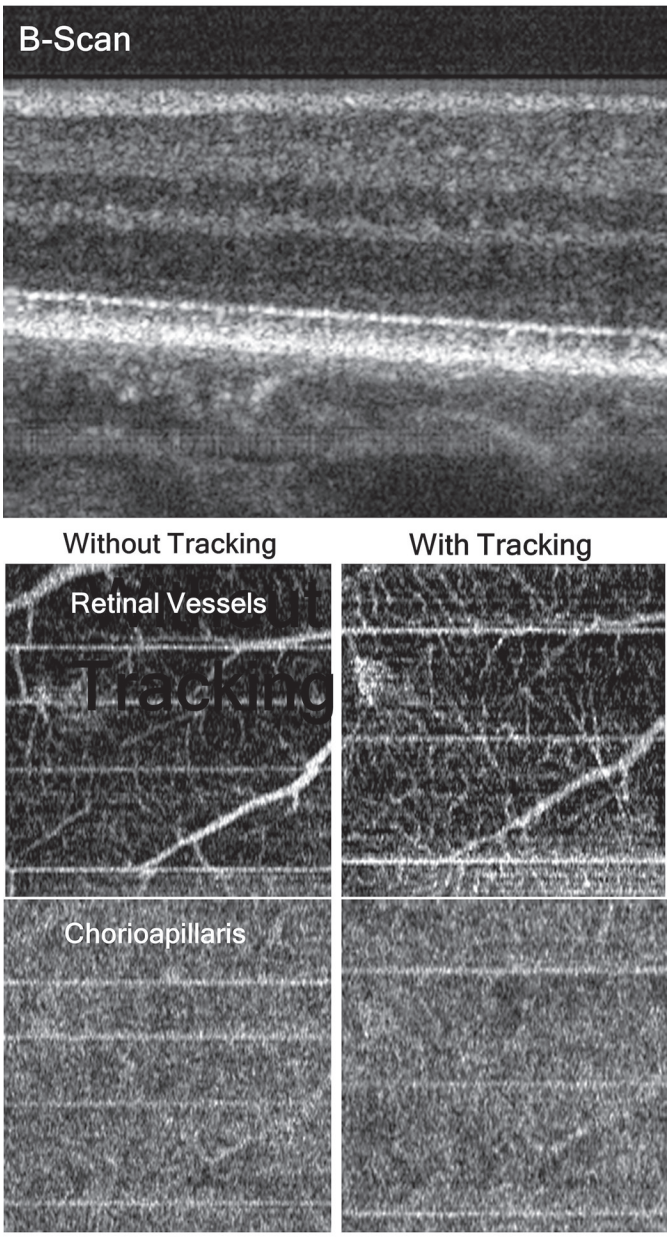

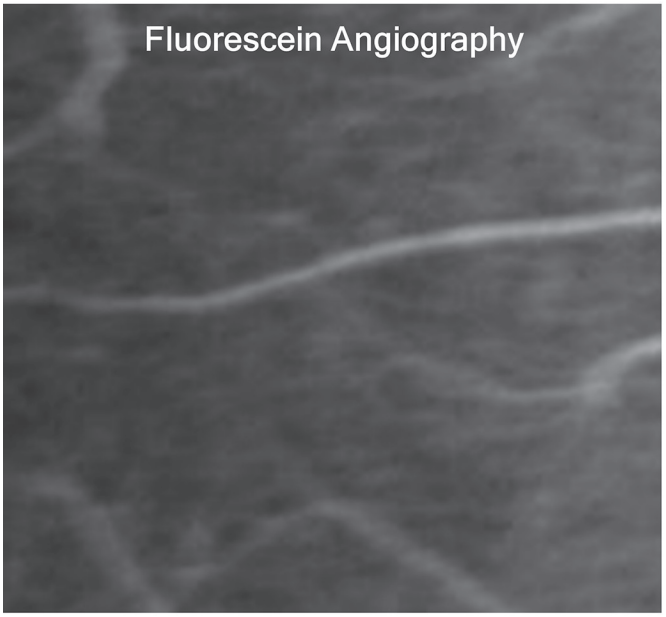

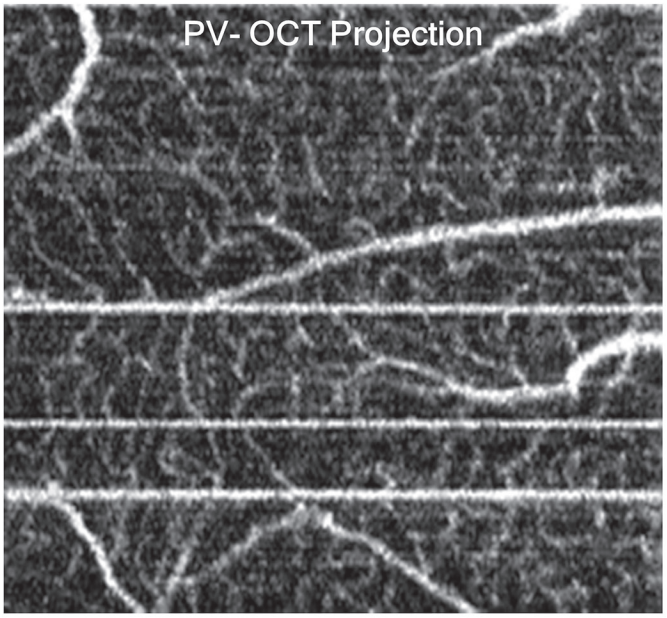

Commercial Relationships: Justin Migacz, None; **Iwona Gorczynska**, None; **Narendran Sudheendran**, None; **Robert J. Zawadzki**, None; **Ala Moshiri**, None; **Susanna S. Park**, None; **Lawrence S. Morse**, None; **John S. Werner**, None
Support: NIE R01 EY024239

Program Number: 5939 **Poster Board Number:** A0110
Presentation Time: 12:00 PM–1:45 PM

Imaging retina in rodent eyes with high resolution polarization sensitive optical coherence tomography

Stanislava Fialová[1, 2], Marco Augustin[1, 2], Roberto Plasenzotti[3], Michael Pircher[1, 2], Christoph K. Hitzenberger[1, 2], Bernhard Baumann[1, 2]. [1]Center for Medical Physics and Biomedical Engineering, Medical University of Vienna, Vienna, Austria; [2]Medical Imaging Cluster, Medical University of Vienna, Vienna, Austria; [3]Division of Biomedical Research, Medical University of Vienna, Vienna, Austria.

Purpose: Animal models play an important role in studies of ocular diseases such as age-related macular degeneration and glaucoma. The purpose of this study is to develop high-resolution polarization sensitive OCT (HR-PS-OCT) for imaging the eyes of rodents and to demonstrate in vivo imaging in rats and mice.
Methods: Spectral domain HR-PS-OCT with an axial resolution of 5.1 μm in air (3.8 μm in tissue) was developed. The central wavelength of the used light source (superluminescent diode) was 840 nm, acquisition speed was 83 kHz. Due to the high scan speed, a whole 3D data set can be acquired in few seconds (1024x200x1536 in 3.44 s) which reduces motion artifacts. In addition to standard OCT images that show sample reflectivity, phase retardation and fast axis orientation images were calculated. PS-OCT images enable the identification of birefringent tissues (such as sclera) and depolarizing tissues (such as retinal pigment epithelium - RPE, choroid).
Results: Healthy non-pigmented/pigmented rats as well as pigmented mice were imaged with the system. On the high-resolution reflectivity images, all retinal layers were observed in all animals. On the phase retardation images, the birefringent properties of the sclera and depolarization properties of the RPE-choroid were observed.
Conclusions: A dedicated HR-PS-OCT system for ocular imaging in rodents was developed and was demonstrated in vivo on rats and mice. On the high-resolution images all retinal layers could be identified. From polarization sensitive images birefringent and depolarizing tissues were identified. OCT represents a non-lethal and non-invasive alternative to histology. Our results demonstrate the feasibility of the system for high speed and high-resolution imaging of the rodent retina in longitudinal studies.

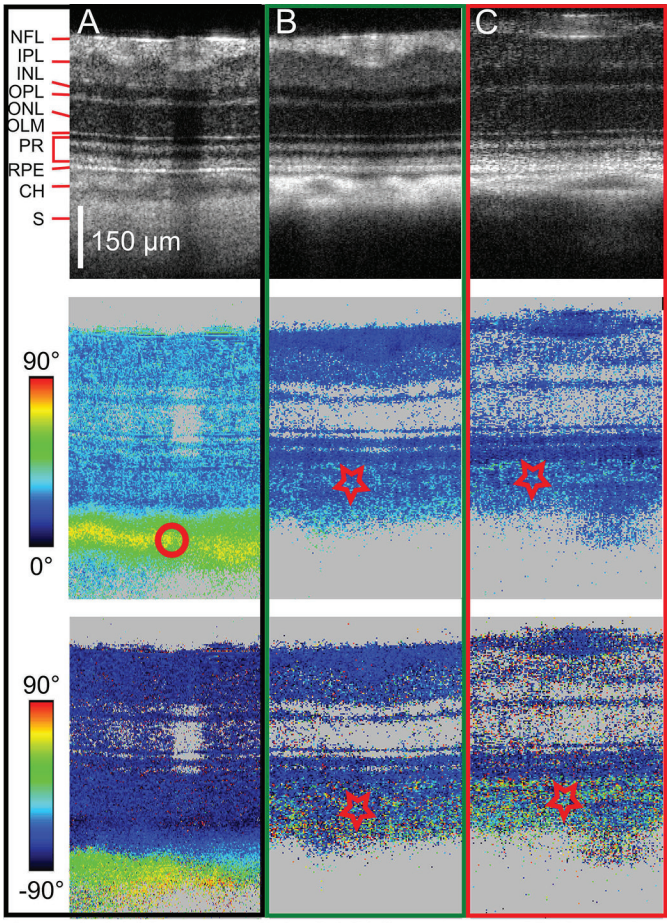

Figure 1: (A) Non-pigmented rat (B) Pigmented rat (C) Pigmented mouse. Averaged of 7 images, in all images (from top to bottom): reflectivity, phase retardation, fast axis orientation. Circle – birefringent tissue, star - depolarizing tissue. In non-pigmented rat penetration of the beam is deeper, sclera is visible, no depolarizing effect in RPE –choroid. In pigmented animals there is depolarizing effect of pigmented tissues in RPE-choroid. NFL – nerve fiber layer, IPL – inner plexiform layer, INL – inner nuclear layer, OPL – outer plexiform layer, ONL – outer nuclear layer, OLM - outer limiting membrane, PR – photoreceptors, RPE – retinal pigment epithelium, CH – choroid, S – sclera.

Commercial Relationships: Stanislava Fialová, None; **Marco Augustin**, None; **Roberto Plasenzotti**, None; **Michael Pircher**, None; **Christoph K. Hitzenberger**, None; **Bernhard Baumann**, None
Support: Austrian Science Fund (FWF) P25823-B24

Program Number: 5940 **Poster Board Number:** A0111
Presentation Time: 12:00 PM–1:45 PM
The sensitivity and specificity of disorganisation of the retinal inner layers on SD-OCT in detecting capillary nonperfusion in diabetic retinopathy
Luke Nicholson, Jayashree Ramu, Ioanna Triantafyllopolou, Namritha V. Patrao, Oliver Comyn, Philip G. Hykin, Sobha Sivaprasad. NIHR Moorfields Biomedical Research Centre, London, United Kingdom.
Purpose: This study was designed to test the sensitivity and specificity of SD-OCT (Heidelberg Spectralis) disorganisation of the retinal inner layers (DRIL) in detecting angiographic evidence of macular capillary nonperfusion in diabetic retinopathy.
Methods: SD-OCT images from 45 separate areas of macular capillary nonperfusion excluding the foveal avascular zone were obtained from 37 eyes and compared with similar images from areas of macular perfusion in the same eye. Each SD-OCT line scan was marked, anonymised, coded and graded by two masked investigators for presence of DRIL with arbitration by a senior clinician.
Results: The intergrader agreement was high (Cohen's Kappa = 0.909). Of the 45 SD-OCT lines scans, DRIL was present in 84.4% (38/45) of nonperfused retina and 0% (0/45) of perfused retina. The sensitivity and specificity of DRIL in detecting angiographic evidence of capillary nonperfusion was 84.4% and 100% respectively. Positive Predictive Value was 100% and the Negative Predictive Value, 86.5%.
Conclusions: The presence of DRIL is highly correlated to areas of nonperfusion but is not a universal finding. The absence of DRIL is very highly correlated with perfused retina. DRIL may be a useful marker for retinal capillary nonperfusion.
Commercial Relationships: Luke Nicholson, None; **Jayashree Ramu**, None; **Ioanna Triantafyllopolou**, None; **Namritha V. Patrao**, None; **Oliver Comyn**, Novartis (R); **Philip G. Hykin**, Allergan (F), Allergan (R), Bayer (F), Bayer (R), Novartis (F), Novartis (R); **Sobha Sivaprasad**, Allergan (F), Allergan (R), Bayer (F), Bayer (R), Novartis (F), Novartis (R), Roche (F), Roche (R)
Support: The research was supported by the National Institute for Health Research (NIHR) Biomedical Research Centre based at Moorfields Eye Hospital NHS Foundation Trust and UCL Institute of Ophthalmology.

Program Number: 5941 **Poster Board Number:** A0112
Presentation Time: 12:00 PM–1:45 PM
Assessment of the Influence of Greater Axial Length on the Accuracy of Partial Coherence Interferometry in Emmetropic and Highly Myopic Patients
Amanda Chi[1, 2], Alexander Vu[1, 2], Jennifer Nguyen[3], Quan V. Hoang[1]. [1]Ophthalmology, Harkness Eye Institute, Columbia University, New York, NY; [2]Institute of Human Nutrition, Columbia University, New York, NY; [3]St. Thomas Aquinas, Overland Park, KS.
Purpose: Accurate axial length measurement is critical in gauging myopic progression. Partial coherence interferometry used in machines such as the Zeiss IOLMaster is the most commonly used method in clinical ophthalmology for measuring axial length. Due to irregularities of slope and shape in the posterior wall of staphylomatous eyes, aberrant reflections are possible and can result in inaccurate measurements. This present work compares IOLMaster-measured axial lengths and manually measured axial lengths on 3-D MRI volume renderings in highly myopic patients with staphyloma to determine if the difference between the two measurements is affected by the eye axial length.
Methods: A prospective study was performed on 34 eyes of 17 patients which included 8 eyes of 4 emmetropic volunteers and 26 eyes of 13 high myopia patients clinically diagnosed with staphyloma. All eyes underwent measurement with both IOLMaster and 3-D MRI scan (Phillips, 3.0T, fat-suppressed T2-weighted cube, a modified 3-D fast-spin echo sequence). Volume renderings of the eyes were generated from high-resolution 3-D data and properly oriented so the eye could be rotated around its visual axis. MRI axial length (from the posterior cornea to the vitreo-retinal interface) was manually measured from 4 different views (each 90 degrees apart) and averaged. Axial length measurement with IOLMaster was compared to that found with the 3-D MRI rendering of the eye. Univariate regression analysis was used to correlate the absolute

difference between the two measurement modalities and axial length as measured by each of the two devices.
Results: Eyes examined ranged in axial length from 21.62 to 39.32 mm on IOLMaster and from 21.69 to 39.31 mm on MRI. The axial length measured by IOLMaster was longer than that measured by MRI in 25 out of 26 eyes (96%) among high myopia patients and 4 out of 8 emmetropic patients (50%). Linear regression did not show an association between the absolute difference between the two measurement modalities and axial length as measured by MRI ($p = 0.511$) or IOLMaser ($p= 0.767$).
Conclusions: Assessment of axial length in staphylomatous eyes may be challenging, potentially influenced by staphyloma location and local slope. Initial studies suggest that differences in axial length measured by IOLMaster versus MRI is not influenced by the magnitude of axial length.
Commercial Relationships: Amanda Chi, None; **Alexander Vu**, None; **Jennifer Nguyen**, None; **Quan V. Hoang**, None
Support: This work was supported in part by Career Development Awards from Research to Prevent Blindness (QVH), K08 Grant (QVH, 1 K08 EY023595, National Eye Institute, NIH) the Louis V. Gerstner Jr. Scholars Program (QVH), AR Peacock Trust (QVH) and JR Peacock Trust (QVH).

Program Number: 5942 **Poster Board Number:** A0113
Presentation Time: 12:00 PM–1:45 PM
Comparison of spectral-domain optical coherence tomography and fluorescein angiography in measuring area of choroidal neovascularization in age-related macular degeneration
Ann Tran, Ellie Corkery, Barbara A. Blodi, Yijun Huang, Zhe Liu, Amitha Domalpally. Ophthalmology, University of Wisconsin, Madison, WI.
Purpose: Fluorescein angiography (FA) is the gold standard for measuring the area of choroidal neovascularization (CNV). Spectral-domain optical coherence tomography (SD-OCT) is increasingly used for monitoring CNV. We developed a methodology for evaluating the area of CNV on SD-OCT and compared to FA.
Methods: We analyzed 17 treatment naïve subjects (17 eyes) with new-onset CNV secondary to age-related macular degeneration (AMD) enrolled in clinical trials. Subjects underwent FA and SD-OCT imaging studies. At the University of Wisconsin Fundus Photograph Reading Center, OCT scans were converted to DICOM images, allowing data from all SD-OCT machines to be displayed in the same software. OCT images were segmented for the inner limiting membrane, top of the retinal pigment epithelial (RPE) lesion complex and Bruchs' membrane layers in a display and analysis platform (Huang, et al, PLoS One. 2013 Dec 26;8(12):e82922). Reading center graders reviewed each volume scan and edited the boundary line placement if required. The central subfield thickness (CSF) and total volume of the RPE lesion complex were obtained. A projection map of the segmented OCT was generated and the area of the RPE lesion complex was delineated using Image J software and subsequently compared to the area of CNV and lesion found on FA.
Results: A total of 17 eyes were included in this study. The mean RPE lesion complex thickness in the CSF was 97.8 ± 57.6 μm with a grid volume of 1.0 mm^3. The mean RPE lesion complex area on SD-OCT was 4.1 mm^2 (SD 2.5). The mean CNV area on FA was 5.4 mm^2 (SD 6.9) and the mean lesion area was 6.0 mm^2 (SD 6.8). The mean difference between area of RPE lesion complex on OCT and CNV area on FA was 1.29 mm^2 (CI -8.97, 11.55). When compared to the lesion area on FA, the mean difference was 1.87 mm^2 (CI -8.09, 11.83)**.**
Conclusions: The use of SD-OCT was able to provide quantitative data about the area and volume of new CNV secondary to AMD. Area measurements from OCT correlated moderately with both CNV and lesion area on FA. Further studies using co-localization between the two modalities and follow-up studies will help evaluate the use of SD-OCT in assessing CNV status. In prospective clinical trials, these findings may substantiate the growing role of SD-OCT in the management of AMD and reduce the need for more invasive testing with FA.
Commercial Relationships: Ann Tran, None; **Ellie Corkery**, None; **Barbara A. Blodi**, None; **Yijun Huang**, None; **Zhe Liu**, None; **Amitha Domalpally**, None

Program Number: 5943 **Poster Board Number:** A0114
Presentation Time: 12:00 PM–1:45 PM
Fluorescence lifetime imaging microscopy on retinal microvascular endothelial cells under high glucose conditions
Yoko Miura[1, 2], Eric Beck[1], Gereon Huttmann[1], Sayon Roy[3], Ralf Brinkmann[1, 4]. [1]Institute of Biomedical Optics, University of Luebeck, Luebeck, Germany; [2]Department of Ophthalmology, University Hospital Schleswig-Holstein, Luebeck, Germany; [3]Department of Medicine and Ophthalmology, Boston University School of Medicine, Boston, MA; [4]Medical Laser Center Luebeck, Luebeck, Germany.
Purpose: High glucose-induced metabolic change in retinal endothelial cells has been suggested to precede the morphological alterations in the pathogenesis of diabetic retinopathy. Fluorescence lifetime imaging microscopy (FLIM) is a new imaging technology, which could be useful to detect cell metabolic changes by measuring the fluorescence lifetime (FLT) of nicotinamide adenine dinucleotide (NADH) autofluorescence. This method utilizes the difference in the FLT of free- and protein-bound-NADH. In this study, we conducted in-vitro NADH FLIM on retinal microvascular endothelial cells under high glucose condition, comparing with the different cell biological status assessed with other experimental methods.
Methods: Cultured human retinal microvascular endothelial cells (HRMEC) were used in the study. Cells were incubated in normal (4.5 mM) or high (30 mM) concentration of glucose for 60 hrs, followed by examination with FLIM combined with two-photon microscopy (TPM; λex=730nm). Amount of intracellular reactive oxygen species (ROS) was estimated with 2',7'-dichlorodihydrofluorescein diacetate (DCFH-DA)-assay, and the protein expression of vascular cell adhesion molecule-1 (VCAM-1) was investigated with Wwestern blotting.
Results: High glucose condition significantly increased intracellular ROS (30%) and VCAM-1 protein (150%) expression. FLIM results demonstrated the significant increase of the fluorescence lifetime of cultured HRMEC (τ_1: 684 ps to 693 ps, τ_2: 3163 ps to 3294 ps, τ_m: 1087 ps to 1126 ps) and the significant decrease in the ratio of the amplitude of shorter and longer lifetime component, which is suggested to indicate the ratio of the amount of free- to protein-bound NADH (a1/a2; whole cells: 7.64 to 6.84, mitochondria: 4.37 to 3.94, nucleus: 12.08 to 8.09) in the cells under high glucose conditions.
Conclusions: The FLIM results suggest that metabolic changes could be documented with TPM-FLIM in living HRMEC undergoing high glucose-induced oxidative stress. TPM-FLIM might be a useful method to detect intracellular oxidative stress and related metabolic changes in retinal vascular cells.
Commercial Relationships: Yoko Miura, None; **Eric Beck**, None; **Gereon Huttmann**, None; **Sayon Roy**, None; **Ralf Brinkmann**, None

Program Number: 5944 **Poster Board Number:** A0115
Presentation Time: 12:00 PM–1:45 PM
Reproducibility of Macular Pigment Optical Density Measurement by Two-wave Length Autofluorescence
Qisheng You[1, 2], Dirk-Uwe G. Bartsch[1], Mark Espina[1], Mostafa Alam[1], Natalia Camacho[1], William R. Freeman[1]. [1]Jacobs Retina Center, Shiley Eye Center, University of California San Diego, San Diego, CA; [2]Beijng Institute of Ophthalmology, Beijing Tongren Hospital, Capital Medical University, Beijing, China.
Purpose: Macular pigment, composed of lutein, zeaxanthin, and meso-zeaxanthin, is postulated to protect against age-related macular degeneration (AMD), likely due to filtering blue light and its antioxidant properties. It was reported that the macular pigment optical density (MPOD) is associated with macular function evaluated by visual acuity and electroretinogram. However, the reproducibility of measurement of MPOD, which is essential for any application purpose, has not yet been determined. The main purpose is to determine the reproducibility of MPOD measurement by two-wave length autofluorescence method.
Methods: Fifty four eyes of 31 persons were enrolled in the study, including 6 normal eyes, 15 wet AMD, 9 dry AMD, 8 macular edema due to diabetic macular, branch retinal vein occlusion or macular telangiectasia and 16 tractional maculopathy including vitreomacular traction, epiretinal membrane and macular hole. MPOD was measured with a two-wave length (488 and 514nm) autofluorescence method with Spectralis HRA+OCT after pupil dilation. The measurement was repeated for each eye 10 minutes later. The Pearson Correlation analysis and Bland-Altman plot were used to assess the reproducibility between the two measurements.
Results: The mean sum of MPOD volume within eccentricities of 1°, 2° and 6° radius was 906.61±440.84, 2332.57±1142.44, 5872.32±3394.97 and 893.74±430.40, 2302.69±1131.46, 5832.13±3416.64 at first and second measurement respectively. The correlation coefficient of the association (r) between the two measurements was 0.994, 0.994 and 0.988 (all P<0.001) respectively, and the Bland-Altman plot showed 9.3%, 3.7% and 5.6% points outside the 95% limits of agreement, indicating an overall excellent reproducibility.The data for the reproducibility did not differ markedly among the various disease and normal eyes.
Conclusions: Under routine examination conditions with pupil dilation, MPOD measurement by two-wave length autofluorescence method showed a high reproducibility.

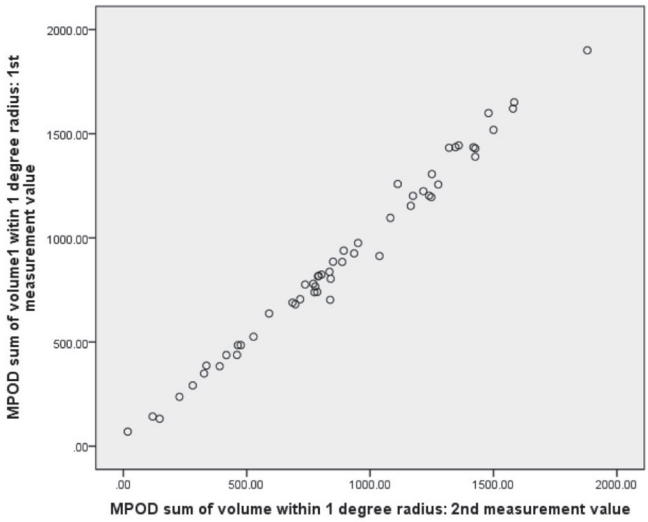

Scatter plot showing the correlation between the 1st and 2nd MPOD measurement within 1 degree radius of fovea

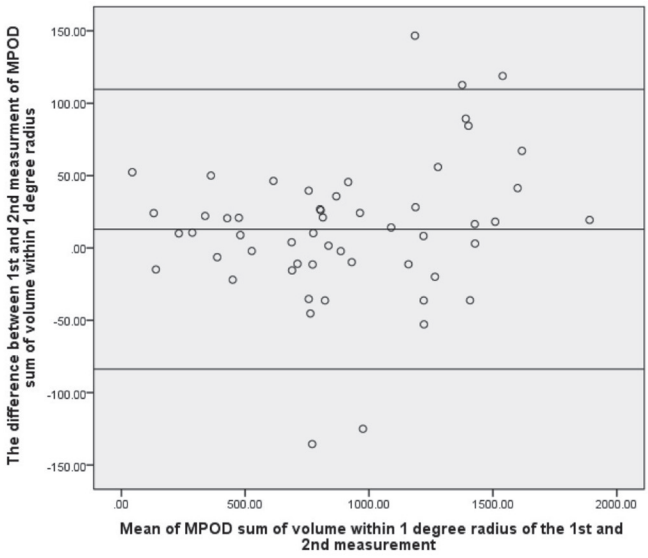

Bland-Altman plot of MPOD within 1 degree radius of the 1st and 2nd measurement. X-axial defined as mean of the 1st and 2nd measurement. Y-axial defined as the first measurement value minus the second measurement value. The mean differences and the 95% confidence limits of the bias are shown as three lines.
Commercial Relationships: Qisheng You, None; **Dirk-Uwe G. Bartsch**, None; **Mark Espina**, None; **Mostafa Alam**, None; **Natalia Camacho**, None; **William R. Freeman**, None

Program Number: 5945 **Poster Board Number:** A0116
Presentation Time: 12:00 PM–1:45 PM
Description and Validation of a new tool for measurement of pigment epithelium detachment (PED) volume: ReVA (Retina Volume Analyzer)
Oudy Semoun[1], Eric H. Souied[1], Violaine Caillaux[1], Bruno Lay[2], Camille Jung[1], Rocio Blanco-Garavito[1]. [1]CHI de Creteil, Creteil, France; [2]ADCIS, Saint-Contest, France.
Purpose: Retinal thickness and volume analysis by Optical Coherence Tomography has recently become a reliable way of

monitoring macular disease activity. Nevertheless, retinal volume can consist of several separate anatomical sections that can vary independently and cannot always be analyzed as a whole. We aim to describe and validate the first results of PED volume quantification by a new software (ReVA) and the follow up results after anti VEGF treatment.
Methods: We included in a prospective fashion patients presenting with vascularized PEDs secondary to exudative AMD, previously diagnosed on the basis of multimodal imaging. All patients had undergone complete ophthalmological examination, fluorangiography and ICG angiography. Spectral Domain Optical Coherence Tomography (SD-OCT) on Enhanced Depth Imaging (EDI) mode (Spectralis HRA+OCT, Heidelberg Engineering GmbH, Heidelberg, Germany) was performed, with an acquisition of a 30 degree retinal volume scan consisting of 61 lines centered on the fovea with an averaging of 9 frames per scan. This information was exported in .XML format to the ReVA software. The information was anonymized. A semi automatic analysis of PED volume was perfomed by three independant readers (OS, VC, RBG), twice, at the beginning and end of a 15 day period. The software allows for semi automated demarcation of PED limits on a two dimesional scan basis, and afterwards calculations are peformed to present PED volume results in cubic millimeters. The results are presented in a 3D volume representation that can be manipulated to be seen from various angles. The Bland Altmann assessment for agreement was used to compare intra and inter-observer observations.
Results: We included 20 eyes of 20 patients presenting with vascularize PED. The Bland-Altman analysis indicates that the 95% limits of agreement between the inter and intra observer measures ranged in average from -0.99 to 1.00 with an average correlation of 0.99.
Conclusions: ReVA analyzer is a reliable tool that can assist in the analysis of PED volume with high precision. This type of separate retinal volume analysis can be of help for monitoring disease activity and therapeutic response in AMD.
Commercial Relationships: Oudy Semoun, None; **Eric H. Souied**, ADCIS (P); **Violaine Caillaux**, None; **Bruno Lay**, ADCIS (P), ADCIS (P); **Camille Jung**, None; **Rocio Blanco-Garavito**, None

Program Number: 5946 **Poster Board Number:** A0117
Presentation Time: 12:00 PM–1:45 PM
Correlation of pre-mortem and post-mortem spectral domain optical coherence tomography (SD-OCT) in examination of normal and diseased human retinas
Meidong Zhu[1, 3], Adil Syed[2, 1], Andrew A. Chang[2, 1]. [1]Save Sight Institute, University of Sydney, Sydney, NSW, Australia; [2]Sydney Institute of Vision Science, Sydney, NSW, Australia; [3]Lions New South Wales Eye Bank, New South Wales Organ and Tissue Donate Service, Sydney, NSW, Australia.
Purpose: Post-mortem human retinal tissues are necessary for studies of macular disease. The lack of clinical information on eyes donated to research frequently limits the scope and accuracy in study of these tissues. Spectral Domain Optical Coherence Tomography (SD-OCT) has been previously used to screen post-mortem retinal changes including age-related macular degeneration (AMD). There are currently no known reports that correlate pre- and post-mortem macular anatomy using SD-OCT on the same eye. The purpose of this study was to describe the features of donated post-mortem retinas and correlate the findings with pre-mortem examination of the same eye using SD-OCT and scanning laser ophthalmoscopy.
Methods: Twelve donated eyes including AMD (n=8), diabetic macular edema (n=3) and normal control (n=1) were examined. All eyes were retrieved within 24 h of donor death. After corneal harvest for transplantation, eye cups were fixed in 4% Paraformaldehyde (PAF) for 72 hours before storage in 2% PAF. Prior to imaging, anterior segment was removed. Four trans-ora serrata sutures were placed to prevent retinal dialysis. During imaging, the eyes were mounted in a flat-topped glass jar filled with 0.9% NaCl or PBS to minimize optical distortions. A 30 diopter handheld indirect lens was used to replicate optical properties. Heidelberg SD-OCT and scanning laser ophthalmoscopy were performed with standard clinical protocols. Student *t* test was used to compare pre- and post-mortem foveal and macular thickness.
Results: Intra-retinal layers were clearly detected on post-mortem OCT scans. Pre-mortem pathological changes including pigment epithelial detachments, drusen, geographic atrophy and intra-retinal cysts were well correlated with post-mortem scans. Fixation-related retinal detachment and loss of sub-retinal fluid were identified in post-mortem images. Adjusting for the detachment, higher foveal thickness (FT) and central macular thickness (CMT) were noted in post-mortem scans compared with pre-mortem images (FT 247.6μm vs.165.8μm, p=0.23; CMT: 387.8μm vs. 229.0μm, p=0.01).
Conclusions: SD-OCT can effectively image fixed post-mortem retinal tissues. Correlation of pre- and post OCT images as well as multicolor fundus imaging may potentially add significant morphological information to the post-mortem retinal research.
Commercial Relationships: Meidong Zhu, None; **Adil Syed**, None; **Andrew A. Chang**, None

Program Number: 5947 **Poster Board Number:** A0118
Presentation Time: 12:00 PM–1:45 PM
Optically Isolating Photoreceptors as AMD Biomarkers using Directional OCT
Brandon J. Lujan[1, 2], Bhavna Antony[2], H. Richard McDonald[1], Robert N. Johnson[1], J. Michael Jumper[1], Arthur D. Fu[1], Emmett Cunningham[1, 3], Sara J. Haug[1], Austin Roorda[2]. [1]West Coast Retina, San Francisco, CA; [2]School of Optometry and Vision Science Graduate Group, University of California, Berkeley, Berkeley, CA; [3]Ophthalmology, Stanford University, Palo Alto, CA.
Purpose: To use Directional Optical Coherence Tomography (D-OCT) to harness the directional reflectivity properties of photoreceptors in eyes with Age-related Macular Degeneration (AMD).
Methods: D-OCT of the Outer Retina in AMD (DOCTORA) is an ongoing IRB-approved one-year natural history study of 48 subjects with drusen and geographic atrophy (GA) and 25 control subjects. A D-OCT acquisition protocol using Cirrus HD-OCT with multiple image sets obtained through multiple pupil entry positions was performed at baseline and every three months. Custom MATLAB analysis was then used to delineate and measure the outer nuclear layer (ONL) and Henle fiber layer (HFL) thicknesses from cross-sectional image sets and volumes from multiple macular cube sets. Custom registration, normalization, and display software was used to visualize reflectivity changes in composite D-OCT images. Visual acuity, fundus photography and autofluorescence measures were compared with D-OCT findings.
Results: D-OCT image sets were successfully acquired by multiple OCT operators using a standardized protocol. 65% (92/142) of baseline cross-sectional D-OCT sets could be successfully registered and analyzed for directional optical effects using a fully automated approach. 95% (132/142) had at least two cross-sectional scans that could be registered using a semi-automated approach. Unambiguous differentiation of ONL and HFL was possible in all registered scans. Increased visualization of the ONL/HFL boundary in the quadrant contrateral to the pupil entry position occurred in each macular cube, which could be integrated to provide average ONL and HFL

measurements within the central 5 mm of the macula. Baseline mean (SD) ONL volume (mm^3) for control eyes was 2.24 (0.18), for drusen eyes was 2.26 (0.18) and for GA eyes was 2.13 (0.29), and were 71%, 72% and 74%, respectively, of what would be measured had HFL been included. Compared to controls, the directional optical effects exhibited by the hyper-reflective photoreceptor bands was altered overlying drusen and near the edges of GA, indicating an abnormal orientation or disruption.

Conclusions: D-OCT provides independent cross-sectional and volumetric measurements of ONL and HFL. Visualization of photoreceptor orientation is also permitted, which may be an indicator of photoreceptor integrity. Analysis of these novel metrics in the DOCTORA study may reveal early imaging biomarkers of AMD progression.

Commercial Relationships: Brandon J. Lujan, 14378083; University of California, Berkeley (P), Allergan (R), Avalanche (C), Genentech, Inc. (F), Genentech/Roche (C), OCTMD, Inc. (S), Regeneron (R); **Bhavna Antony**, OCTMD, Inc. (C); **H. Richard McDonald**, None; **Robert N. Johnson**, None; **J. Michael Jumper**, None; **Arthur D. Fu**, None; **Emmett Cunningham**, None; **Sara J. Haug**, None; **Austin Roorda**, 14378083; University of California, Berkeley (P)

Support: Beckman Initiative for Macular Research, Foundation Fighting Blindness TA-CL-0613-0621-UCB

Program Number: 5948 **Poster Board Number:** A0119
Presentation Time: 12:00 PM–1:45 PM

Quantification of retinal blood flow in swept-source Doppler OCT

Maximilian G. Gräfe[1, 3], Leah S. Wilk[1, 3], Boy Braaf[1], Jan H. de Jong[3], Jelena Novosel[3, 2], Koenraad A. Vermeer[3], Johannes F. De Boer[1]. [1]Department of Physics and Astronomy, VU University, LaserLab, Amsterdam, Netherlands; [2]Faculty of Applied Science, Delft University of Technology, Delft, Netherlands; [3]Rotterdam Ophthalmic Institute, Rotterdam, Netherlands.

Purpose: Doppler OCT is an extension of standard OCT and is sensitive to moving particles due to signal decorrelation between consecutive A-lines, resulting in phase differences in the OCT signal. Based on Bayesian statistics the flow velocity is estimated quantitatively from these phase differences.

Methods: A high-speed fiber-based Doppler OCT system (Braaf *et al.*, Opt. Express 2011) was used to acquire repeated A-lines with a time interval of 2.5ms using a backstitched B-scan pattern that measures each lateral tissue location twice (Braaf *et al.,* Opt. Express 2012). Previously, Bouwens *et al*. (Opt. Let. 2014) used a model to directly calculate flow velocities from the mean and standard deviation of phase differences. Here, this model is extended to include influences of noise and a *maximum a posteriori* (MAP) estimator is introduced to determine flow velocities without the bias that occurs in the direct calculation.

Results: Figure 1 presents an *en face* plane from an age related macular degeneration (AMD) patient. It shows the removal of bias for flow estimation (grayscale is normalized to the highest flow). a) was processed with the method of direct calculation and b) with the MAP estimator. The backstitched scan pattern can be seen in the bias due to gradual changes in the background noise caused by revisitation error (i.e. the error in rescanning the same location). This induced an offset in method a) but the MAP estimator could isolate the flow from it. Figure 2 shows quantitative flow in the same *en face* plane processed with the MAP estimator to provide flow velocities. The determined flow velocities are within the expected range for retinal capillaries of 0.2 to 3.3 *mm/s*.

Conclusions: A new estimator was developed to quantify flow velocities of retinal capillaries directly from *in vivo* Doppler-OCT measurements. The method removes erroneous flow estimates due to revisitation errors and produces results that are in the expected velocity range. This method is potentially interesting for studying retinal pathology such as AMD.

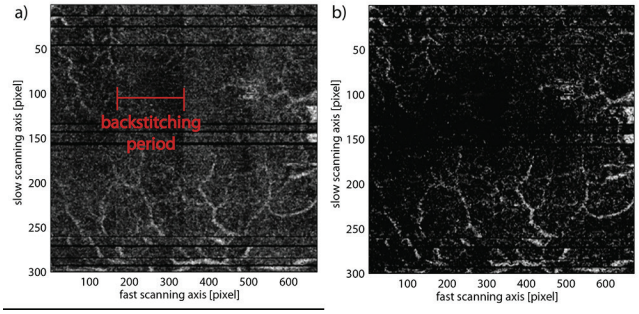

Flow estimation by a) direct flow calculation and (b) MAP estimator, showing removal of bias in the flow estimates due to backstitched scanning which appear as vertical stripes in the background signal. Black horizontal lines are motion artifacts which were taken out.

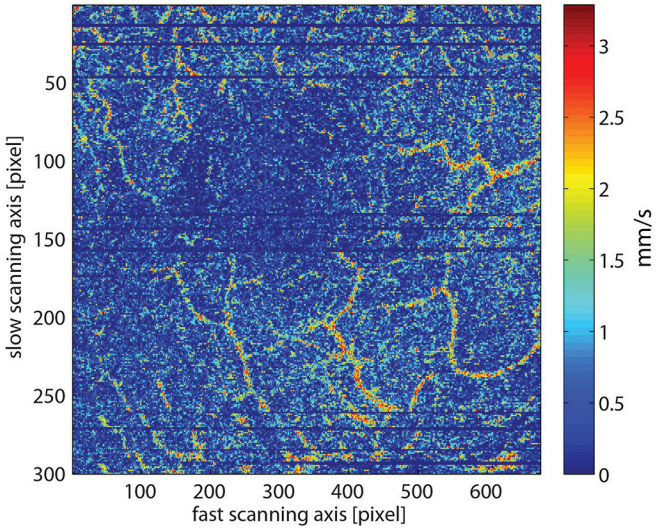

Three-pixel-layer *en face* plane of quantitative flow estimation with MAP. Flow velocity is displayed in false color.

Commercial Relationships: Maximilian G. Gräfe, None; **Leah S. Wilk**, None; **Boy Braaf**, None; **Jan H. de Jong**, None; **Jelena Novosel**, None; **Koenraad A. Vermeer**, None; **Johannes F. De Boer**, Heidelberg Enginering (F), Heidelberg Enginering (P), Nidek (P)

Support: STW Grant 12822

Program Number: 5949 **Poster Board Number:** A0120
Presentation Time: 12:00 PM–1:45 PM
***In vivo* imaging of human retinal microvasculature in sickle cell retinopathy using adaptive optics scanning light ophthalmoscope fluorescein angiography and offset pinhole imaging**
Nadim Choudhury[2, 1], Nikhil Menon[2, 1], Alexander Gan[2], Moataz M. Razeen[2], Alexander Pinhas[2, 1], Nishit Shah[2], Ronald C. Gentile[2, 4], Toco Y. Chui[2, 1], Alfredo Dubra[3, 5], Richard B. Rosen[2, 1]. [1]Icahn School of Medicine at Mount Sinai, New York, NY; [2]Department of Ophthalmology, New York Eye and Ear Infirmary of Mount Sinai, New York, NY; [3]Department of Ophthalmology, Medical College of Wisconsin, Milwaukee, WI; [4]Department of Ophthalmology, Winthrop University Hospital, Mineola, NY; [5]Department of Biophysics, Medical College of Wisconsin, Milwaukee, WI.
Purpose: Purpose: To detect and monitor microvascular changes cross-sectionally and longitudinally in patients with sickle cell retinopathy (SCR) using adaptive optics scanning light ophthalmoscope (AOSLO) fluorescein angiography (FA) and offset pinhole (OP) imaging.
Methods: The maculae of 7 patients (mean age 39, range 23-56) and 25 control subjects (mean age 27, range 21-54) were imaged using AOSLO FA and OP. AOSLO FA images were montaged to create a 6x6 degree perfusion map; OP images created a structural map of the vessels both perfused and non-perfused. In 2 subjects, longitudinal imaging was performed 2 and 3 times, respectively, with 6-8 months between sessions to assess vasculopathic changes over time. Quantitative analysis including vessel density and capillary tortuosity index (TI) within 100 μm of the foveal avascular zone (FAZ) margin, FAZ area and perimeter, and perifoveal intercapillary width (PICW) were quantified using custom MATLAB programs.
Results: All patients showed multiple vasculopathic features including microaneurysms, non-perfused vessels, vessel looping, and tortuous vessels. The SCR group had significantly larger FAZ area and perimeter than the controls. While mean vessel density was found to be lower in the SCR group compared to healthy controls, this difference was not significant (mean 32.54±5.83 vs. 33.40±3.71 mm^{-1}, d_f=30, p=0.63). PICW was significantly larger in SCR (93±21 vs 77±10μm, d_f=30, p=0.01). The mean TI in SCR patients was significantly higher than that of controls (1.56±0.61 vs. 1.17±0.09, d_f=30, p=0.003). Quadrant analysis for TI yielded statistically significant differences in all quadrants except the superior between SCR and controls. Longitudinal imaging in SCR patients revealed vascular changes that included recanalization, vessel loop formation and remodeling in a span of 6-8 months.
Conclusions: AOSLO FA and OP revealed microvascular changes both cross-sectionally and longitudinally. Quantitative measures including TI within 100 microns and PICW may be useful in future studies to monitor SCR patients.
Commercial Relationships: Nadim Choudhury, None; **Nikhil Menon**, None; **Alexander Gan**, None; **Moataz M. Razeen**, None; **Alexander Pinhas**, None; **Nishit Shah**, None; **Ronald C. Gentile**, Alcon (Vitreoretinal) (C), Genentech (F), Quark (F), Regeneron (F); **Toco Y. Chui**, None; **Alfredo Dubra**, Canon USA Inc. (C), RPB Career Development Award (F), US Patent 8,226,236 (P); **Richard B. Rosen**, Advanced Cell Technologies (C), Allergan (C), Carl Zeiss Meditech (C), Clarity (C), OD-OS (C), Opticology (I), Optovue (C)
Support: Marrus Family Foundation, Wise Family Foundation, Glaucoma Research Foundation Catalyst for a Cure, RPB Career Development Award.

Program Number: 5950 **Poster Board Number:** A0121
Presentation Time: 12:00 PM–1:45 PM
Individual Retinal Capillary Network Visualization on Optical Coherence Tomography Angiography Based on Retinal Layer Segmentation
Masanori Hangai[1], Takuhei Shoji[1], Takeshi Katsumoto[1], Shin Yoneya[1], Yasuhiro Furuuchi[2], Masaaki Hanebuchi[2]. [1]Ophthalmology, Saitama Medical University, Iruma, Japan; [2]NIDEK Co., Ltd., Gamagori, Japan.
Purpose: Retinal capillary system is comprised of four capillary networks. The purpose of this study was to develop a method to visualize each of the four capillary networks using optical coherence tomography (OCT) angiography technology.
Methods: Raster scans of 256A-Scan×256B-Scan by spectral-domain OCT (SD-OCT) were repeated four times within the 4.5 mm × 4.5 mm square macular region. Three-dimensional angiographic images were reconstructed by a motion-contrast method from the four data set. Automated layer boundary segmentation was performed on the intensity-based OCT images generated from the same data set. Angiographic images between the posterior boundary of and *x*-pixel (1 pixel= 4.2 μm) anterior line of the retinal nerve fiber layer (RNFL) were defined as RNFL capillary plexus (RNFLP). Angiographic images between the two lines *y*-pixel, anterior and posterior to the anterior boundary of the inner nuclear layer (INL) were defined as intermediate capillary plexus (ICP). Angiographic images between the two lines *z*-pixel, anterior and posterior to the posterior boundary of the INL were defined as deep capillary plexus (DCP). Angiographic images between RNFLP and ICP were defined as superficial capillary plexus (SCP). Visualization of capillary patterns were compared by changing the number of *x*, *y*, and *z* pixels in ten normal eyes.
Results: Images of the four capillary networks showed distinct capillary patterns. A complete image of RNFLP was obtained when $x \geq 3$ pixels. Even if the number of *x*-pixels was increased, no capillary patterns were obtained in the parafoveal region and temporal raphe. SCP, ICP and DCP showed dense mesh patterns, which were different among the three networks. However, a partial overlap of capillary patterns of ICP was observed with that of SCP, and an overlap of some capillary patterns of SCP was observed with that of ICP. These partial overlaps changed with the number of *y*, but it did not disappear. In contrast, little overlap of the other plexus was found in the DCP. More than seven pixels in *z* were required to obtain a complete image of DCP.
Conclusions: Visualization of individual retinal capillary networks was possible based on segmentation of layer boundaries. No visualization of capillary patterns of RNFLP in the parafovea and temporal raphe and overlaps of partial capillary signals between SCP and ICP need to be addressed.
Commercial Relationships: Masanori Hangai, Nidek (C), Nidek (F); **Takuhei Shoji**, None; **Takeshi Katsumoto**, None; **Shin Yoneya**, Nidek (C), Nidek (F); **Yasuhiro Furuuchi**, Nidek (E); **Masaaki Hanebuchi**, Nidek (E)

Program Number: 5951 **Poster Board Number:** A0122
Presentation Time: 12:00 PM–1:45 PM
Luminance flicker-induced retinal venule dilation is improved by euglycemic clamp in type 1 diabetes
Jonathan E. Noonan[1], Glenn M. Ward[3, 4], Ryan Man[2], Ecosse L. Lamoureux[1, 2]. [1]Ophthalmology, Centre for Eye Research Australia, Melbourne, VIC, Australia; [2]Singapore Eye Research Institute, Singapore, Singapore; [3]Endocrinology and Diabetes, St Vincent's Hospital, Melbourne, VIC, Australia; [4]Clinical Biochemistry, St Vincent's Hospital, Melbourne, VIC, Australia.

Purpose: Luminance flicker-induced retinal vasodilation is reduced in type 1 diabetes. Whether this relates to short-term glycemic control is unclear. We studied the effect of euglycemic clamp (normal glucose levels with insulin and glucose infusions) on these responses in people with type 1 diabetes.
Methods: 12 otherwise healthy adult non-smokers with type 1 diabetes and no known complications were studied. Retinal imaging was performed with the Dynamic Vessel Analyzer (DVA, IMEDOS, Germany) after an overnight fast and repeated after 1 h of insulin infusion (6 pmol/kg/min; Actrapid, Novo Nordisk, Australia) and 30 min of euglycemia (6 ±1 mmol/l). Arteriole and venule calibers were measured in units (MU) under green light (130 cd/m^2) at a rate of 25 Hz. Responses to 12.5 Hz luminance flicker were recorded from the mean of 3 consecutive intervals of 100 sec: 30 sec of constant light, 20 sec of flicker and 50 sec of constant light. Repeated tests used the same vessels. Within-subject changes in pre-flicker calibers, maximum relative dilations and area under the curve (AUC) during flicker were compared by ANOVA.
Results: Subjects were (mean [standard deviation]) aged 25.5 (5.9) years with 11.0 (7.5) years of diabetes. From baseline to euglycemia, plasma glucose levels decreased from 8.4 (3.6) mmol/l to 6.1 (0.8) mmol/l (P = 0.004) and insulin levels increased from 64.6 (24.3) pmol/l to 333.6 (63.1) pmol/l (P < 0.001), respectively. Pre-flicker arteriole and venule calibers were unchanged between tests (both P > 0.05). From baseline to euglycemia, arteriole maximum dilations were 3.2 (2.4) % and 3.6 (2.4) %, while AUC were 31.2 (32.3) % x sec and 35.8 (32.1) % x sec, respectively (Figure 1**;** both P > 0.05). However, corresponding venule maximum dilations were 3.3 (3.4) % and 5.0 (4.1) % (P = 0.002), and AUC were 15.9 (44.1) % x sec and 44.6 (50.8) % x sec (Figure 2; P = 0.001), respectively.
Conclusions: Euglycemic clamp improves luminance flicker-induced retinal venule dilation in type 1 diabetes. Arteriole responses are not significantly affected. Glucose normalization with insulin may improve retinal blood flow regulation in type 1 diabetes.

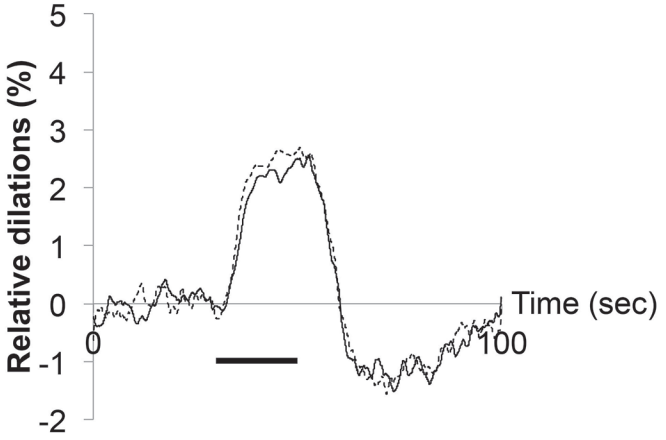

Figure 1. Mean relative arteriole dilations at baseline (solid line) and euglycemia (dashed line). Black bar indicates flicker.

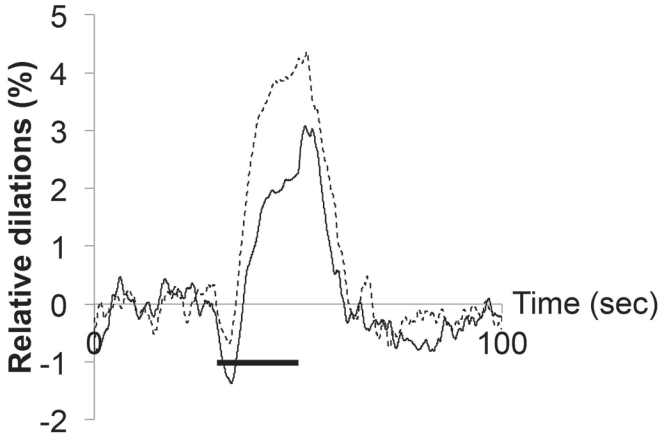

Figure 2. Mean relative venule dilations at baseline (solid line) and euglycemia (dashed line). Black bar indicates flicker.
Commercial Relationships: Jonathan E. Noonan, None; **Glenn M. Ward**, None; **Ryan Man**, None; **Ecosse L. Lamoureux**, None
Support: JDRF (Australia) Pilot and Feasibility Grant 290591

Program Number: 5952 **Poster Board Number:** A0123
Presentation Time: 12:00 PM–1:45 PM
The application of optical coherence tomography angiography in diabetic retinopathy
Pearse A. Keane[1], Dawn A. Sim[2], Rupesh Agrawal[4], Nicholas Koutramanos[2], Javier Zarranz-Ventura[5], Marcus Fruttiger[3], Catherine A. Egan[1], Adnan Tufail[1]. [1]NIHR Biomedical Research Centre for Opht, Moorfields Eye Hospital NHS Foundation Trust, London, United Kingdom; [2]Medical Retina, Moorfields Eye Hospital NHS Foundation Trust, London, United Kingdom; [3]Institute of Ophthalmology, University College London, London, United Kingdom; [4]Ophthalmology, Tan Tock Seng Hospital, Singapore, Singapore; [5]Institut Clínic d'Oftalmologia, Hospital Universitario Sagrat Cor, Barcelona, Spain.
Purpose: To investigate the parafoveal vessel density in diabetic retinopathy using optical coherence tomography (OCT) angiography (Avanti Angiovue SDOCT (Optovue, Inc. Fremont, CA, USA).
Methods: OCT angiography images were acquired from normal subjects and patients with diabetic retinopathy within a 3x3mm area of the central macula. The flow imaging was based on split-spectrum amplitude decorrelation angiography (SSADA), which can assess the vasculature in distinct layers of the retina. The layers assessed were the superficial retinal vascular plexus, deep retinal vascular plexus, avascular outer retina, and choriocapillaris. Parameters quantified include the area of the foveal avascular zone (FAZ) (mm^2), parafoveal vessel density (%), and parafoveal vessel flow to no flow index.
Results: A total of 60 eyes were included; 30 eyes from normal subjects and 30 eyes with DR. A marked difference in parafoveal vessel density was observed between normal (49.1 ± 11.2%) and eyes with diabetic retinopathy (36.1 ± 11.0%) (P = .0001) in the superficial retinal vascular plexus. This was also observed in the deep retinal vascular plexus (Normal: 39.6 ± 14.0% vs diabetic retinopathy: 22.9 ± 10.0%) (P=0.001), and choriocapillaris (Normal: 86.9 ± 9.6% vs diabetic retinopathy: 77.6 ± 13.2%) (P=0.01). The FAZ and parafoveal flow index was significantly different only in the superficial and deep retinal vascular plexi.
Conclusions: OCT angiography has for the first time provided an insight into the characteristics of perfusion in all layers of the retina. Although the FAZ is an established parameter in determining the severity of diabetic retinopathy, we observed that parafoveal vessel

density, in the retina and choriocapillaris may be more indicative of disease.
Commercial Relationships: Pearse A. Keane, None; **Dawn A. Sim**, None; **Rupesh Agrawal**, None; **Nicholas Koutramanos**, None; **Javier Zarranz-Ventura**, None; **Marcus Fruttiger**, None; **Catherine A. Egan**, None; **Adnan Tufail**, None

Program Number: 5953 **Poster Board Number:** A0124
Presentation Time: 12:00 PM–1:45 PM
Feasibility of automated interface segmentation of Cirrus HD-OCT data in normal and mild non proliferative diabetic retinopathy eyes
Torcato Santos[1], Antonio Correia[1], Catarina A. Neves[2], Christian Schwartz[2], Telmo Miranda[1], Ana Rita Santos[2], Jose G. Cunha-Vaz[3]. [1]Centre of New Technologies for Medicine, Association for Innovation and Research on Light and Image, Coimbra, Portugal; [2]Coimbra Ophthalmology Reading Centre, Association for Innovation and Biomedical Research on Light and Image, Coimbra, Portugal; [3]Association for Innovation and Biomedical Research on Light and Image, Coimbra, Portugal.
Purpose: Implementation and validation of a graph based segmentation algorithm on Optical Coherence Tomography (OCT) acquired data from eyes with preserved retinal structure, using normal control and mild Non Proliferative Diabetic Retinopathy (NPDR) populations.
Methods: The graph theory segmentation algorithm in [1] was implemented to automatically identify 8 retinal interfaces namely Vitreous to Inner Limiting Membrane (ILM), Retinal Nerve Fiber to Ganglion Cell Layers, Inner Plexiform (IPL) to Inner Nuclear Layers (INL), INL to Outer Plexiform Layer (OPL), OPL to Outer Nuclear Layer (ONL), ONL to Inner Segment (IS), Outer Segment to Retinal Pigment Epithelium (RPE) and RPE to Choroid. The algorithm was applied on Cirrus HD-OCT (Carl Zeiss Meditec, Dublin, CA, USA) acquired data from 86 eyes of 47 healthy volunteers aged from 23 to 55 years (m±SD: 38.30±9.10) and from 72 eyes of 72 NPDR patients, including subclinical and clinical macular edema (DRCRnet criteria), aged from 39 to 75 years (m±SD: 60.01±8.70).
Results: Root mean square errors (RMSE) between automatic and human grader segmentations for healthy volunteers and for NPDR patients are of the same order of magnitude. Larger RMSE were found at the OS/RPE interface ranging from 3.97 to 16.61 (m±SD: 6.92±2.21) [μm] and from 0.66 to 17.76 (m±SD: 4.24±2.69) [μm] for healthy subjects and for NPDR patients respectively. Interfaces at the Central Sub Field have larger RMSE relatively to other ETDRS areas, ranging from 2.58 to 9.02 [μm] and from 0.79 to 8.50 [μm] for healthy subjects and for NPDR patients respectively. Lower RMSE were found at the outer rings for all interfaces with the exception of the vitreous/ILM and ONL/IS for healthy volunteers and vitreous/ILM and IPL/INL for NPDR patients.
Conclusions: RMSE between automatic and human grader segmentations are close to the device 5 μm axial resolution in tissue which makes this segmentation algorithm well suited for detecting individual retinal layer changes in situations where the retinal structure is well preserved, such as mild NPDR, contributing to identify the relative role of the different retinal cells in the retinopathy development.
[1] Li K., Wu X., Chen D., Sonka M., "Optimal Surface Segmentation in Volumetric Images – A Graph-Theoretic Approach", IEEE Trans. Pattern Analysis and Machine Intelligence, vol. 28, no. 1, pp. 119-134, January 2006.
Commercial Relationships: Torcato Santos, None; **Antonio Correia**, None; **Catarina A. Neves**, None; **Christian Schwartz**, None; **Telmo Miranda**, None; **Ana Rita Santos**, None; **Jose G. Cunha-Vaz**, Carl Zeiss Meditec (C)
Clinical Trial: NCT01145599

Program Number: 5954 **Poster Board Number:** A0125
Presentation Time: 12:00 PM–1:45 PM
Three-dimensional vascular remodeling in inner nuclear layer using swept-source optical coherence tomography in diabetic retinopathy
Tomoaki Murakami, Yoko Dodo, Kiyoshi Suzuma, Akihito Uji, Shin Yoshitake, Masahiro Fujimoto, RIMA GHASHUT, Rina Yoza, Nagahisa Yoshimura. Ophthalmology & Visual Sciences, Kyoto Univ Grad Sch of Med, Kyoto, Japan.
Purpose: As one of microvascular complications by diabetes, diabetic retinopathy (DR) is accompanied by the remodeling of retinal capillaries, i.e., microaneurysms, intraretinal microvascular abnormalities (IRMA), and nonperfused areas (NPA). In this study, we evaluated the morphologies and location of deep INL capillary network in DR.
Methods: We retrospectively reviewed 42 eyes of 31 patients suffering from DR (6 eyes with no apparent retinopathy, 4 with mild NPDR, 9 with moderate NPDR, 9 with severe NPDR, and 16 with PDR) on whom 3x3mm volume scans of sufficient quality were obtained using swept-source optical coherence tomography (SS-OCT; DRI OCT-1, Topcon). After B-scan images were aligned by the flattening using the border between inner plexiform layer (IPL) and inner nuclear layer (INL), en face OCT images were constructed by the average of three pixels in z-axis in order to delineate the deep INL capillary network. We then counted the pixels (1 pixel = 2.6μm) from Henle's layer to deep INL capillary network in order to measure the distance.
Results: Eyes with no apparent retinopathy had the homogeneous diameter and density of deep INL capillary network, whereas such capillaries in eyes with DR showed the heterogeneity in the diameter and density. Eyes with DR but not CSME tended to have larger distances between Henle's layer and deep INL capillary network than those with no apparent retinopathy, but without statistical significance (4.6±1.4 pixels vs 6.1±2.8 pixels; p=0.208). Especially, the distances were larger in eyes with PDR than those with NPDR (5.1±1.9 pixels vs. 7.3±3.4 pixels; p=0.037). In eyes with CSME, cystoid spaces reside mainly in INL and OPL. The deep INL capillary network was delineated within the septa between cystoid spaces in INL, but not beneath them. The areas with cystoid spaces in INL were accompanied with the larger distances than those without such cystoid spaces (24.2±8.8 vs. 5.2±1.6 pixels; p<0.001).
Conclusions: En face images of SS-OCT showed three-dimensional vascular remodeling in the deep INL capillary network of DR.
Commercial Relationships: Tomoaki Murakami, None; **Yoko Dodo**, None; **Kiyoshi Suzuma**, None; **Akihito Uji**, None; **Shin Yoshitake**, None; **Masahiro Fujimoto**, None; **RIMA GHASHUT**, None; **Rina Yoza**, None; **Nagahisa Yoshimura**, None

Program Number: 5955 **Poster Board Number:** A0126
Presentation Time: 12:00 PM–1:45 PM
***In Vivo* Characterization of Retinal Vascularization Morphology Using Optical Coherence Tomography Angiography**
Bruno Lumbroso[1], Cristina M. Savastano[2, 1], Marco Rispoli[3, 1]. [1]Centro Italiano Macula, Rome, Italy; [2]Ophthalmology, Catholic University, Rome, Italy; [3]"Nuovo Regina Margherita" Hospital, Rome, Italy.
Purpose: To evaluate retinal vessel morphology using Split-spectrum Amplitude-Decorrelation Angiography with Optical Coherence Tomography (SSADA-OCT) in healthy eyes.

Methods: Fifty-two eyes of 26 healthy volunteers (age range from 35 to 48 years old; mean age 41.94 years; SD: ± 4.13) were evaluated by OCT-angiography in the macular region. The protocol acquisition consisted of a 216 x 216 A-scan that was repeated five times in the same position, in 3x3 mm centered into the fovea.
Results: All 52 eyes showed two separate vascular networks in the inner retina: the *superficial network,* located in the nerve fiber layer and in the ganglion cell layer, and the *deep network,* detected in the outer plexiform layer. The superficial and deep networks showed interconnections of vertical vessels. The reference planes to observe the two networks were defined, respectively, at 60 µm, with an inner limiting membrane reference (6 µm offset) and 30 µm with an inner plexiform layer reference (60 µm offset).
Conclusions: OCT-Angiography can separately detect the superficial vascular and the deep vascular networks. These networks are overlaid and seem to be fused when seen with standard angiographies. Furthermore, OCT-Angiography technology allows for the visualization of abnormal blood column and vessel wall details.
Commercial Relationships: Bruno Lumbroso, None; **Cristina M. Savastano**, None; **Marco Rispoli**, None

Program Number: 5956 **Poster Board Number:** A0127
Presentation Time: 12:00 PM–1:45 PM

Characterization of retinal structure and diagnosis of peripheral acquired retinoschisis using high-resolution ultrasound B-scan
Nathan V. Harms[1], Aniruddha Agarwal[1], Shan Fan[1], Alessandro Invernizzi[2], Diana V. Do[1], Quan Nguyen[1], Yasir J. Sepah[1].
[1]Ophthalmology, University of Nebraska Medical Center, Omaha, NE; [2]Ophthalmology, University of Milan, Luigi Sacco Hospital, Milan, Italy.
Purpose: Using conventional B-scan, it may not be possible to differentiate individual retinal layers to distinguish retinoschisis (RS) from retinal detachment (RD). We performed a retrospective study to report the ability of high-resolution ultrasonography (USG) B-Scan in differentiating between acquired RS and RD, and compared the findings with spectral-domain optical coherence tomography (SD-OCT).
Methods: Patients with acquired peripheral RS and RD undergoing imaging with high resolution B-scan USG and SD-OCT were included in the study. RS was considered in the presence of an immobile, dome-shaped visible elevation of the peripheral retina. SD-OCT images were obtained with the Spectralis OCT. A 20°×15° horizontal raster-line scan, encompassing the attached and detached retina was obtained for each patient. B-scan USG was performed using Ellex Eye Cubed ®. Descriptive analysis was performed on the images obtained by high-resolution B-scan USG and SD-OCT to identify various retinal layers.
Results: Six eyes of 5 patients (2 males) with RS, 7 eyes of 4 patients (3 males) with RD and 1 eye of a patient with schisis-detachment were included in the study. In all eyes of patients with RS, the attached outer retina demonstrated the presence of two hyper-reflective layers corresponding to the outer plexiform layer (OPL) and retinal pigment epithelium (RPE). Eyes with RD demonstrated two hyper-reflective layers in the detached portion, corresponding to the nerve fiber layer and OPL, whereas the attached portion demonstrated the presence of the third hyper-reflective layer, i.e. RPE (figure). These findings correlated well with SD-OCT.
Conclusions: Analysis of retinal layers on high-resolution USG B-scan may allow precise differentiation of acquired RS from RD by identification of various retinal layers. These findings correlate well with SD-OCT.

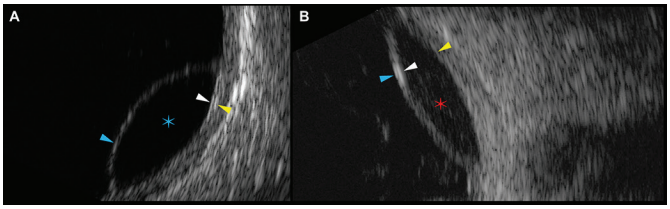

High-resolution ultrasound (USG) B-scan of eyes with (A) RS and (B) RD. (A) shows that eyes with RS demonstrate a thin single hyper-reflective line representing RNFL (blue arrowhead). Schisis cavity is marked by a blue asterisk. The attached OPL and RPE layers are shown with a white and yellow arrowhead. (B) shows that eyes with RD demonstrate the presence of two hyper-reflective lines representing RNFL and OPL (blue and white arrowheads). The red asterisk marks subretinal space overlying RPE layer, which is attached (yellow arrowhead)
Commercial Relationships: Nathan V. Harms, None; **Aniruddha Agarwal**, None; **Shan Fan**, None; **Alessandro Invernizzi**, None; **Diana V. Do**, None; **Quan Nguyen**, None; **Yasir J. Sepah**, None

Program Number: 5957 **Poster Board Number:** A0128
Presentation Time: 12:00 PM–1:45 PM
The Range of Foveal Avascular Zone (FAZ) Size and Vessel Density Around the FAZ in Healthy Eyes as Measured from OCT Angiography En-Face Images
Michal Laron[1], Mary K. Durbin[1], Lin An[1], Utkarsh Sharma[1], Renee W. Lamb[1], Jose G. Cunha-Vaz[2]. [1]R&D, Carl Zeiss Meditec, Inc, Dublin, CA; [2]AIBILI and Faculty of Medicine, University of Coimbra, Coimbra, Portugal.
Purpose: To characterize the range of FAZ size and vessel density around the FAZ in healthy eyes, and compare manual versus automated FAZ measurements from OCT angiography en face images at different retinal layers.
Methods: Three OCT angiography scans were performed on each of 22 healthy subjects. The range of subjects' age was 21-63 years (mean±SD; 40±10.7), and best corrected visual acuity was 20/25 or better. OCT field was 3x3 mm and vascular information was extracted by repeating each b-scan several times while evaluating change in contrast between consecutive b-scans at the same location. The average area and perimeter of FAZ in both the superficial retinal layer (SRL) and the deeper retinal layer (DRL), was calculated both manually and by using an automated algorithm.
Results: The range of SRL FAZ area was 0.06-0.53/0.12-0.49 mm^2 (automated/manual). DRL range was 0.38-0.89/0.29-1.00 mm^2. SRL FAZ perimeter range was 1.07-3.21/1.21-2.47 mm (automated/aanual), and DRL range was 2.68-4.52/1.90-3.55 mm. Regression analysis comparing manual vs. automated measurements of FAZ showed high correlations for area and perimeter of FAZ in both layers ($P<0.0001$ for all). The correlations were higher for SRL ($R^2=0.87/0.85$, area/perimeter), compared to DRL ($R^2=0.63/0.62$, area/perimeter). Vessel density in the SRL was on average 19% around the FAZ, increased to 47% in the 200-400µm zone, and further increased to 58% for eccentricities beyond 400µm from FAZ border. In DRL, vessel density was on average 23% around the FAZ, increased to 44% in the 200-400µm zone, and further increased to 54% for eccentricities beyond 400µm.
Conclusions: Our study shows that there is a large variability in size of the FAZ in the normal population. However, the reliable identification of the FAZ both in the SRL and DRL make it a new tool to follow progression of capillary closure in retinal vascular diseases.
Commercial Relationships: Michal Laron, Carl Zeiss Meditec, Inc. (E); **Mary K. Durbin**, Carl Zeiss Meditec, Inc. (E); **Lin An**, Carl

Zeiss Meditec, Inc. (E); **Utkarsh Sharma**, Carl Zeiss Meditec, Inc. (E); **Renee W. Lamb**, Carl Zeiss Meditec, Inc. (E); **Jose G. Cunha-Vaz**, Carl Zeiss Meditec, Inc. (C)

Program Number: 5958 **Poster Board Number:** A0129
Presentation Time: 12:00 PM–1:45 PM
Repeatability and Reproducibility of Quantifying Parafoveal Vessel Density in Normal Subjects with OCT-based Microangiography

Zhongdi Chu[1], Qinqin Zhang[1], Chieh-Li Chen[1], Fengyi Luo[1], Cecilia Lee[2], James L. Kinyoun[2], Ruikang K. Wang[1, 2]. [1]Bioengineering, University of Washington, Seattle, WA; [2]Ophthalmology, University of Washington, Seattle, WA.

Purpose: To demonstrate the reliability of OCT-based microangiography (OMAG) for non-invasive, label-free in vivo imaging of the retinal microvasculature in macular region of normal subjects and for the measurement of vessel density in central fovea and parafoveal quadrants.

Methods: A prospective, observational study was conducted with ten normal subjects (twenty eyes; age = 30.9±7.17). Each subject was scanned three times per eye with a Cirrus HD-5000 OCT-angiography prototype using OMAG scanning protocol. The retinal microcirculation was depicted as an *en face* image. Two masked graders performed segmentation of the resulting OMAG images, outlined the foveal avascular zone (FAZ) with ellipse or free-hand drawing approach and performed independent vessel density quantification. The parafoveal and foveal regions were outlined with circles of diameters of 2.5mm and 1.5mm; vessel density was calculated for central foveal region (FAZ excluded) and in quadrants for parafovea. Descriptive statistics, repeatability and reproducibility were calculated.

Results: The vessel density of defined sub-field varied among subjects (range of 0.136-0.288). The mean values of each sub-field were 0.223±0.022 for parafoveal superior quadrant, 0.22±0.022 for parafoveal inferior quadrant, 0.234±0.022 for parafoveal nasal quadrant, 0.23±0.024 for parafoveal temporal quadrant and 0.222±0.02 for central fovea. There were no statistically significant differences among four parafoveal quadrants, but statistically significant differences were observed between parafoveal nasal and central foveal regions (p = 3e-5) as well as between parafoveal temporal and central foveal regions (p = 0.0149). The measurements were reliable: the repeatability (%) was 9.7% (Sr = 0.021), the reproducibility (%) was 5.3% (SR = 0.012), and the intra-class coefficient (ICC) was 0.96 while the coefficient of variance was 5.4%.

Conclusions: OMAG is a noninvasive 3D imaging technique that can provide depth-resolved retinal microvasculature information with capillary level resolution in real-time. Blood flow distribution in macular region can be easily identified and allow repeatable and reproducible parafoveal vessel density measurements.

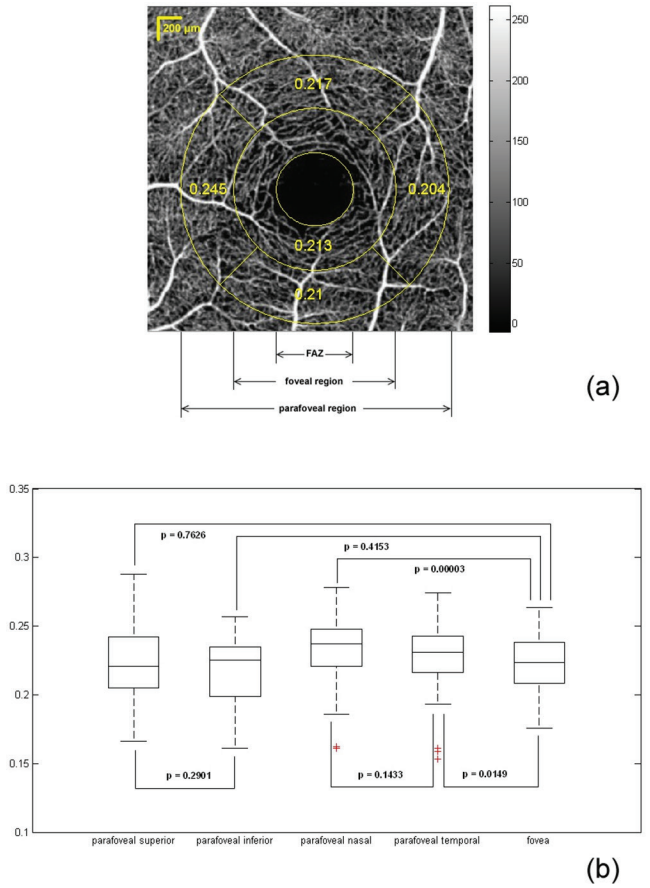

Fig.1 Vessel density quantification. (a) Illustration of vessel density measurement in defined sub-fields; (b) Box-and-whisker plot of vessel density measurement and correspongding p value.

Commercial Relationships: Zhongdi Chu, None; **Qinqin Zhang**, None; **Chieh-Li Chen**, None; **Fengyi Luo**, None; **Cecilia Lee**, None; **James L. Kinyoun**, None; **Ruikang K. Wang**, Carl Zeiss Meditec (F), Carl Zeiss Meditec (P)

Program Number: 5959 **Poster Board Number:** A0130
Presentation Time: 12:00 PM–1:45 PM
Reproducibility of Disorganization of the Retinal Inner Layers (DRIL) Grading Across Spectral Domain Optical Coherence Tomography (SDOCT) Model and Scan Types in Eyes with Diabetic Macular Edema (DME)

Marwan Abdulaal[1, 3], Michael M. Lin[1], Migil Ledesma[2], Cloyd Pitoc[2], Paolo S. Silva[1], Michael Cheney[1], Jan Lammer[4, 1], Tahera Doctor[1], Lloyd Paul Aiello[1, 3], Jennifer K. Sun[1, 3]. [1]Beetham Eye Institute, Joslin Diabetes Center, Boston, MA; [2]Philippine Eye Research Institute, Manila, Philippines; [3]Ophthalmology, Harvard Medical School, Boston, MA; [4]Department of Ophthalmology and Optometry, Medical University Vienna, Vienna, Austria.

Purpose: To evaluate reproducibility of DRIL evaluation in eyes with DME imaged by 2 SDOCT instruments (Zeiss Cirrus HD-OCT 4000D and Heidelberg Spectralis 6 mode) with high speed and high resolution settings.

Methods: A cross sectional study enrolled eyes with current or recently resolved (<3 month) center-involved DME (ciDME) defined using gender/machine specific values equivalent to time domain CST≥250µm. For each eye, 2 Cirrus (Macular Cube 512x128 [Cube]

and HD 5 Line Raster [5 Line]) and 2 Spectralis (20x20°, 49 B-scans, 16 ART Mean: high res [HR] and high speed [HS] settings) scans were acquired. The 1 mm area centered on the fovea was graded using customized MATLAB software for 7 B-scan substacks in HR, HS and Cube scans and all 5 B-scans for 5 Line scans. Presence and extent of DRIL, intraretinal cysts and cone outer segment tip (COST) visibility were determined. DRIL causes were assessed as either generalized inner retinal layer boundary blurring (blur), presence of intraretinal cysts crossing boundary lines (cysts) or hyperreflective foci (HR) obliterating layer demarcations.
Results: In 24 eyes of 18 patients, mean±SD CST was 360±94µm, 67% (N=16) had current and 33% (8) had recently resolved ciDME. Mean age was 61±15 years and 47% were female. Intraclass correlation coefficients (ICC) and 95% confidence limits (CL) between HR scans and each of the other scan types for extent of DRIL, DRIL cause, intraretinal cyst boundary area (horizontal x vertical extent), and COST visibility are reported in Table 1. ICCs were highest for overall DRIL extent, DRIL caused by blur or cysts, and cyst boundary area. Grading was most reproducible between HR and HS scans, followed by HR and Cirrus Cube scans.
Conclusions: Reproducibility for SDOCT parameters of DRIL and intraretinal cysts was high overall and excellent across OCT models and scan types, especially between Spectralis HR and HS scans. These data suggest that evaluation of DRIL and other SDOCT variables is feasible using these different OCT models and scan types in eyes with DME.

Variable	Spectralis HR vs Spectralis HS ICC (95% CL)	Spectralis HRvs Cirrus 512x128Cube ICC (95% CL)	Spectralis HRvs Cirrus 5 Line Raster ICC (95% CL)
DRIL Horizontal Extent	0.93 (0.88, 0.96)	0.84 (0.74, 0.91)	0.77 (0.64, 0.87)
DRIL Caused by Blur	0.97 (0.95, 0.98)	0.86 (0.76, 0.92)	0.77 (0.63, 0.86)
DRIL Caused by Cysts	0.95 (0.92, 0.97)	0.91 (0.84, 0.95)	0.89 (0.81, 0.94)
DRIL Caused by HR	0.73 (0.58, 0.84)	0.79 (0.66, 0.88)	0.67 (0.50, 0.81)
Cyst Boundary Area	0.97 (0.95, 0.98)	0.93 (0.88, 0.96)	0.95 (0.91, 0.97)
COST Visibility	0.91 (0.84, 0.95)	0.76 (0.62, 0.86)	0.59 (0.40, 0.76)

Table 1. ICCs and 95% CL for SDOCT parameter grading between scan types
Commercial Relationships: Marwan Abdulaal, None; **Michael M. Lin**, None; **Migil Ledesma**, None; **Cloyd Pitoc**, None; **Paolo S. Silva**, None; **Michael Cheney**, None; **Jan Lammer**, None; **Tahera Doctor**, None; **Lloyd Paul Aiello**, None; **Jennifer K. Sun**, Boston Micromachines (F), Genentech (F), Kowa (C), Novartis (C), Optovue (F), Regeneron (C)
Support: NEI 1R01EY024702-01, JDRF 2-SRA-2014-264-M-R, Eleanor Chesterman Beatson Childcare Ambassador Program Foundation Grant, Massachusetts Lions Eye Research Fund, Inc.

Program Number: 5960 **Poster Board Number:** A0131
Presentation Time: 12:00 PM–1:45 PM
VESGEN Analysis of Generational Branching Patterns in Arteries and Veins for Investigating Diabetic Retinopathy by Spectralis® Angiographic Imaging
Patricia A. Parsons-Wingerter[1], Krishnan Radhakrishnan[2], K V Chalam[3], Maria B. Grant[4]. [1]Space Biosciences Research Branch, NASA Ames Research Center, Moffett Field, CA; [2]Internal Medicine, University of Kentucky, Lexington, KY; [3]Ophthalmology, University of Florida, Jacksonville, FL; [4]Ophthalmology, Glick Eye Institute, Indiana University, Indianapolis, IN.

Purpose: We hypothesize that site-specific patterning within branching generations of arterial and venous trees in the human retina can be mapped and quantified by VESsel GENeration Analysis (VESGEN) software. Using images acquired by 30° Spectralis® fluorescein angiography (FA), we demonstrate that the methodology may be useful for analysis of longitudinal progression of diabetic retinopathy (DR).
Methods: The retina of a patient diagnosed with mild nonproliferative DR was photographed at 12.5µm/pixel with 30° Heidelberg Spectralis® imaging following fluorescein injection. Binary (black/white) vascular patterns of branching arterial and venous trees were extracted from the grayscale photograph (768768 pixels) as described previously for 50° FA (IOVS 2010, 51:498). The resulting arterial and venous images served as sole inputs to the VESGEN software. The vascular patterns were automatically mapped by VESGEN to generate vessel branching generations (G_x) and to quantitatively analyze them by computing numerous vascular parameters, including the densities of vessel length (L_v), area (A_v), number (N_v), and the fractal dimension (D_f). Results for the branching generations were further assigned by VESGEN into two groups of large (G_{1-3}) and small ($G_{\geq 4}$) vessels.
Results: L_{v1-3} and A_{v1-3} were 5.02E-4 µm/µm^2 and 4.50E-2 µm^2/µm^2 for large arteries, and 5.42E-4 µm/µm^2 and 4.85E-2 µm^2/µm^2 for large veins. For small arteries, $L_{v\geq 4}$ and $A_{v\geq 4}$ were 9.26E-4 µm/µm^2 and 3.37E-2 µm^2/µm^2, compared to 1.10E-3 µm/µm^2 and 4.41E-2 µm^2/µm^2 for small veins. Trends for A_v and L_v were confirmed by D_f and N_v. Agreement among these several key parameters reveal that the density of small veins was greater than that of small arteries.
Conclusions: Our study supports the future feasibility of VESGEN analysis for highly sensitive mapping and quantification of remodeling of retinal arterial and venous trees from clinical images obtained by 30° Spectralis® fluorescein angiography. The VESGEN mapping methodology will support evidence-based conclusions for ongoing longitudinal studies on how and where site-specific remodeling occurs and progresses within the human retina.
Commercial Relationships: Patricia A. Parsons-Wingerter, NASA (P); **Krishnan Radhakrishnan**, None; **K V Chalam**, None; **Maria B. Grant**, None
Support: NIH Grant NHLBI R01HL110170 and NASA 2012 NRA

Program Number: 5961 **Poster Board Number:** A0132
Presentation Time: 12:00 PM–1:45 PM
Novel patchy lesions in inner retinal layers of diabetic retinopathy using en face optical coherence tomography
Rina Yoza, Tomoaki Murakami, Akihito Uji, Kiyoshi Suzuma, Masahiro Fujimoto, Shin Yoshitake, Yoko Dodo, RIMA GHASHUT, Nagahisa Yoshimura. Kyoto University, Kyoto city, Japan.
Purpose: It have been reported that ganglion cells are degenerated in diabetic retinopathy (DR), which is supported by the clinical data using fundus imaging to some extent. We herein investigated the findings in the nerve fiber layer (NFL) and ganglion cell layer (GCL) of DR on the en face images of swept-source optical coherence tomography (SS-OCT).
Methods: Fifty eyes from 34 patients with DR were included in this study (10 eyes with each grade of international DR severity scale). We obtained three-dimensional images in 6x6mm centering the fovea using SS-OCT (DRI OCT-1, TOPCON). After individual B-scan images were aligned by the 'flattening' function using the border between NFL and GCL, we observed en face images constructed by 256 B-scan images. We characterized the patchy lesions which had both lower reflectivity than the surrounding areas in NFL and higher reflectivity in GCL.

Results: The patchy lesions in NFL and GCL had the various shapes on en face OCT images, and their areas were 0.125±0.057 mm^2 at the level of NFL. Most lesions resided within NFL and GCL, and did not show any findings in the corresponding areas on color fundus photography. We further investigated the association between findings on fluorescein angiography (FA) and OCT in 23 eyes on whom both images were obtained. Mild hypofluorescence was accompanied with retinal capillaries in the areas corresponding to 78 patchy lesions on OCT images, and typical nonperfused areas were depicted in 8 lesions. Eyes with moderate nonproliferative diabetic retinopathy (NPDR), severe NPDR, and proliferative diabetic retinopathy were accompanied with the patchy lesions (the numbers in the individual grades were 4.4±3.7, 3.3±3.7, and 4.3±4.8, respectively), compared to no such lesions in eyes with no apparent retinopathy or mild NPDR.
Conclusions: We characterized a novel finding, the patchy lesion, at the levels of NFL and GCL on en face OCT images in DR, most of which did not correspond to any fundus findings but to mild hypofluorescence on FA images.
Commercial Relationships: Rina Yoza, None; **Tomoaki Murakami**, None; **Akihito Uji**, None; **Kiyoshi Suzuma**, None; **Masahiro Fujimoto**, None; **Shin Yoshitake**, None; **Yoko Dodo**, None; **RIMA GHASHUT**, None; **Nagahisa Yoshimura**, None

Program Number: 5962 **Poster Board Number:** A0133
Presentation Time: 12:00 PM–1:45 PM
Analysis of the Bruch's Membrane/RPE Complex in Normal and Dry AMD Subjects with Avanti SD-OCT
Xingwei Wang, Ben K. Jang, Qienyuan Zhou. Optovue, Inc, Fremont, CA.
Purpose: To analyze the retinal pigment epithelium (RPE) elevation and choroid illumination pattern in normal and dry AMD subjects using Avanti SD-OCT (Optovue, Fremont, CA).
Methods: 20 normal subjects (age 26 to 60, 15 male and 5 female) and 19 dry age related macular degeneration - AMD patients (age 66 to 90, 7 male and 12 female) were enrolled following an IRB approved study protocol. The 19 dry AMD patients consist of 10 early AMD patients and 9 GA patients. One eye per subject were included in the study. Each subject had three repeated 3D OCT scans of 8mm x 8mm in scan filed with integrated motion correction technology (MCT). 117 scans were acquired excluding 6 scans (5.1%) due to poor signal or poor fixation, a total of 111 scans were included in the analysis.
Results: Areas of RPE elevation and increased choroid illumination were measured in the grid sectors of Early Treatment Diabetic Retinopathy Study (ETDRS) (Figure 1). For normal subjects, 93.3% (56/60) and 95% (57/60) of the total 60 scans have no detection of the RPE elevation and the increased choroid illumination, respectively. The (min, mean, max) of the detection areas (mm^2) in the total ETDRS region for RPE elevation and increased choroid illumination are (0.000, 0.016, 0.090) and (0.000, 0.056, 0.880), respectively. For early AMD subjects, the (min, mean, max) of the RPE elevation areas are (0.550, 1.133, 2.293) with the repeatability of 0.069 mm^2. For GA subjects, the (min, mean, max) of increased choroid illumination areas are (0.460, 6.180, 13.477) with the repeatability of 0.350 mm^2.
Conclusions: The analysis shows promising detection results for both normal and AMD subjects in Avanti SD-OCT system.

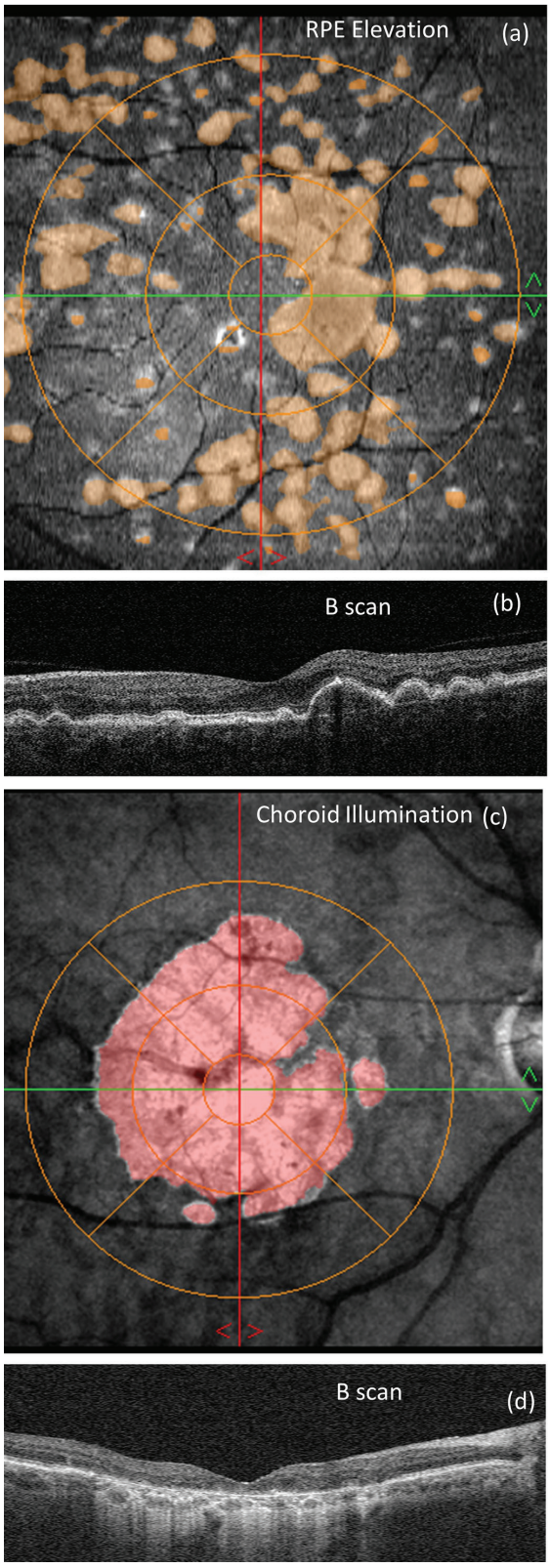

Figure 1: (a) Detected area of RPE elevation in an early AMD case. (b) B-scan OCT image at the green line of (a). (c) Detected area of increased choroid illuminaon in a GA case. (d) B-scan OCT image at the green line of (c).

Commercial Relationships: Xingwei Wang, optovue, Inc (E); **Ben K. Jang**, Optovue, Inc (E); **Qienyuan Zhou**, Optovue, Inc (E)

Program Number: 5963 **Poster Board Number:** A0134
Presentation Time: 12:00 PM–1:45 PM
Evaluation of Neovascularization Elsewhere using Optical Coherence Tomography based Microangiography
Mary K. Durbin[1], Scott Lee[2], Cecilia Lee[3], Qinqin Zhang[4], Patty Chung[2], Kasra Attaran Rezaei[3], Michal Laron[1], Lin An[1], Ruikang K. Wang[3, 4]. [1]R & D, Carl Zeiss Meditec, Inc, Dublin, CA; [2]East Bay Retina Consultants, Inc., Oakland, CA; [3]Department of Ophthalmology, University of Washington, Seattle, WA; [4]Department of Bioengineering, University of Washington, Seattle, WA.
Purpose: OCT based microangiography (OMAG) is a non-invasive imaging technique that allows 3D images of dynamic blood perfusion within the retina. This study describes the OMAG imaging characteristics of neovascularization elsewhere (NVE) in cases of proliferative diabetic retinopathy (PDR).
Methods: Three patients with PDR, diagnosed by fundus examination and fluorescein angiography (FA), were imaged with OMAG, and depth encoded en face images were generated, including an en face image located just internal to the internal limiting membrane (ILM). Clinical characteristics and funduscopic findings of NVE were correlated to OMAG images.
Results: Three cases were imaged, two with type 1 and one with type 2 diabetes. In one case, clinical exam revealed neovascularization elsewhere (NVE) in temporal macula of the left eye. OMAG of the left eye revealed multiple lesions that breached the ILM and blood flow was detected in all NVEs (Figure 1, left). In a second case, multiple NVEs appeared inactive on clinical exam, and OMAG revealed multiple NVEs without blood flow (Figure 1, right). In a third case, clinical exam showed new active neovascularization superotemporal and temporal to the macula. Late FA showed profuse leakage from both areas of NVE. OMAG confirmed the presence of a "bow-tie" shaped frond of neovascularization with active blood flow superotemporal to the macula and an irregular branching network also with active blood flow temporal to the macula.
Conclusions: This study highlights the OMAG characteristics of diabetic neovascularization elsewhere. With blood perfusion information, OMAG supports the clinical diagnosis of either active or inactive NVEs, suggesting that OMAG can provide information on PDR including the blood flow characteristics within the neovascular complex.

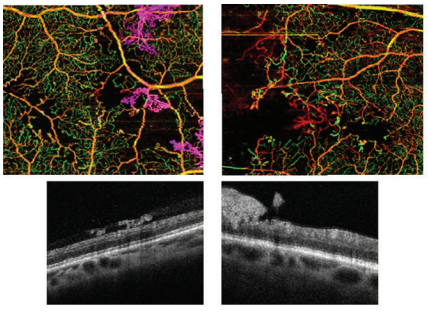

Depth encoded OMAG images of (top left) active NVE and (top right) inactive NVE, with (bottom) OCT intenstiy B-scans. Inner (red), deeper (green), and vessels outside the ILM (purple).
Commercial Relationships: Mary K. Durbin, Carl Zeiss Meditec, Inc. (E); **Scott Lee**, Carl Zeiss Meditec, Inc. (C); **Cecilia Lee**, None; **Qinqin Zhang**, Carl Zeiss Meditec, Inc. (R); **Patty Chung**, None; **Kasra Attaran Rezaei**, None; **Michal Laron**, Carl Zeiss Meditec, Inc. (E); **Lin An**, Carl Zeiss Meditec, Inc. (E); **Ruikang K. Wang**, Carl Zeiss Meditec, Inc. (R)

Program Number: 5964 **Poster Board Number:** A0135
Presentation Time: 12:00 PM–1:45 PM
Does pooling in fluorescence angiography correlate with cyst imaging in transverse section OCT?
Josef Pretzl, Nikolaus Luft, Michael Ring, Siegfried Priglinger, Matthias Bolz. Ophthalmology, Allgemeine Krankenhaus der Stadt Linz, Linz, Austria.
Purpose: Transverse section analysis (TSA) of optical coherence tomography (OCT) scans offers the opportunity to image the distribution of intraretinal cysts or subretinal fluid in a single en face image. Pooling is a phenomenon caused by dye accumulation in retinal cysts during a late phase fluorescence angiography. The aim of this study was to reveal if FA can be replaced by TSA scans in imaging retinal cysts in diabetic macular edema.
Methods: In 25 eyes of 25 patients with clinically significant diabetic macular edema a FA examination and OCT TSA scan at minute 5 were performed simultaneously using Spectralis HRA and OCT (Heidelberg engineering). Transverse section full retina analysis and FA images were then superimposed and correlated regarding (1) the location and (2) the planimetric dimension of intraretinal cyst formation in OCT and the area of pooling or hyperfluorescence in FA (MATLAB 2012a, The MathWorks). Furthermore, for each area of intraretinal fluid accumulation in OCT the source of leakage was analysed in both imaging techniques.
Results: There was no significant correlation between the location of intraretinal cysts in TSA images and visible pooling in FA images at minute 5. Further, there was no correlation between the planimetric dimension of intra-retinal cyst areas and detectable local pooling or hyperfluorescence areas in FA. The source of leakage was defined in FA images by detecting microaneurysms, capillary non-perfusion or capillary leakage depending on the individual edema type graded by the SAVE grading system. These changes in FA were not detectable in TSA images.
Conclusions: OCT transverse section analysis and FA offer complementary information and are not interchangeable in imaging intra-retinal cyst formation. TSA reveals the amount and location of intraretinal fluid accumulation in more detail than pooling or changes in fluorescence in FA. FA in contrast to TSA is capable to detect the individual source of leakage and cyst formation. Hence, it remains to be clarified if a combination of TSA and OCT angiography together can replace FA in certain cases of clinically significant diabetic macular edema.
Commercial Relationships: Josef Pretzl, None; **Nikolaus Luft**, None; **Michael Ring**, None; **Siegfried Priglinger**, None; **Matthias Bolz**, None

Program Number: 5965 **Poster Board Number:** A0136
Presentation Time: 12:00 PM–1:45 PM
Repeatability of retinal thickness measurements with fast 3D motion correction technology (MCT) in optical coherence tomography in normal subjects and retinal patients
Wei Feng, Ben K. Jang, Kent Pham, Qienyuan Zhou, Tony H. Ko. Optovue Inc, Fremont, CA.
Purpose: To evaluate repeatability of quantitative retinal thickness measurements with and without fast 3D motion correction in 30 normal subjects and 30 retinal patients.
Methods: Using Avanti SD-OCT system (Optovue, Inc.), 3 scan repeats with each collecting two pairs of orthogonal (fast x,

hereinafter FX and fast y, hereinafter FY) 3D volumes on the retina were performed on each subject. The scan area was 8x8mm^2 and matrix size was 320x320x640(widthxheightxdepth), with a sample resolution of 25x25x3.2 μm^3. One FX and one FY volume were fed into a modified and GPU-accelerated version of the motion correction technology (MCT) proposed by Kraus et al. [1]. The resulting MCT-corrected was used to quantitatively assess the retinal thickness map in 9 areas in the ETDRS grid. For comparison, the same analyses were performed on the selected FX volume. Multivariate analysis of variance with a linear model taking into account of 5 factors, including repeats, patient groups, retinal areas, subjects and processing methods, was performed on the measurements to assess repeatability and agreement between MCT and non-MCT corrected images.

Results: Motion artifacts in individual scan volumes were removed or significantly reduced in all cases with an average processing time of about 10 seconds. Figures 1 and 2 show motion correction for a normal subject and a retinal patient, respectively. It is seen that MCT was able to remove the motion artifacts in single scan volumes and achieve a much better SNR (red and green arrows). The difference in retinal thickness within ETDRS grid induced by repeats and processing methods (with or without MCT) were both insignificant (p=0.95 and p=0.88, respectively).

Conclusions: Our modified and GPU-accelerated motion correction technology was fast and able to remove most motion artifacts without impacting the repeatability of quantitative retinal thickness analysis.

[1] Kraus M et al. *Biomedical Optics Express* 2014;5(8):2591-2613

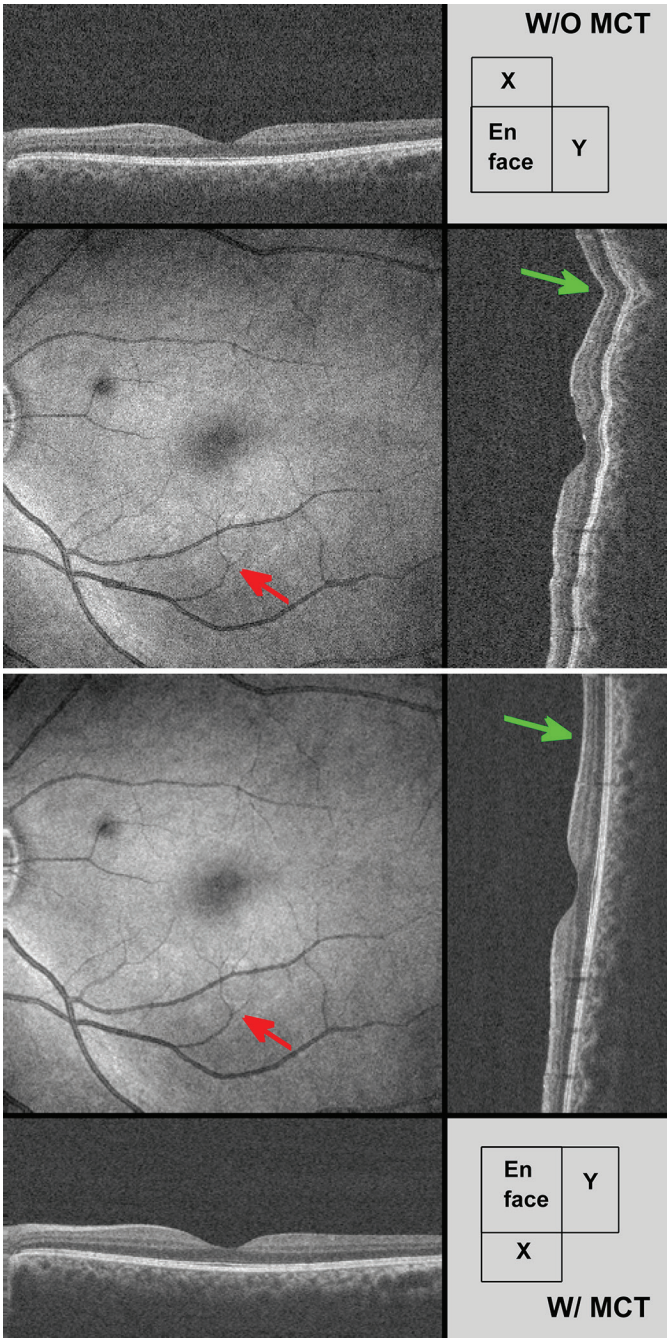

En face and central B scans for a normal subject with and without MCT. Red arrows point to clear SNR improvement in vessel delineation with MCT and green arrows point to MCT performance in central B scan.

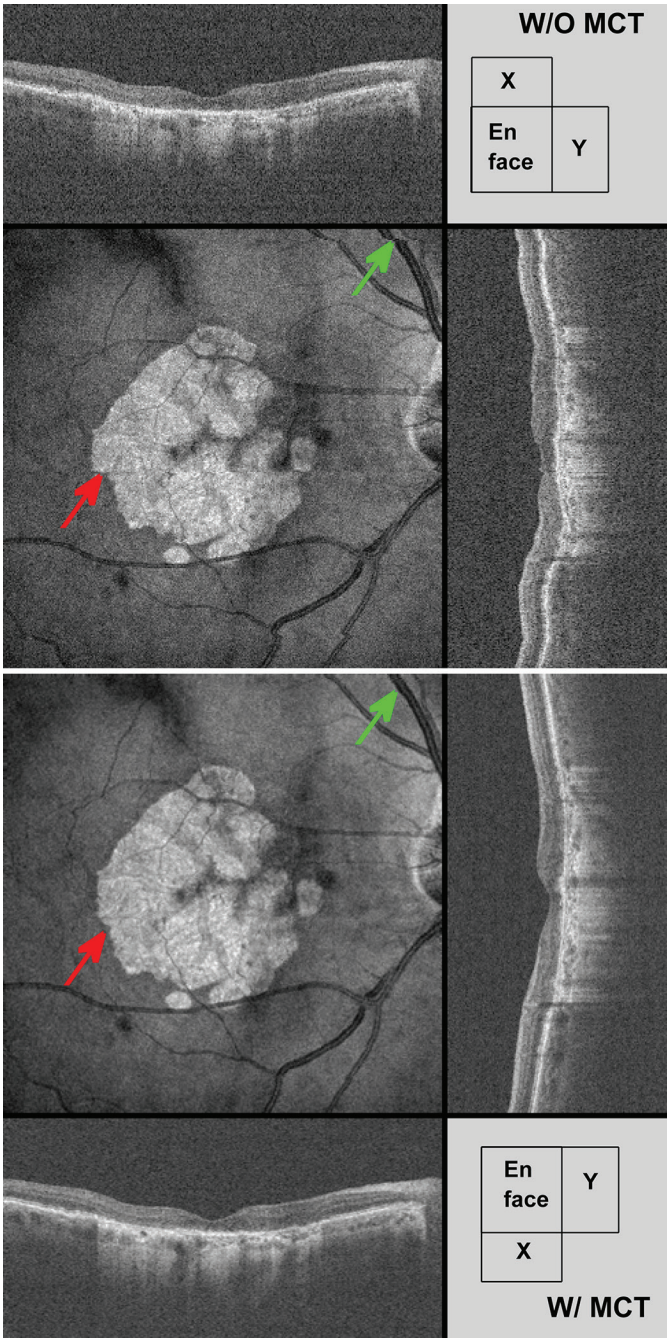

En face and central B scans for a retinal patient with and without MCT. Red and green arrows point to motion correction performance in en face image.

Commercial Relationships: Wei Feng, Optovue Inc (E); **Ben K. Jang**, Optovue (E); **Kent Pham**, Optovue (E); **Qienyuan Zhou**, Optovue (E); **Tony H. Ko**, Optovue (E)

Program Number: 5966 **Poster Board Number:** A0137
Presentation Time: 12:00 PM–1:45 PM

Anatomically-accurate graphing and flow modeling of the retinal vasculature using Doppler OCT and angiography

Conor Leahy[1], Harsha Radhakrishnan[1], Geoffrey Weiner[2], Jeffrey L. Goldberg[2], Vivek J. Srinivasan[1]. [1]Biomedical Engineering, University of California, Davis, Davis, CA; [2]Shiley Eye Center, University of California-San Diego, San Diego, CA.

Purpose: Normal functioning of the retina is dependent upon a sufficient supply of oxygen and other nutrients by a network of blood vessels. In this study, we present an optical coherence tomography (OCT) angiography-based graphing protocol for imaging and reconstructing the inner retinal vascular network over a field of view of 3 x 3 mm in the rat inner retina. Based on this data, we provide detailed and comprehensive characterization of the vascular branching patterns in the rodent inner retina.

Methods: Rat eyes were imaged with a 1300 nm spectral/Fourier domain OCT microscope. OCT angiography techniques were applied to enhance the contrast of the red blood cells (RBCs) within the vasculature. Additionally, flow velocity axial projections were obtained using Doppler OCT. A topological model of the inner retinal vascular network was obtained from the OCT angiography data using image processing techniques. By using experimentally-quantified flow in major retinal vessels as boundary conditions, the flow in each vessel branch down to the capillary level was inferred by modeling the vasculature as a resistive network.

Results: We present a 3D vectorized representation of the inner retinal vasculature, derived from OCT image data. We show computed vessel branch lengths and diameters, which are combined with the vectorized data to form a topologically accurate model of the retinal vasculature. We show capillary-level hemodynamics computed from this model, which could be directly cross-validated against other capillary speed and flow imaging metrics.

Conclusions: The image processing and modeling methods we have presented can yield accurate 3-D graphs that may be useful for general studies of retinal vasculature and metabolism. Vascular branching patterns within the capillary plexuses are also represented in great detail, which may open new possibilities for the investigation of neurovascular coupling and control in the retina. We anticipate that accurate biophysical models such as the one presented here, when informed by independent *in vivo* measurements of flow and metabolism, will advance our understanding of the relationship between flow, metabolism, and neuronal activity elsewhere in the central nervous system, and constitute a baseline to characterize changes in numerous retinal diseases.

Commercial Relationships: Conor Leahy, None; **Harsha Radhakrishnan**, None; **Geoffrey Weiner**, None; **Jeffrey L. Goldberg**, None; **Vivek J. Srinivasan**, None

Support: National Institutes of Health (R00NS067050, R01EB001954), the American Heart Association (IRG5440002), the National Eye Institute (P30-022589), Research to Prevent Blindness Inc., and the Glaucoma Research Foundation Catalyst for a Cure 2

Program Number: 5967 **Poster Board Number:** A0138
Presentation Time: 12:00 PM–1:45 PM

OCT angiography guided by SLO eye tracker

Daniel Ruminski, Maciej Szkulmowski, Dawid Borycki, Iwona Gorczynska, Maciej Wojtkowski. Institute of Physics, Faculty of Physics, Astronomy and Informatics, Nicolaus Copernicus University, Toru, Poland.

Purpose: To demonstrate applicability of recently developed Scanning Laser Ophthalmoscope combined with Optical Coherence Tomography technique for noninvasive visualization of retinal

microcapillary network (RMN) in retinal diseases. RMN maps are provided by OCT technology while SLO provides fast eye tracking system.
Methods: The study was performed with high resolution and high speed spectral OCT (100 kHz A-scan rate, 4.5 um axial resolution, 91 dB detection sensitivity). Constant 30 Hz retinal preview is provided by SLO device and is used to guide the OCT scanning to the region of interest. Dedicated algorithm is used to detect eye motion on SLO images and calculate the translation to update the OCT scanner trajectory to compensate the motion of the eye. Complex difference and phase-variance algorithms are used to provide flow contrast on RMN maps. To increase RMN visualization area mosaic protocols were used. In case of eye blink or data corruption OCT guided by SLO can still provide good quality RMN maps as corrupted B-scans are rejected and reacquired.
Results: RMN maps obtained in the eyes of healthy volunteers and 12 patients with diabetic retinopathy, branch retinal vein occlusion and central retinal vein occlusion will be presented. 3D data will be visualized including depth color-coded projection. We will show that OCT can easily identify no perfusion areas and can visualize superficial and deep capillary plexus independently. We compare complex difference and phase-variance algorithms for RMN maps generation.
Conclusions: Recent reports on OCT angiography techniques show that these methods are well suited for visualization of 3D RMN in the healthy and pathologic eyes as well. However data acquisition time still needs to be shortened in order to provide good quality maps. Having no possibility to dramatically shorten time measurement we focused on small tracked areas that can be finally integrated on wide field mosaic. Our data suggest that OCT angiography has potential in the early diagnosis of retinal vascular diseases. Moreover real time eye tracking system highly improves data acquisition quality.
Commercial Relationships: Daniel Ruminski, None; **Maciej Szkulmowski**, None; **Dawid Borycki**, None; **Iwona Gorczynska**, None; **Maciej Wojtkowski**, None
Support: NCBR PBS1/A9/20/2013